Università degli Studi di Padova

DIPARTIMENTO DI FISICA E ASTRONOMIA"G. GALILEI"

Corso di Laurea Magistrale in Fisica

Tesi di Laurea Magistrale

THEORETICAL STRATEGIES FOR COMPARING DARK MATTER SEARCHES

Laureando:
Davide Racco

Relatori:
Dott. Andrea Wulzer
Prof. Fabio Zwirner

Anno Accademico 2013 – 2014

Contents

Introduction

Nearly a century ago, astronomers began to realise that there is a large discrepancy between the amount of mass deduced by the analysis of gravitational interactions in galaxies and clusters of galaxies and the mass that interacts with us through electromagnetic fields. The name "dark matter" was introduced to denote the hypothesis that this discrepancy is due to a component of matter subject to the gravitational interaction but not to the electromagnetic one, resulting as an opaque component of the mass budget inside the structures of the universe. Decades of subsequent astronomical observations, and the recent striking developments in observational cosmology, have nearly ruled out alternative proposals to explain this discrepancy, such as the possibility that it is due to compact objects formed of ordinary matter, or that it is our understanding of the gravitational interaction that is inadequate. This explains why the idea that dark matter is made of a new type of particle (or even more than one), subject to yet unknown interactions with ordinary matter, is widely shared today in the scientific community.

The quest for the dark matter particle(s) is today a compelling issue of Particle Physics, Cosmology and Astrophysics. There is a large set of models that contain a dark matter particle candidate, and within them there are different mechanisms responsible for the production of dark matter in the early universe. The most promising one is the freeze out mechanism, because of the striking coincidence (the so-called "WIMP miracle", where WIMP stands for Weakly Interactive Massive Particle) between the mass range preferred by this production mechanism and the mass scale required for new physics to appear in order to solve the gauge hierarchy problem of the Standard Model. Within this framework, the dark matter particle should have interactions with ordinary matter with a strength comparable with that of the electroweak interactions, which open good chances for the experimental detection of dark matter particles. But this is only one among the possible types of viable candidates: other production mechanisms are possible, and candidates from physics beyond the Standard Model show a remarkable variety of mass ranges and interactions with ordinary matter.

The variety of viable dark matter candidates proposed in theoretical models is accompanied by a rich set of very different experimental searches: direct searches could detect the flux of dark matter particles on the Earth, indirect searches look for the products of annihilations of dark matter happening today in the universe in many possible final states, and collider searches look for signals of dark matter production in high-energy reactions. The interplay among these different searches is crucial to test the properties of a possible positive detection, and to check that they can fit in the history of our universe.

The complex task of constraining many models with bounds coming from various experi-

ments forces both theorists and experimentalist to identify a theoretical framework that allows to draw conclusions and exclusion limits as independently as possible from a specific model. This need has motivated the use of effective theories to parametrise dark matter and its interactions with the Standard Model: effective field theories consist in the mapping of a model containing a certain number of particles and interactions into a model in which only the degrees of freedom below a given energy scale, also called cut-off scale, are present. This approach, although being extremely general because the number of possible effective operators with a given mass dimension is limited, relies on the assumption that the energy scale involved in the interaction of dark and ordinary matter is lower than the cut-off scale, which depends on the detail of the specific model under exam. If this hypothesis is not satisfied, then the predictions of the effective theory deviate from those of the corresponding complete model, until they reach the limit in which the effective theory is no longer reliable. This is a subject of concern for theorists and experimentalists, because the energy scale of the interactions in experiments aimed at dark matter detection are likely to approach or even reach the cut-off scale of the effective theory, especially at colliders. This is the reason why an increasing attention has been paid to understanding when the effective theory is reliable, and what is the possible bias induced by the effective approach on the interpretation of experimental results.

The aim of this thesis is to analyse carefully the regime of validity of the predictions of the effective theory when extracting limits from different types of measurements. To do so, it is necessary to compare the effective theory with the full one, thus to specify a model: to keep the approach as general as possible, the most sensible option is to identify *simplified models*, i. e. models containing a minimal set of fields, defined by Lagrangians containing only renormalisable operators. These models allow a control over the regime of validity of the effective theory, but keep the fundamental property of parametrising the essential features of a larger class of models beyond the Standard Model. This is a relevant advantage, since we do not have a compelling candidate dark matter model among the large set of available ones. Then we choose as case studies two representative simplified models, with a fermionic dark matter particle and a vector or a scalar mediator, respectively, and we critically discuss the reliability of the predictions of the corresponding effective theories with respect to the complete models.

The content of the thesis is the following. In chapter 1, we review the history of dark matter, and discuss the main evidences that prove its existence. Then we motivate the introduction of a new particle as the explanation for dark matter, by discussing two alternative approaches that are today basically excluded, or at least strongly disfavoured, by cosmological observations. We continue by reviewing the possible mechanisms for the production of dark matter in the early universe, and the main candidates for dark matter that are not WIMPS. In chapter 2, we describe in detail the three categories of searches for dark matter (direct, indirect and collider searches) and the most relevant WIMP candidates for dark matter. The main part of the thesis consists of chapter 3, which contains the original contribution of this work. After a discussion of the motivations for the use of simplified models and a description of the two models chosen for this thesis, we derive the constraints coming from the relic abundance of dark matter, and from direct, indirect and collider searches, for each of the two models. We finally summarise our conclusions and the prospects of future work. Some more technical material is collected in two appendices: appendix A contains relevant formulæ and conventions on Dirac and Majorana fermions, while in appendix B we present the detailed calculation of the relic density through the freeze out mechanism.

CHAPTER 1

Evidence and candidates for particle dark matter

In this chapter, we will review [1, 2, 3] the history of the discovery of dark matter (DM) on a broad range of scales in our Universe (sec. 1.1). The increasing amount of evidence led physicists and astronomers to propose various alternative explanations, along two possible approaches: either by changing our model for gravity on the galactic scale (sec. 1.2.2) or by adding other components of matter, which could be ordinary non-luminous matter (sec. 1.2.1) or some yet unknown particle (sec. 1.4). Many decades of astronomical and cosmological observations eventually showed that the latter is the most viable option, and today a wide range of possible candidates are predicted by many theories beyond the Standard Model (BSM).

Before discussing these possibilities, we will review the possible production mechanisms of dark matter in the early universe after the primordial inflation (sec. 1.3), to point out the relevant features that a viable candidate must possess to be consistent with the relic density of dark matter observed today and with the standard cosmological model (the so-called ΛCDM).

1.1 Evidence for dark matter

1.1.1 Observations on the galactic scale

The first observations of non-luminous matter were done by Oort in 1932. His measurements of the brightest stars in the Milky Way suggested that part of the gravitational mass of the galaxy was missing if one only considered those stars, and this fact brought him to claim that the disk of the galaxy was composed for two thirds by "dark matter" including stars less luminous than the Sun, and gas and dust in the interstellar medium. Many years later, in 1959, Kinman observed some deviations in the velocities of the globular clusters contained in the Milky Way with respect to what expected from a pure disk mass model, and already suggested a linearly rising mass distribution beyond the disk.

Also the observations of the spiral galaxy nearest to us, M31 (Andromeda), done by Babcock in 1939, suggested that the ratio between gravitational and luminous mass was increasing in the outer regions of the galaxy. Later measurements of the rotation curve of this galaxy in 1957 and 1975 showed a flat region. The studies were deepened in the following years, in particular by Vera Rubin, who showed that, for a large sample of spiral galaxies, the rotation curve of stars inside the galaxy did not fall off as predicted by Keplerian gravity, but kept a flat profile

for a large distance outside the main disk. Since the radial velocity, in the approximation of a circular motion and spherical symmetry, is given by $v = \sqrt{GM(r)/r}$ (where $G = 6.67 \times 10^{-11}\,\mathrm{N \cdot m^2 kg^{-2}}$ is the gravitational constant and $M(r)$ is the gravitational mass contained inside a sphere of radius r centered in the barycenter of the galaxy) these results imply a dark matter mass density proportional to r^{-2} within a large region outside the main disk of the galaxy (see fig. 1.1).

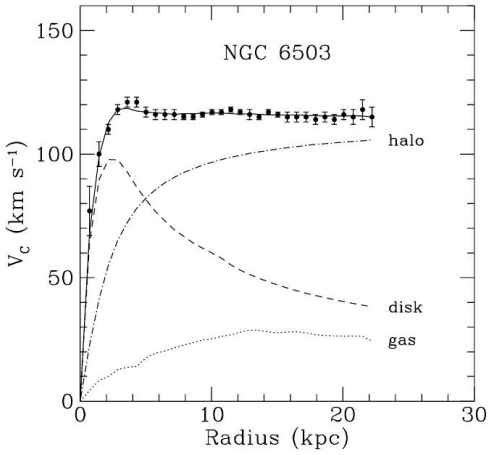

Figure 1.1: Rotation curve of stars in the galaxy NGC 6503: this plots reports the rotation velocity as a function of the radial distance, for many stars inside that galaxy. The dotted, dashed and dash-dotted lines are respectively the contributions of gas, disk and dark matter to the gravitational mass contained in the galaxy (from [2]). The profile of the rotation curve remains nearly constant for a large distance outside the main disk radius, while, if the luminous mass and the gas were the only component of the galaxy, Newtonian gravitational law would predict a fall-off proportional to $1/\sqrt{r}$.

1.1.2 Observations on the intergalactic and cosmological scale

One year after Oort (1933), Fritz Zwicky measured the velocities of galaxies within the Coma galaxy cluster, and deduced that the gravitational mass contained in the cluster was hundreds of times greater than the luminous mass. Among the few possible explanations, he also quoted Oort's proposal of "dark matter".

The large set of observations gathered from the early '30s to the end of the '80s provided plenty of evidence that, in the framework of general relativity, a large part of the mass inside and surrounding galaxies is not interacting through electromagnetic or nuclear interactions.

The first detailed observations of the Cosmic Microwave Background (CMB) on small angular scales (Maxima, Boomerang in 2000 and WMAP in 2003) allowed to measure the spectrum of the anisotropies in the temperature of the CMB, which constrains many cosmological parameters, including Ω_m (the sum of dark matter and baryon energy densities over the critical density). Ω_m affects the shape of the spectrum through many mechanisms, but mainly influences the heights of the first peaks. Already the first measurements of Maxima and Boomerang pointed to a value of Ω_m around 30%, and the current best measurement of the CMB, obtained by the Planck satellite, gives $\Omega_m = 31.6\%$ [4], and an energy density of dark matter equal to 26.7% of the total one.

Another important probe for the distribution of dark matter is the observation of strong gravitational lensing, i. e. the study of images of far galaxies bent or replicated because of the passage of light near a very massive galaxy cluster. This kind of observations showed that

the most massive clusters are largely dominated by dark matter, with ratios of gravitational to luminous matter of the order of some hundreds.

We conclude this brief summary with an important and suggestive evidence, the observation of the *Bullet cluster* in 2006 [5]. This system is composed of two primary galaxy concentrations, which passed through each other $\approx$ 100 Myr ago. As a result of this collision, the various components of the two galaxy clusters (dark matter, X-ray emitting plasma, and galaxies visible in the optical spectrum) underwent different interactions with the components of the other cluster. While the ordinary matter components slowed down during the collision because of their electromagnetic interactions, the dark matter components passed through each other without significant consequences, in the hypothesis that they can interact only gravitationally or through a very weak self-interaction. Under these conditions, the outcome of the collision is a displacement between the barycentres of the hot gas distribution (visible in the X-ray spectrum by the Chandra satellite) and the dark matter distribution (which can be inferred by the analysis of the weak gravitational lensing of background structures). The result is displayed in fig. 1.2. This spectacular observation is very important, because it allows to constrain the strength of dark matter self-interactions, and because it is a strong argument against the proposals of modified gravitation (sec. 1.2.2). Indeed, if one rejects the dark matter hypothesis, it is hard to explain without contradicting very basic assumptions on the nature of gravity why the weak gravitational lensing points to a barycentre displaced with respect to the centre-of-mass of the ordinary matter distribution.

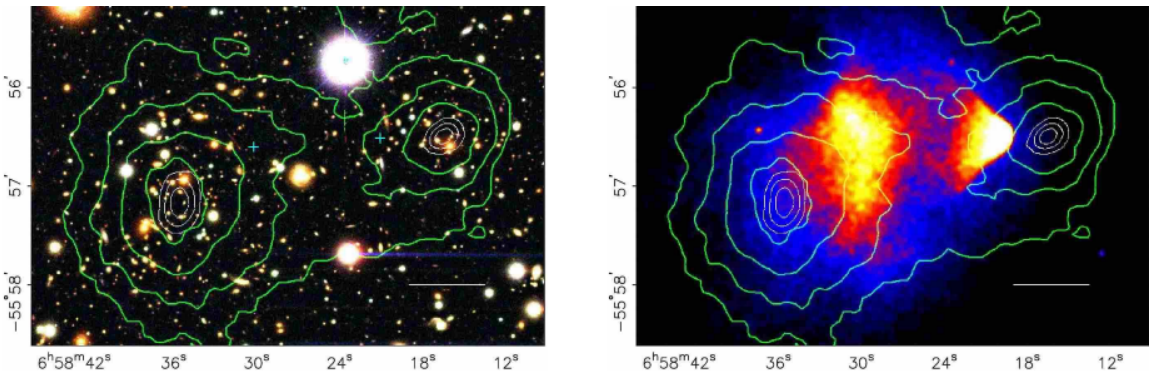

Figure 1.2: Images of the Bullet cluster. In the left panel, a colour optical image showing the galaxies, which make up only a few percent of the mass of the cluster. In the right panel, an X-ray image from the Chandra telescope, showing where the bulk of the gas in the cluster is located. In both panels, the green contours show the mass distribution inferred from gravitational lensing [5].

1.2 Attempted explanations for DM without new particles

In this section we will discuss two possible explanations for the effects described in the previous section. The two logical alternatives are modifying the Newtonian gravitational laws on the galactic scale, to predict for some reason a gravitational attraction much stronger with respect to the Newtonian one (at larger distances, or for lower accelerations as in the MOND case) in order to explain the flat trend in rotation curves outside the galactic disk, or adding other components of non-luminous matter. In the latter case, a conservative but relevant remark is that we could have a poor understanding of non-luminous ordinary matter in the galaxies: sec. 1.2.1 discusses this possibility. The former possibility is then discussed in sec. 1.2.2, following the discussion of [6, 7]: apart from possible theoretical inconsistencies of these models, also their

phenomenological viability faces relevant difficulties. Nevertheless, as long as dark matter is not observed through interactions different from the gravitational one, modified gravity could still be considered, from an epistemological point of view, in order to confront the dark matter paradigm with a contrasting one.

1.2.1 MACHOs: Massive Astrophysical Compact Halo Objects

To explain the strong hierarchy between the gravitational and luminous mass in galaxies, the most straightforward proposal is that we do not correctly model the population of low mass stars, stellar remnants and planetary mass bodies [1]. Compact astronomical bodies that constitute a significant component of the mass of the galaxy are referred to as Massive Astrophysical Compact Halo Objects (MACHOs). Their luminous faintness or opacity prevents us from searching for MACHOs in direct imaging, leaving as the only probe the search for their gravitational effects, in particular the gravitational lensing that they induce. In the case of the images of single stars, the passage of a massive lensing body has the effect of a brightening of the star on a time scale related to the mass and velocity of the intervening object, and typically ranges between a few weeks and a year.

Various experiments in the past two decades have investigated the number density of MACHOs in the Milky Way through this effect of microlensing (MACHO project, Optical Gravitational Lensing Experiment, Expérience pour la Recherche d'Objets Sombres), and found no conclusive evidence, placing strong upper limits on the number of massive bodies in the galaxy in the mass regime of $(10^{-7} \div 30)\ M_\odot$, where $M_\odot$ denotes the mass of the Sun.

For opaque bodies of masses greater than $\sim 100\ M_\odot$, the time scale of microlensing is a few years, therefore the efficiency for detecting objects in this mass range through this tipe of surveys drops significantly. In this mass range, the most efficient methods rely on the study of the lifetime of wide binary stars in the galaxy (which are likely broken up by the near passage of massive bodies), bringing to the estimate that MACHOs of mass $(10 \div 10^7)\ M_\odot$ comprise no more than $\sim 50\%$ of the galactic halo, or on indirect studies of the velocity dispersion of the galactic disk, which pose strong constraints on MACHOs with mass $\gtrsim 10^7\ M_\odot$.

Today, even if further analyses of stellar remnants and primordial black holes are in progress, galactic searches for dark matter in the form of MACHOs have reached a significant level of maturity, and have firmly established that dark matter does not dissipate energy (because of its very weak self-interactions) to clump into objects as massive as stars or planets, and that the dominant matter component in galactic halos is more diffusely distributed [1, 8].

1.2.2 MOND: MOdified Newtonian Dynamics

The evidence for dark matter came from the observation of an inconsistency between the observations and the Newtonian model for the gravitational interaction. In analogy to similar crises faced by astronomy in the past (discovery of Neptune as "dark matter"[1], and precession of the perihelion of Mercury explained through a modification of gravity), a possibility is that the radial velocities of stars far from the centre of the galaxy are higher than expected because they are subject to a gravitational force stronger than the Newtonian one.

This was the perspective of the proposal by Milgrom (1983) of MOND (MOdified Newtonian Dynamics). He postulated the following equation for the motion of a test particle subject

[1] In the 18th century, the observations of the motion of Uranus were in contrast with the Newtonian laws applied to the known content of the Solar system; the proposal of introducing a new ingredient to the matter components, i. e. the introduction of a new planet, led to the discovery of Neptune.

to a gravitational field $-\vec{\nabla}\Phi_N$:

$$\widetilde{\mu}\left(\frac{|\mathbf{a}|}{a_0}\right)\mathbf{a} = -\vec{\nabla}\Phi_N\,, \qquad \widetilde{\mu}(x) \to \begin{cases} 1 & \text{for } x \to \infty\,, \\ x & \text{for } x \to 0\,, \end{cases} \tag{1.1}$$

where $a_0 \approx 10^{-8}$ cm s^{-2} is a preferred scale of acceleration. Outside the mass distribution of a galaxy, at a radial distance r, $|\vec{\nabla}\Phi_N| = GM/r^2$, where M understands only the baryonic mass. Eq. (1.1) implies the Newtonian limit for accelerations greater than a_0, while for $a \ll a_0$ (therefore for extremely weak gravitational fields) the acceleration is the geometric mean of the Newtonian one and a_0. As a consequence, eq. (1.1) is able to predict a flat rotation curve for galaxies (fig. 1.1) and also to explain the Tully-Fisher correlation, i. e. the experimentally observed proportionality between the total baryonic mass of a disk galaxy and the fourth power of the asymptotic rotation velocity [6].

Apart from these results, from a more theoretical point of view it is not clear from eq. (1.1) if the deviation from the Newtonian limit comes from a modification of the inertial mass, or the gravitational mass, or the second Newton's law, or the gravitational force, and any of these possibilities opens the door to many theoretical or experimental inconsistencies. Eq. (1.1) does even violate momentum conservation, since the time derivative of the total momentum $m_1\mathbf{v}_1 + m_2\mathbf{v}_2$ of an isolated system of two particles interacting gravitationally does not vanish, because the values of the factor $\widetilde{\mu}$ will generally be unequal. Milgrom then suggested that this equation is meaningful only for test particle motion in a background gravity field.

There have been some attempts to derive eq. (1.1) from a variational principle. The resulting non-relativistic Lagrangian is

$$L = -\int \left[\frac{a_0^2}{8\pi G}\,F\!\left(\frac{|\vec{\nabla}\Phi|^2}{a_0^2}\right) + \rho\,\Phi\right] \mathrm{d}^3x\,, \tag{1.2}$$

where ρ is the visible matter density, and F is a positive function such that $\widetilde{\mu}(x) = F'(x)$. The asymptotic trends of F are $F(X^2) \to X^2$ for $X^2 \to \infty$ (so that $\widetilde{\mu}$ is constant) and $F(X^2) \to \frac{2}{3}X^{3/2}$ for $X^2 \to 0$. This Lagrangian, which for extremely weak gravitational fields deviates from the Newtonian behaviour (which corresponds to $F(X^2) = X^2$) is referred to as AQUAL (AQUAdratic Lagrangian). It is clear that this formulation is non-local, since F cannot be a polynomial in $|\vec{\nabla}\Phi|$, and frame dependent: indeed, it is not sensible to consider a ratio $|\vec{\nabla}\Phi|/a_0$ without specifying the frame in which the vector $\vec{\nabla}\Phi$ should be evaluated.

A relativistic formulation that reduces to the MOND equation in the weak field limit was proposed by Bekenstein in 2004, and is called TeVeS (Tensor-Vector-Scalar theory). In this formulation, one needs to introduce a timelike 4-vector field $\mathcal{U}_\alpha$, together with a scalar field ϕ, to define a Jordan metric

$$\widetilde{g}^{\text{Jordan}}_{\alpha\beta} = e^{-2\phi}g^{\text{Einstein}}_{\alpha\beta} - (e^{2\phi} - e^{-2\phi})\mathcal{U}_\alpha\mathcal{U}_\beta\,.$$

By requiring that $\mathcal{U}_\alpha$ points in the time direction, it is possible to deduce the gravitational lensing effect [6]. Such a recipe would violate the general covariance of the model, since the prescription that a 4-vector should point in the time direction obviously is not a covariant one. In order to get this constraint dynamically, Bekenstein proposed the following action:

$$S_{\text{TeVeS}} = -\frac{1}{32\pi G}\int \Big[K_1 g^{\alpha\beta}g^{\mu\nu}\mathcal{U}_{[\alpha,\mu]}\mathcal{U}_{[\beta,\nu]} + K_2(g^{\alpha\beta}\mathcal{U}_{\alpha;\beta})^2 - 2\lambda(g^{\mu\nu}\mathcal{U}_\mu\mathcal{U}_\nu + 1)\Big]\sqrt{-g}\;\mathrm{d}^4x\,. \tag{1.3}$$

The first term is a Maxwell-like one, the second one is a gauge fixing term and the third term fixes $\mathcal{U}^2 = -1$ through a Lagrange multiplier. This model manages to reproduce the additional

lensing far from the centres of galaxies, which is needed to reconcile the observations with the visible matter content of galaxies.

The TeVeS formulation gives a viable theoretical framework leading to the MOND equation (1.1). The main problems of this modified gravity approach are the following three [7].

First of all, MOND does not explain well the dynamics of galaxy clusters. The most remarkable example is given by the *Bullet cluster*, discussed in sec. 1.1.2. The arguments proposed by the supporter of TeVeS are that we should not draw conclusions from a single observation, that also the CDM paradigm has some difficulties in modelling this cluster, and that the full calculations for this case of axisymmetric lens have not been performed so far in TeVeS: these are true statements, but not very convincing, pointing out that the dark matter paradigm explains much more successfully galaxy cluster dynamics.

As a second point, the spectrum of the anisotropies of the CMB in the TeVeS paradigm has difficulties in reproducing the observed height of the third peak, which should be very small in a baryon dominated model that lacks the extra gravitational force supplied by dark matter.

Finally, TeVeS gives completely different predictions about the power spectrum of matter perturbations (fig. 1.3): in the ΛCDM paradigm, the so-called Baryon Acoustic Oscillations (the peaks in the power spectrum of the matter distribution, linked to the propagation of sound waves in the baryon-photon fluid before the recombination) are highly suppressed as the baryons fall into the potential wells created by dark matter, while in a model without dark matter the oscillations should be as apparent in the baryonic matter distribution as in the CMB.

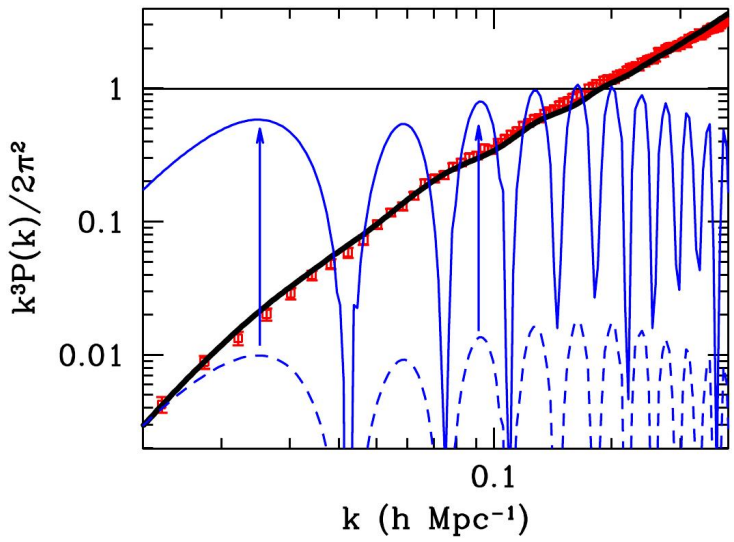

Figure 1.3: The power spectrum of matter extracted from the data of the Sloan Digital Sky Survey (red points with error bars), compared with the predictions of the ΛCDM model (black line), a no dark matter model with $\Omega_b \approx 0.2$, $\Omega_{\rm DE} \approx 0.8$ (blue dashed line), and the TeVeS predictions (blue solid line). The TeVeS model, which amplifies the perturbations with respect to the dashed line prediction, reaches the amount of inhomogeneities needed for the structure formation, but is in total disagreement with respect to the observed power spectrum, whose "bumps" (the so-called Baryon Acoustic Oscillations) are highly suppressed (from [7]).

1.3 Production mechanisms of DM in the early universe

In the rest of this thesis, we will assume the DM paradigm, which seems today by far the most viable hypothesis to explain the anomalies mentioned in sec. 1.1 and to fit the vast amount of detailed cosmological observations.

In this section, we will briefly discuss how DM fits in the history of the early Universe, i. e. we will explain the main features of the most plausible mechanisms by which dark matter has been produced in the universe after the end of the inflation (the so-called reheating phase), and has reached the current abundance.

1.3.1 Freeze out

Freeze out is the simplest mechanism that fixes the abundance of a species in an expanding Universe [8, 3].

If two particles, say A and X, can interact with each other through the reaction $AA \leftrightarrows XX$, then, when initially the Universe is very hot (at energies much greater than the masses of the two particles), the two species annihilate into each other maintaining the chemical equilibrium. When the temperature T of the Universe drops below the higher of the two masses, say m_X, then the number density n_X of X, in the hypothesis that X remains in thermal equilibrium, must follow the non-relativistic Boltzmann distribution, which includes a suppression factor $e^{-m_X/kT}$. Hence, the particles X will annihilate into particles A so as to follow the Boltzmann distribution.

Therefore, n_X should drop to zero as the Universe cools down, unless the reaction $XX \to AA$ at a certain point becomes inefficient. This will happen indeed because of the expansion of the Universe, which dilutes the concentration of non-relativistic particles proportionally to a^{-3}, where a is the scale factor[2]. Then, when the annihilation rate $n_X\langle\sigma v\rangle$ (where $\langle\sigma v\rangle$ is the thermally averaged cross section for the reaction $XX \to AA$) will decrease below the Hubble rate of expansion $H \equiv \dot{a}/a$, the annihilation of the X particles will substantially cease. The consequence is that n_X keeps the same value it had at the moment of the *freeze out*, when $n_X\langle\sigma v\rangle \approx H$.

This mechanism could be specialised to the case of dark matter, if we denote by X the corresponding particle and we assume that it can interact with another species (through some yet unknown interaction, or possibly only through gravitational ones), and that it is in thermal equilibrium in the early Universe.

This discussion can be made quantitative through the numerical solution of the Boltzmann equations, a set of differential equations that describe the evolution of the number densities of interacting species in an expanding universe. In the case we are discussing, the equation for n_X reads (we understand the subscript X for n)

$$\frac{\mathrm{d}n}{\mathrm{d}t} = -3Hn - \langle\sigma v\rangle\left(n^2 - n_{\mathrm{eq}}^2\right), \tag{1.4}$$

where n_{eq} is the equilibrium number density of X. The first term on the right hand side of eq. (1.4) accounts for the dilution due to the expansion, the second term comes from the $XX \to AA$ process, while the third one comes from the opposite reaction $AA \to XX$. This equation can be solved numerically, with the result shown in fig. 1.4.

[2]The scale factor is the the function of time that multiplies the spatial part of the Friedmann-Robertson-Walker metric,

$$\mathrm{d}s^2 = c^2\mathrm{d}t^2 - a^2(t)\left[\frac{\mathrm{d}r^2}{1-kr^2} + r^2\mathrm{d}^2\Omega\right],$$

where $k = -1$, 0 or +1 depending on the geometry on the Universe, and $\mathrm{d}^2\Omega = \mathrm{d}\theta^2 + \sin^2\theta\,\mathrm{d}\phi^2$.

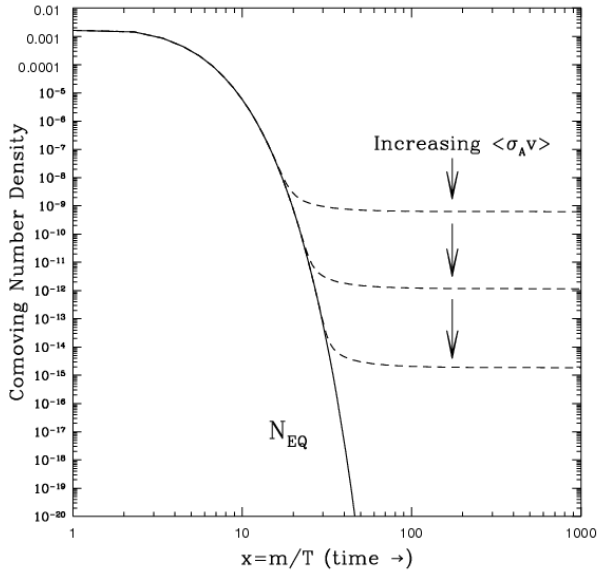

Figure 1.4: A scheme of the comoving number density (na^3) of a stable species X during the process of thermal freeze out, as a function of $x = m_X/T$. The larger is the cross section for the process $XX \to AA$, the lower is the thermal relic density of X (from [9]).

In appendix B, we will describe in detail the derivation, from the definition of the thermally averaged cross section $\langle\sigma v\rangle$ that appears in eq. (1.4), of a simpler (exact) formula involving only a one-dimensional integral, and then we will derive an approximate formula in the limit of low temperature with a low velocity expansion. Then, we will show how to compute, with an approximate solution of the Boltzmann equation, the relic abundance of dark matter $\Omega_{\rm DM}$. In the remainder of this section, we show through a qualitative estimate of $\Omega_{\rm DM}$ what we can infer about the fundamental properties of the DM particle X.

Let us focus on the freeze out moment (denoted with a subscript f): the condition $n\langle\sigma v\rangle = H$, together with the Friedmann equation for a radiation dominated Universe, $H^2 \sim T_f^4/M_{\rm P}^2$ (by the symbol $\sim$ we will denote rough estimates, valid up to $O(1)$ factors, and by $M_{\rm P}$ the reduced Planck mass $1/\sqrt{8\pi G}$), brings to

$$n_f \sim \frac{T_f^2}{M_{\rm P}\langle\sigma v\rangle}\,. \tag{1.5}$$

It is customary to define $x \equiv m/T$, and the yield $Y \equiv n/s$, where s is the entropy density of the Universe. The thermal relic density of X is then (the subscript 0 denotes present-day quantities)

$$\Omega_X = \frac{m_X n_0}{\rho_c} = \frac{m_X T_0^3}{\rho_c}\frac{n_0}{T_0^3} \sim \frac{m_X T_0^3}{\rho_c}\frac{n_f}{T_f^3} \sim \frac{x_f T_0^3}{\rho_c M_{\rm P}}\frac{1}{\langle\sigma v\rangle}\,, \tag{1.6}$$

where the first approximation follows from $Y_f = Y_0$ and $s_f = s_0$ (isoentropic expansion of the universe) with the approximation $g_{*f} \approx g_{*0}$ [9], and in the last passage we used eq. (1.5). If we impose $\Omega_X \sim 0.3$ in eq. (1.6), and we assume that X is weakly interacting with A and therefore we write[3] on dimensional grounds $\langle\sigma v\rangle \sim g_{\rm weak}^4/(16\pi^2 m_X^4)$, then m_X turns out to be in the range 100 GeV – 1 TeV. Then, a weakly interacting particle with a weak scale mass (which is the most straightforward requirement to solve the gauge hierarchy problem) naturally leads to the

[3]From now, we will usually assume $c = 1$, $\hbar = 1$, unless specified otherwise.

correct relic abundance. This exciting coincidence was called "*WIMP miracle*", where WIMP stands for Weakly Interacting Massive Particle, and motivated in the last decades a wide belief that the most likely particle candidate for dark matter is a WIMP[4].

An important point in this result is that the thermal relic density is mainly dependent on the cross section σ, rather than on the mass m_X, which appears in eq. (1.6) only through x_f, which is typically of the order of 20 for a WIMP candidate and does not vary much for different choices of m_X. Moreover, this mechanism is independent of the early thermal history of the Universe and of the interactions at high energy scales.

We conclude this discussion about the freeze out mechanism by recalling the corresponding requirements for dark matter: the DM particle X should be stable on cosmological scales and in thermal equilibrium in the early Universe (moreover, its mass should be lower than the reheating temperature), it should annihilate to other particles, and the corresponding cross section must satisfy a lower bound, so that X is not over-abundant. The consequence of the two last requirements is that it is possible to probe the existence of dark matter through one of the strategies described in sec. 2.1 (if X can annihilate into Standard Model particles). A peculiarity of the freeze out mechanism is that a weakly interacting particle X with a mass of the order of the weak scale implies the correct total relic abundance of dark matter.

1.3.2 Freeze out and decay

A slightly more sophisticated mechanism with respect to the freeze out might offer a viable option to get the correct relic abundance, even in a scenario in which the particle X undergoing the freeze out has a mass a bit higher than the weak scale (for example around 1 TeV), or it is electrically charged, but unstable on long time scales because of extremely weak interactions (e. g. gravitational ones).

This mechanism, which opens many possibilities from the particle physics point of view, goes under the name of "*freeze out and decay*". In this case, the species X undergoes the freeze out mechanism yielding a thermal relic density Ω_X. Then, because of very weak interactions (as gravitational ones), X can further decay to some particle Y with a decay $X \to Y + \ldots$; if this coupling is weak, the effect of Y on the freeze out of X is negligible. The result at late times is that the species X nearly disappears, leaving a relic density for Y given by (if each X produces only one particle Y)

$$\Omega_Y = \frac{m_Y}{m_X}\Omega_X \,.$$

If we now specialise this general framework, by assuming that X is a WIMP (now with a more relaxed constraint on m_X), and that m_Y is comparable or slightly lower than m_X, then Y turns out to have the correct relic abundance to be the DM candidate: a name used to denote this species is "*superWIMP*", as it should interact super-weakly and have a mass of the order of the weak scale.

In this case, since X is unstable and is not the DM particle, it does not need to be neutral (for a further discussion, see sec. 1.4.2).

If the decay channel of X includes, together with Y, some Standard Model (SM) particles, a limit on the lifetime of X comes from the requirement that it does not decay after the nucleosynthesis, in order not to introduce a late time production of SM particles that could influence the nucleosynthesis in a way incompatible with observations.

[4]This belief has put down so strong roots that in some references the acronym WIMP is occasionally used as a synonym of dark matter; another commonplace led in sporadic cases to the use of "neutralino" as a synonym of WIMP (see sec. 2.2). In this work, we will pay attention to the distinction of these terms.

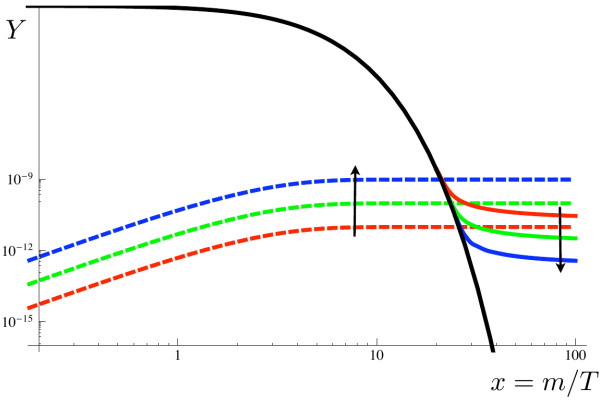

Figure 1.5: Evolution of the relic yield Y for the freeze out mechanism (solid coloured lines) and freeze in via a Yukawa interaction (dashed coloured), deviating from the equilibrium density (solid black). The arrows indicate the effect of increasing the coupling strength for the two processes (from [10]).

1.3.3 Freeze in

The production mechanism called *freeze in* can be seen for various reasons as the "opposite" with respect to the freeze out mechanism, in particular for its constraints on the properties of the dark matter candidate. We will sketch here only its basic features, and refer to [10] for a more detailed discussion[5], including BSM candidates and their possible experimental signatures.

The basic framework of this production mechanism is the following. The assumptions about the initial conditions of the dark matter candidate X are that, unlike for freeze out, the species X is thermally decoupled from the thermal bath because it is weakly interacting with its components. Another assumption is that the initial number density of X is negligible, for example because after reheating the reactions that produce X in the final state are inefficient. Although the interactions with the thermal bath are feeble, X is still produced, with a yield which turns out to be inversely proportional to the temperature T, and therefore increasing in time (we will show later the formulæ that justify this statement). Then the number density of X keeps growing until the temperature drops below m_X, and the reactions that produce X become kinematically disfavoured. From that moment on, the number density of X will substantially remain frozen because the interaction rate will be lower than the Hubble rate.

The most relevant feature of this mechanism is that the number density of X is greater for higher couplings of X to the thermal bath, contrarily to the freeze out case (see fig. 1.5).

We will now estimate the yields expected for two possible renormalisable interaction terms, to show that they turn out to be decreasing with temperature (and hence increasing with time). The yield, being an adimensional quantity (once we set $k = 1$) must be the ratio of the two dimensionful quantities which are involved, the decay rate Γ (for a three field interaction, or $n\langle\sigma v\rangle$ for a two-to-two particles scattering) and the Hubble rate $H \sim T^2/M_{\mathrm{P}}$.

For a Yukawa interaction $\lambda\psi_1\psi_2 X$ among three fields with masses $m_1 > m_2,\ m_X$, the decay rate in the rest frame of ψ_1 must be $\Gamma^{\mathrm{RF}} \sim \lambda^2 m_1$. The corresponding rate in the comoving frame can be obtained by dividing for the boost factor T/m_1; then $Y_X \sim \Gamma/H \sim \lambda^2 m_1^2 M_{\mathrm{P}}/T^3$. By evaluating the yield for the temperature $T \approx m_1$ at which the production is dominant (with

[5] An earlier application of this mechanism had already been done in [11] for the specific case of a gauge singlet complex scalar S, interacting with the Higgs boson through the so-called *Higgs portal*, i. e. through an interaction term $\lambda S^\dagger S H^\dagger H$, which brings to a possible decay of the Higgs boson to $S\overline{S}$ after electroweak symmetry breaking.

respect to later times when $T < m$) we get

$$Y_X \sim \lambda^2 \frac{M_P}{m_1}\,.$$

In the case of the quadrilinear interaction $\mathcal{L}_{int} = \lambda X^2 \psi_1^2$, the corresponding cross section will be proportional to λ^2/T^2 for dimensional reasons (for early times, the two species are relativistic, $T \gtrsim m_1,\ m_X$), $n \sim T^3$ and $Y_X \sim n\langle\sigma v\rangle H^{-1} \sim \lambda^2 M_P/T$ which gives a final yield (for $T \approx m_1$) of the same order as before, $Y_X \sim \lambda^2 M_P/m_1$.

Even if the details of the freeze in mechanism and of the calculation of the relic density change from case to case, the relevant point that emerges from this estimates is that the yield predicted by this mechanism has opposite features with respect to the one predicted by freeze out. We can estimate the latter from eq. (1.5) by inserting $\langle\sigma v\rangle \sim \lambda^2/m_X^2$ and $T \sim m_X$:

$$Y_{FO} \sim \frac{1}{\alpha^2}\frac{m_X}{M_P}\,.$$

We can see that the two mechanisms generally yield the correct relic abundance of dark matter for different regimes of the mass scales and interaction couplings (see fig. 1.6).

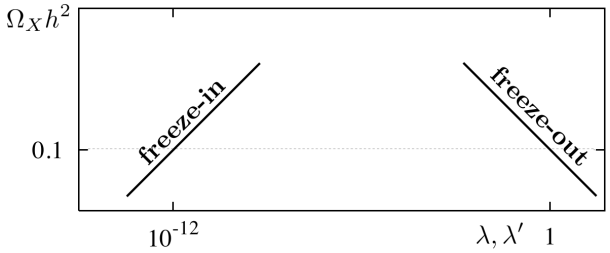

Figure 1.6: Schematic picture of the relic abundances due to freeze in and freeze out as a function of coupling strength (from [10]).

We conclude by observing that the yield predicted by the freeze in mechanism mainly depends on the particle (ψ_1 in our notation) which produces the dark matter particle X, while the prediction from the freeze out depends on X. Moreover, the comparison between the two results shows that, in order to get $\Omega_X \approx 0.3$, the coupling constant must be of the order of the ratio between the weak scale and the Planck mass, $\lambda \sim v/M_P$: therefore, freeze in candidates are likely to arise in theories where small couplings arise at linear order in the weak scale. For a further discussion about possible candidates from supersymmetry or extra dimensions, see [10].

1.3.4 Asymmetric dark matter

The mechanisms we have discussed until now give relic abundances of dark matter that depend on microscopic quantities related to the interaction and couplings of the dark sector. For example, we have seen that in the freeze out mechanism Ω_{DM} depends in first approximation only on the annihilation cross section for the process $XX \to AA$.

Now, in our Universe the densities of dark matter and baryonic matter are comparable, $\Omega_{DM} \approx 5\Omega_b$. The two energy densities are both proportional to a^{-3}, so they keep the same ratio as the Universe expands. Then, the production mechanisms for the two species brought to similar yields even if they took place in different times, and with completely different dynamics. This is a quite surprising coincidence if we assume the freeze out mechanism for dark matter

and some different scenario for baryogenesis: this can be an accident, or could be discussed on anthropic grounds, or could be the dynamical result of two related production mechanisms for the two species. The latter framework goes under the name of "*asymmetric dark matter*" [12, 13], for reasons that will be clear in the following.

The current proposals about the explanation of the abundance of baryonic matter are linked to the so-called baryon asymmetry, the strong disparity between the amount of matter and antimatter in the Universe. This asymmetry is quantified by the difference between baryon and antibaryon number densities, over the photon number density, $\eta = (n_b - n_{\bar{b}})/n_\gamma$, and is experimentally measured as 6×10^{-10}. In order to explain dynamically this asymmetry, the following conditions have to be fulfilled: baryogenesis must have happened out of the thermal equilibrium, and there must be interactions that violate the baryon number B and C, CP transformations.

One of the most promising options to solve this problem is to link it to the main experimental problem of the minimal version of the Standard Model, the neutrino masses. If we add the right-handed neutrinos to the SM with a Majorana mass term and Yukawa couplings to the lepton and Higgs doublet, then the total leptonic number L is violated, and non-perturbative phenomena[6] could have communicated an L violation to the baryonic sector during the leptogenesis.

Independently from the mechanism that explains a slight initial asymmetry between baryons and antibaryons in the early Universe, later annihilations of baryon and antibaryons remove the symmetric part of the two components (decaying eventually into photons), leaving only the asymmetric part, until this reaction is efficient. The result of this process is indeed that the component which had a slightly smaller number density nearly disappears.

At this point, it is clear that the coincidence of the orders of magnitude of $\Omega_{\rm DM}$ and $\Omega_{\rm b}$ is unexpected. Starting from these considerations, many production mechanisms for dark matter, similar to the baryogenesis paradigm, stem out: some CP violating process (which must also violate the quantum number that makes DM stable) creates an asymmetry between dark matter particles and antiparticles, to an amount comparable to the baryonic asymmetry. Then, annihilations of dark matter leave only the asymmetric component which turns out to have a number density comparable to $\Omega_{\rm b}$.

Without entering into the details of any specific model, we only sketch the generic features of this mechanism [12].

- An asymmetry between particle and antiparticle number density is initially created in the visible and/or the dark sector, through some specific mechanism, at the same time or at different ones.

- Some process communicates the asymmetry between the two sectors and then decouples, "freezing in" their amounts.

- The symmetric components, in each of the two sectors, must finally annihilate away through some efficient reaction. In analogy with the SM, this could happen in the dark sector through the annihilation of particle and antiparticle into the vector mediators of some dark force, or maybe with other higher dimension operators.

[6] The chiral anomaly for the global symmetries B and L implies non-perturbative configurations (called *sphalerons*) that violate B and L, but preserve their difference $B - L$.

1.4 Particle candidates for dark matter

1.4.1 WIMPs: Weakly Interactive Massive Particles

As we have discussed in sec. 1.3.1, the freeze out mechanisms presents a "*WIMP miracle*", i. e. it naturally predicts a correct $\Omega_{\rm DM}$ for a weakly interacting particle with a mass of the order of the weak scale. The requirement that there are new particles at the weak (or TeV) scale (with some non-negligible interaction with the Standard Model) is the most straightforward one to solve the hierarchy problem. The coincidence that two very different problems at the microscopic and the macroscopic scale pointed to the same prediction has motivated for some decades a strong belief in the particle physics community that this should be the common solution to both problems.

Furthermore, the mass scale and the interaction strength (comparable to the weak one of the SM) of the WIMP motivate some hope of a relatively easy detection (at least with respect to the other possibilities mentioned in this section) with some of the methods described in section 2.1, because the freeze out mechanism offers a lower bound on the interaction rate with the SM. Because of its relevance to the collider searches that will be the focus of this thesis, we postpone a more detailed discussion of WIMP candidates to sec. 2.2.

1.4.2 SuperWIMPs

SuperWIMP candidates are related to the production mechanism called "freeze out and decay", described in sec. 1.3.2. The extremely weak interactions of this candidate could seem to disfavour any possibility of detection; nevertheless the interesting point about this production mechanism is that it reduces the requirements about its producer (that we denoted by X), which in this scenario can be a more generic WIMP with a mass also above the TeV and does not need to be neutral, since it is not the DM candidate.

The classic example of this possibility is a weak scale gravitino as a superWIMP [3]. The gravitino $\widetilde{G}$ is the spin-3/2 partner of the graviton, and supergravity theories predict[7] a mass $m_{\widetilde{G}} = M_{\rm susy}^2/(\sqrt{3}M_{\rm P})$, where $M_{\rm susy}$ is the supersymmetry breaking scale (not to be confused with the mass of supersymmetric particles): this value can range from the Planck scale to the milli-elettronvolt scale. In gravitino superWIMP scenarios, the role of the WIMP is played by the Next to Lightest Supersymmetric Particle (NLSP), which can be a charged slepton, or the sneutrino, or the chargino, or the neutralino (see sec. 2.2.1 for a discussion about supersymmetric models and WIMP candidates). The gravitino then couples SM particles to their superpartners through gravitino-sfermion-fermion interactions and gravitino-gaugino-gauge boson interactions: these could be the interactions that lead to the decay of the WIMP to the superWIMP, if the lifetime of the NLSP is sufficiently long that the decay of the WIMP does not interfere with the freeze out mechanism, but not too long otherwise dark matter would be produced too late.

Other candidates of superWIMP include axinos (the supersymmetric partners of axions, mentioned in sec. 1.4.4), and graviton and axion states in extra-dimensional models.

1.4.3 Sterile neutrinos

As already mentioned, a possible solution to the problem of extending the Standard Model to give mass to the neutrinos is the introduction of the right-handed neutrinos $\nu_{\rm R}$. These fermions would be gauge singlets, and therefore it would possible to write a Majorana mass term for

[7] This formula holds once $\langle V \rangle = 0$ has been imposed, which is perfectly motivated since cosmological observations tell us that the vacuum energy density is $\rho_{\rm vacuum} \approx (0.003\ {\rm eV})^4$.

them, in addition to the Yukawa couplings to the left-handed lepton doublet $L_{\rm L}$ and the Higgs $SU(2)_{\rm L}$ doublet Φ. The corresponding Lagrangian for the so-called νMSM (Neutrino Minimal Standard Model) [14] is[8] (here we restrict for simplicity to one lepton family)

$$\mathcal{L}_{\nu\rm MSM} = \mathcal{L}_{\rm SM} - Y_\nu \overline{L_{\rm L}} \Phi^{\rm c} \nu_{\rm R} - \tfrac{1}{2} M \overline{(\nu_{\rm R})^{\rm c}} \nu_{\rm R} \,.$$

The mass eigenstates for the neutrinos, after electroweak symmetry breaking, are a mixture of $\nu_{\rm L}$ and $\nu_{\rm R}$; let us call the corresponding eigenvalues m_ν and M_ν, and the corresponding eigenstates ν and N. In the limit $M \gg Y_\nu v$, where $v = 246$ GeV is the so-called electroweak scale, linked to the vacuum expectation value (vev) of the neutral component H of the Higgs doublet, $\langle H \rangle = v/\sqrt{2}$, we can write the following relation of inverse proportionality between them (this is the so-called *type-I see-saw* mechanism):

$$M_\nu \approx M \approx \frac{Y_\nu^2 v^2}{2 m_\nu} \,. \tag{1.7}$$

In this limit, the mixing between the two fermions is negligible, therefore the more massive neutrino (that we will denote by N_i if we are including three lepton families) will nearly coincide with $\nu_{\rm R}$, and therefore it is called "*sterile neutrino*", because it has gauge interactions with the SM only through the small mixing with the left-handed neutrino.

If we try to get the orders of magnitude in eq. (1.7), by assuming $m_\nu \sim 0.1$ eV and $Y_\nu \sim 1$ we recover $M \sim 10^{14}$ GeV: this scenario offers a further motivation for the study of Grand Unification Theories (GUT).

Another option is to get a sterile neutrino mass of the order of a few keV, by postulating tiny Yukawa couplings, of the order of 10^{-10}, a value which is some orders of magnitude below the smallest Yukawa coupling in the SM ($Y_e \approx 3 \cdot 10^{-6}$). This option is motivated by the possibility of solving through this minimal modification of the SM three great puzzles such as neutrino masses, dark matter and baryogenesis (see [14], and references therein).

In this scenario, the lightest sterile neutrino, say N_1, is the dark matter candidate. Given its low mass, the main physical decay channel appears only at one loop through the small mixing with $\nu_{\rm L}$ (see fig. 1.7). The overall result is a decay $N \to \nu_{\rm L}\gamma$, with a peculiar experimental signature given by the observation of an X-ray with defined energy $M/2$. This is indeed the experimental search that has the best possibilities to probe this scenario.

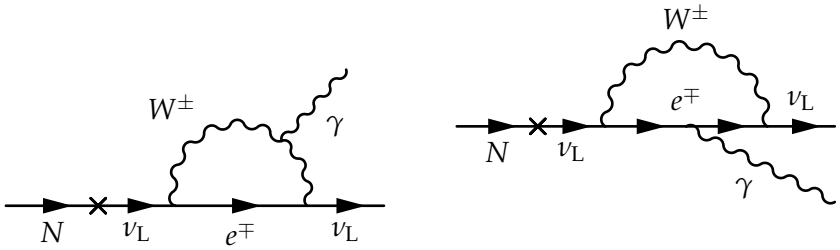

Figure 1.7: Feynman diagrams at one loop for the decay of a sterile neutrino N into a photon and a left-handed neutrino $\nu_{\rm L}$. The cross on the fermionic line denotes the $\nu_{\rm L}$ component of the mass eigenstate N, which is a mixture of $\nu_{\rm L}$ and $\nu_{\rm R}$.

This keV sterile neutrino is a candidate of Warm Dark Matter (WDM). Depending on the velocity distribution of the dark matter particles[9], three classes of candidates are distinguished: Cold Dark Matter (CDM), Warm Dark Matter and Hot Dark Matter (HDM). The latter is strongly

[8] By $\Phi^{\rm c}$ and $(\nu_{\rm R})^{\rm c}$ we denote the conjugate $SU(2)_{\rm L}$ doublet and Lorentz spinors, respectively. For our notation and conventions on Dirac and Majorana spinors, see appendix A.

[9] The velocity distribution depends on the mass but also on the production mechanism and the interaction rates of this particle.

constrained as it poorly enhances the formation of structure, and the current bound is that HDM can constitute no more than 1% of $\Omega_{\rm DM}$. The difference between CDM and WDM is crucial for low scales: indeed, during the history of structure formation, WDM washes out the structures at a scale below 100 kpc because of its higher kinetic energy which causes the escape of DM from gravitational wells. Instead, for CDM this effect is relevant only for scales of 10 kpc or below: therefore, the astrophysical observations of dwarf satellite galaxies, objects within this range of dimensions, can help to distinguish between the two possibilities [15].

There are hints in the direction of WDM from the discrepancy between the low number of satellite galaxies observed in the Universe with respect to the predictions of CDM simulations: this phenomenon, the so-called *missing satellite problem*, is still under discussion, but seems to favour the WDM case. Another problem of the CDM paradigm is the predicted steep profile for the dark matter density near the centre of galaxies, because of the lower velocity profile which binds more particles to the bottom of the potential. It is difficult to check this prediction experimentally, and this is the reason why there is still debate about this so-called *cuspy halo problem*.

1.4.4 Axions

Another possible dark matter candidate is given by a particle proposed to solve the so-called "*strong CP problem*", the axion. Before discussing its cosmological implications, we review the strong physical motivations underlying this proposal [16, 17].

In a generic gauge theory, we could add to the Lagrangian a term proportional to $\mathrm{tr}(F_{\mu\nu}\widetilde{F}^{\mu\nu})$, where $\widetilde{F}^{\mu\nu} = \frac{1}{2}\varepsilon^{\mu\nu\rho\sigma}F_{\rho\sigma}$ and $F^{\mu\nu}$ is the non-Abelian field strength tensor. This term violates parity and time reversal, but not charge conjugation, therefore it violates CP. This insertion could seem useless, because this term is a four-divergence,

$$F^a_{\mu\nu}\widetilde{F}^{a\,\mu\nu} = \partial_\mu K^\mu \equiv \partial_\mu\left[\varepsilon^{\mu\nu\rho\sigma}\left(A^a_\nu F^a_{\rho\sigma} - \frac{g}{3}f_{abc}A^a_\nu A^b_\rho A^c_\sigma\right)\right], \tag{1.8}$$

and we could expect that the surface integral $\int_\Omega \mathrm{d}^4x F^a_{\mu\nu}\widetilde{F}^{a\,\mu\nu} = \int_{\partial\Omega}\mathrm{d}\sigma^\mu K_\mu$ vanishes[10]. This is not the case, however, in a non-Abelian gauge theory, where the physical requirement that $F_{\mu\nu} \underset{r\to\infty}{\to} 0$ does not imply $A_\mu \underset{r\to\infty}{\to} 0$, but that A_μ is a gauge transformed of 0, and indeed solutions can be found with $F_{\mu\nu} \underset{r\to\infty}{\to} 0$ without $A_\mu \underset{r\to\infty}{\to} 0$. This implies that the surface term is not vanishing, and that the term $F\widetilde{F}$ is not superfluous.

On the other hand, this term is linked to the *chiral anomaly*. This anomaly is associated to the chiral (or axial) transformation, which transforms the fermions ψ of the theory into $\psi' = e^{i\beta\gamma_5}\psi$: in the absence of a mass term for ψ, this is a symmetry of a gauge theory at the classical level. In the case of QCD, this symmetry is only approximate, but it is sensible to take the limit m_u, $m_d \to 0$ since the light quark masses are quite smaller than $\Lambda_{\rm QCD}$. At the quantum level, instead, the axial symmetry does not hold[11], because in the path integral formulation

[10] In this section, we are assuming that a Wick rotation has been performed, in order to work with a Euclidean metric.

[11] This anomaly provides a solution to the so-called $U(1)_A$ problem [16], a puzzle of the first years of study of QCD. In the limit of massless up and down quarks, QCD is invariant under a global symmetry $U(2)_V \times U(2)_A$; this symmetry is spontaneously broken by quark condensates $\langle\bar{u}u\rangle$, $\langle\bar{d}d\rangle$ to $U(2)_V \simeq SU(2)_{\rm Isospin} \times U(1)_B/\mathbb{Z}_2$. Therefore we would expect four pseudo Nambu-Goldstone bosons as a consequence of the breaking of the approximate $U(2)_A$, but in the hadron spectrum only the three pions have a reasonably low mass, while the η, η' mesons have respectively $m_\eta = 548$ MeV and $m_{\eta'} = 958$ MeV. This was called the η- or $U(1)_A$-problem by Weinberg in 1975, who proposed that for some reason the symmetry $U(1)_A$ was not present. This turned out to be the correct answer, as it was shown in 1976 by 't Hooft in the discussion of the chiral anomaly, i. e. the absence of the symmetry $U(1)_A$ at the quantum level.

this transformation should be seen as a change of integration variables, which is accompanied by the introduction of the Jacobian of the transformation. The computation of this Jacobian brings to the addition in the Lagrangian of a term proportional to $F^a_{\mu\nu}\widetilde{F}^{a\,\mu\nu}$, which implies that the divergence of the axial current $j^\mu_5 = i\overline{\psi}\gamma^\mu\gamma_5\psi$ (in the massless case) is given by

$$\partial_\mu j^\mu_5 = \frac{g^2 N}{32\pi^2} F^a_{\mu\nu}\widetilde{F}^{a\,\mu\nu}\,, \tag{1.9}$$

where N is the number of light quark flavours.

The crucial point of the strong CP problem is the following: the right-hand side of eq. (1.9) must appear explicitely in the effective action of a non-Abelian gauge theory once we take into account the structure of the vacuum of the theory: the instantonic configurations (to be defined below) imply indeed the presence in the Lagrangian of the term (1.8), multiplied by the θ angle. We are going to explain this fact in the following.

Because of the existence of the *instantons*, localised, topologically non-trivial solutions of the Yang-Mills equations with a self-dual field strength tensor ($F_{\mu\nu} = \widetilde{F}_{\mu\nu}$), the true vacuum of a non-Abelian gauge theory will be the superposition of vacuum configurations $|n\rangle$ characterised by different winding numbers (or Pontryagin indices) n, associated to the A_μ field configuration:

$$n[A] = \frac{g^2}{32\pi^2}\int \mathrm{d}^4x\, F^a_{\mu\nu}\widetilde{F}^{a\,\mu\nu}\,.$$

Under a gauge transformation T_1 characterized by a winding number of 1, the vacuum $|n\rangle$ gets transformed into $T_1|n\rangle = |n+1\rangle$. Gauge invariance implies that T_1 commutes with the Hamiltonian, therefore the true vacuum is an eigenstate of the operator T_1, and is called θ-*vacuum*:

$$|\theta\rangle = \sum_n e^{-in\theta}|n\rangle\,, \qquad T_1|\theta\rangle = e^{i\theta}|\theta\rangle\,.$$

If we now consider the vacuum-to-vacuum transition amplitude, we can see that (we denote with an argument OUT, IN, the state of the system respectively for $t\to+\infty$, $t\to-\infty$, and we denote the field strength by $G_{\mu\nu}$ to specialise to QCD)

$$\langle\theta,\,\mathrm{OUT}|\theta,\,\mathrm{IN}\rangle = \sum_\nu e^{i\nu\theta}\sum_n \langle n+\nu,\,\mathrm{OUT}|n,\,\mathrm{IN}\rangle\,,$$

where we recall that $\nu = \frac{g^2}{32\pi^2}\int \mathrm{d}\sigma^\mu K_\mu = \frac{g^2}{32\pi^2}\int \mathrm{d}^4x\, G^a_{\mu\nu}\widetilde{G}^{a\,\mu\nu}$.

Using the path integral definition of the vacuum-to-vacuum transition amplitude, we get

$$\begin{aligned}
\langle\theta,\,\mathrm{OUT}|\theta,\,\mathrm{IN}\rangle &= \sum_\nu e^{i\nu\theta}\sum_n \langle n+\nu,\,\mathrm{OUT}|n,\,\mathrm{IN}\rangle = \sum_\nu e^{i\nu\theta}\sum_n \langle n+\nu|\int \mathcal{D}G\, e^{i\mathcal{S}_{\mathrm{QCD}}}|n\rangle = \\
&= \sum_\nu e^{i\nu\theta}\int \mathcal{D}G\, e^{i\mathcal{S}_{\mathrm{QCD}}}\,\delta\left(\nu - \frac{g^2}{32\pi^2}\int \mathrm{d}^4x\, G^a_{\mu\nu}\widetilde{G}^{a\,\mu\nu}\right) = \\
&= \sum_\nu \int \mathcal{D}G\, e^{i\left[\mathcal{S}_{\mathrm{QCD}} + \theta\frac{g^2}{32\pi^2}\int \mathrm{d}^4x\, G^a_{\mu\nu}\widetilde{G}^{a\,\mu\nu}\right]}\,\delta\left(\nu - \frac{g^2}{32\pi^2}\int \mathrm{d}^4x\, G^a_{\mu\nu}\widetilde{G}^{a\,\mu\nu}\right),
\end{aligned}$$

where in the passage from the first to the second line we are imposing that the only contribution to the matrix elements are those for which $\mathcal{S}_{\mathrm{QCD}}|n\rangle = |n+\nu\rangle$, i. e. the configurations of G_μ characterised by a winding number ν.

We see that the presence of instantons produces a non-trivial vacuum characterised by a parameter θ which appears in the action as a coefficient of the term (1.8): this makes explicit

the anomalous four-divergence of the axial current, eq. (1.9), and introduces a potentially large source of CP violation in the Lagrangian.

In the Standard Model, containing the electroweak theory and QCD, the θ coefficient of the term (1.8) gets an additional contribution [16] from the presence of the quark mass matrix, which is in general complex: starting from a generic $\mathcal{L}_{\text{mass}} = \overline{q}_{\text{R}\,i}\, M_{ij}\, q_{\text{L}\,j} + \text{h. c.}$, the diagonalisation of the mass matrix involves a chiral transformation with parameter $\frac{1}{2}\arg(\det M)$, which brings to a shift in the θ angle: in other words, the coefficient of the term (1.8) actually reads

$$\overline{\theta} = \theta + \arg(\det M)\,.$$

The introduction of the term $\overline{\theta} G\widetilde{G}$ in the QCD Lagrangian has relevant physical consequences [17]. For example, its contributions to the vacuum energy turns out to be $m_\pi^2 f_\pi^2 \cos(\overline{\theta})$, where f_π is the pion decay constant; the most relevant consequence is anyway its contribution to the neutron electric dipole moment. Indeed, the presence of this term leads to an electric dipole moment of the neutron proportional to $\overline{\theta}$, contradicting the experimental null detection. The experimental bound $|d_n| < 3 \times 10^{-26}\, e{\cdot}\text{cm}$ constrains $\overline{\theta} \lesssim 10^{-9}$. The absence of an explanation in the SM for the tiny value for this parameter is the *strong CP problem*.

This fine tuning problem can be faced either by invoking a spontaneous breaking of CP or an additional dynamics that leads to a nearly vanishing $\overline{\theta}$.

The most straightforward option, originally put forward by Peccei and Quinn, is to make $\overline{\theta}$ somehow a dynamical variable: in this way, the minimisation of its potential energy (which we have mentioned to be $\propto \cos\overline{\theta}$) brings to $\overline{\theta} = 0$. This can be done for example by introducing a real scalar field a (the *axion*) coupled to QCD with

$$\mathcal{L}_{\text{axion}} = (\partial_\mu a)^2 + \frac{a/f_a + \overline{\theta}}{32\pi^2} G\widetilde{G}\,,$$

where f_a is called axion decay constant, and by imposing a symmetry under the shift $a' = a + \alpha$ with constant α[12]. Therefore, the potential energy for this field is periodic and proportional to $\cos(a/f_a + \overline{\theta})$, and would be minimised by a value of a which dynamically cancels the term (1.8) from the QCD Lagrangian, eventually solving the strong CP problem.

We can finally discuss the phenomenological consequence of the existence of the axion. Its mass turns out to be $m_a^2 \approx m_\pi^2 f_\pi^2 / f_a^2$, i. e. $m_a \approx (6\,\mu\text{eV}) \times (10^{12}\,\text{GeV}/f_a)$: hence, for a value of f_a around the TeV we get $m_a \sim$ keV, while for higher values of f_a around the GUT scale we obtain $m_a \sim 10^{-9}$ eV.

The couplings of the axion to matter are all suppressed by f_a^{-1}; therefore, if the axion decay constant is large enough, it is extremely hard to detect its interactions with matter. The strongest limits on m_a come from the lifetime of red giant stars: indeed, the axion emission during their evolution contribute with the neutrino emission to the energy loss of the star, and the observed age of red giants implies an upper bound for m_a around 600 μeV. Another important astrophysical constraint comes from supernovæ: indeed, the observation of the neutrino emission from the supernova SN1987A (19 events over 10 seconds) in the IMB (Irvine-Michigan-Brookhaven) and Kamiokande detectors was in good accord with core-collapse model, and precludes axions in the mass range $10^{-3}\,\text{eV} < m_a < 2\,\text{eV}$ [18].

An experimentally interesting signature of axions is offered by their coupling to photons through a $f_a^{-1} a F\widetilde{F} = f_a^{-1}\, a\, \vec{E}\cdot\vec{B}$: this interactions implies that the passage of an axion in a very strong magnetic field can bring to its conversion in a photon. This is the phenomenon exploited

[12] This shift invariance can be imposed by introducing a scalar field $\sigma \equiv |\sigma| e^{i\frac{a}{f_a}}$ and a $U(1)_{\text{PQ}}$ global chiral symmetry, under which σ and the fermion fields are charged. If the potential of σ has a minimum for $|\sigma| = f_a$, a is the Goldstone boson associated to the spontaneous breaking of $U(1)_{\text{PQ}}$.

by various current experiments (ADMX, CAST), which are expected to reach soon interesting sensitivities in the parameter space.

What are the cosmological implications of axions? First of all, the hypothesis of a standard thermal relic production with $\Omega_a \approx \Omega_{\rm DM}$ requires a mass m_a around 80 eV. On the other hand, this value would imply a decay time for an axion in two photons too short on cosmological scales [3].

Therefore, some other production mechanism for the axion must take place: we can distinguish two possible cases, depending on whether the energy scale $T_{\rm PQ}$ of the breaking of $U(1)_{\rm PQ}$ is over or below the reheating temperature T_R at the end of inflation [18, 3]. In any of these cases, axions behave as cold dark matter, even if their mass is tiny, because they are produced out of the thermal equilibrium with a low energy distribution.

Before the breaking of $U(1)_{\rm PQ}$, the axion mass is negligible.

In the case $T_{\rm PQ} > T_R$, the spontaneous breaking of $U(1)_{\rm PQ}$, which generates different values of $\langle a \rangle$ in various patches of the spacetime, happens before inflation, and our Universe today originated from a region that was very small before inflation, and very likely had an homogeneous value of $\langle a \rangle$. In that case, the relevant contribution of axions came when QCD effects became relevant, at an energy scale around 1 GeV. At this point, the field a rolls from its initial value (some initial phase that we denote by θ_i) towards the true minimum, where it begins to oscillate and contributes to the local energy density as non-relativistic matter; this phenomenon is called *vacuum realignment*. The current axion energy density is then

$$\Omega_a \simeq 0.15 \left(\frac{f_a}{10^{12}\,\text{GeV}} \right)^{\frac{7}{6}} \theta_i^2 \,.$$

If inflation occurs before the Peccei-Quinn phase transition, our observable Universe should consist of a mixture of many patches with different expectation values $\langle a \rangle$. Along their boundaries there could lie topological defects, as domain walls, or axionic strings, with observable effects. The axion production from domain wall decay is expected to be sub-dominant to vacuum realignment, but the relic density radiated by axionic string may be of the same order, or even an order of magnitude larger [3, 19].

We conclude this section with two plots that summarise the limits on the axion's mass, decay constant and coupling constant to photons (figs. 1.8 and 1.9).

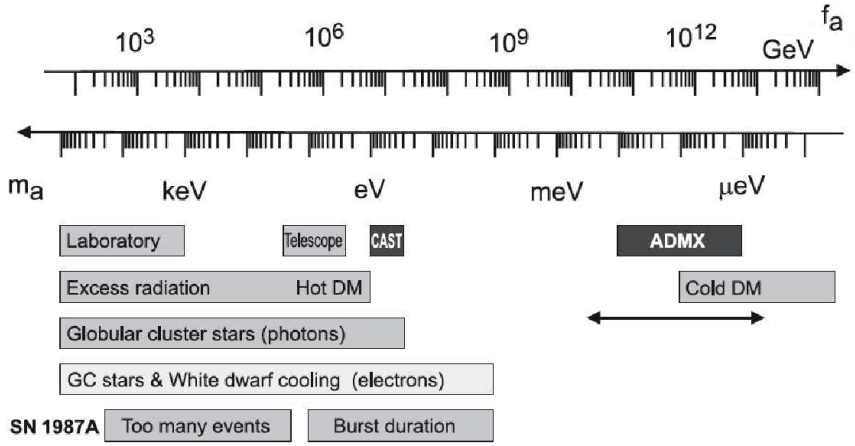

Figure 1.8: Exclusion ranges for m_a (and correspondingly for f_a). The dark intervals are the approximate CAST and ADMX search ranges. The lighter constraints are more model dependent (from [20]).

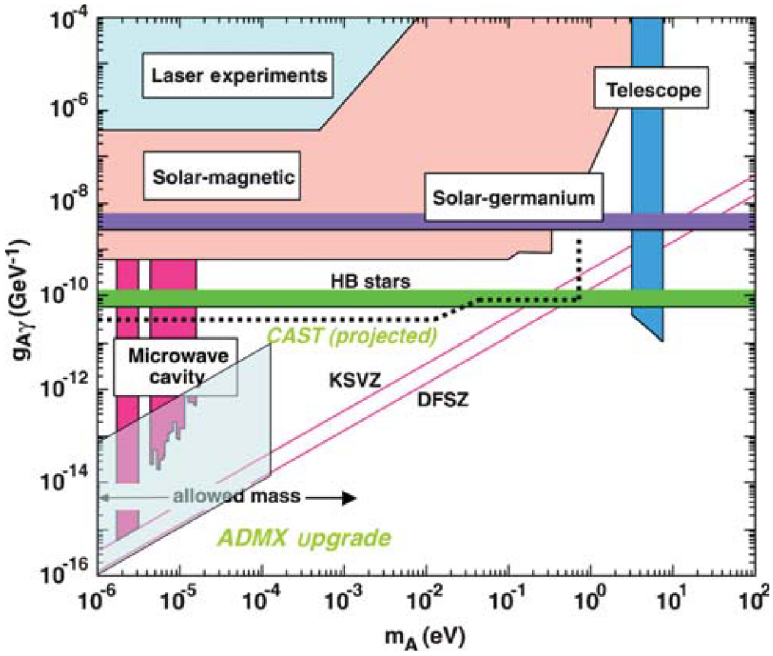

Figure 1.9: Current constraints (shaded) and theoretical predictions for two specific models (KSVZ, DFSZ) in the (m_a, $g_{a\gamma}$) plane (by $g_{a\gamma}$ we denote the coupling constant between axions and photons of the term $aF\widetilde{F}$). "Allowed mass" denotes the window of axion allowed by the upper bound on m_a from astrophysical observations (red giants, for example) and the lower bound due to the energy density predicted by the vacuum realignment mechanism (from [3]).

CHAPTER 2

WIMP candidates

In this chapter, we will describe, following the lines of [1, 2, 3], the possible experimental searches for dark matter, distinguishing three broad categories: direct, indirect and collider searches. Then we will focus on the WIMPs, the DM candidates which offer by far the best chances for detection colliders, and will be the focus of this thesis.

2.1 Searches for dark matter

Keeping in mind the discussion of sec. 1.3 about the possible scenarios for the production of DM in the early Universe, we can argue that apart from the gravitational interaction, to which (according to General Relativity) all the particles in Nature are subject, dark matter must couple also to some of the other components of the Universe with some other (weak) interaction. Indeed, to be produced after inflation, the DM particle must couple to the inflaton or to some of the particles generated during the reheating phase (the period after the inflationary expansion during which the inflaton field decays into the SM particles). Moreover, each of the mechanisms discussed in sec. 1.3 involves an interaction which, although possibly very weak, must have been efficient at least at some time in the history of the Universe. In particular, the freeze out mechanism produces consistent relic densities in the hypothesis of an interaction with the SM with a strength comparable to the one of the SM $SU(2)_{\mathrm{L}}$ interaction: this possibility leaves room for detection in the near future with some of the methods described below.

Because of these reasons, it is reasonable to assume that there is a non-gravitational interaction between DM and the SM. The generic Feynman diagram involving two DM particles (that we will denote by X) and two SM particles on the external lines implies three possible search channels, depending on the temporal direction assumed for the interaction (fig. 2.1).

From this scheme, it is clear that a positive result from any of these searches could be probed by the other ones, depending on the regions of higher sensitivity specific to each experiment. Therefore, it is likely that the best constraints we can get about any DM candidate will come from an interplay of all of the three research channels. A crucial point is to understand in which limits and with which model (i. e. with which effective field theory parametrisation) we can compare these constraints. This will be the main conceptual point of the work of this thesis.

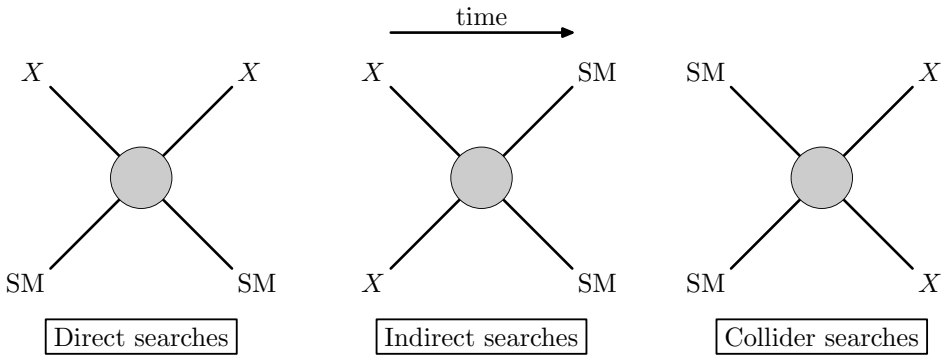

Figure 2.1: Schematic Feynman diagrams involved in the three possible searches for dark matter, which suppose some interaction between the dark matter particle (X) and some of the Standard Model particles (SM).

2.1.1 Direct searches

Direct searches try to detect the motion of Earth through the DM distribution of our galaxy. Indeed, the relative motions of the Earth with respect to the Sun (at a speed of 30 km/s) and of the Sun with respect to the galaxy and therefore with respect to the DM distribution (at a speed around 220 km/s) imply a relatively large flux of DM particles through the Earth. This flux, also called "*DM wind*", can be quantified as $\Phi_{\mathrm{DM}} \sim 10^{11}\ \mathrm{m}^{-2}\mathrm{s}^{-1}/(m_\chi/\mathrm{GeV})$.

Hence a possible experimental search consists in monitoring a large detector made of a specific material with high density, in order to maximise the cross section of a DM particle with one of the nuclei of the detector (see fig. 2.1). The expected signal is extremely low, and can be observed only if the background of cosmic rays and other sources is minimised: this is accomplished by putting the detectors underground, usually in mines or inside a mountain under a thick layer of rock. This choice reduces the background from cosmic rays with respect to the surface of the Earth at the order of one over a thousand. Eventually, an important point that can allow to distinguish the expected signal from the background is the periodicity: indeed, the flux of DM through the Earth should show an annual modulation, as we will discuss below.

In order to quantify the expected number of events, many inputs from different research fields must be specified:

- *Astrophysical* input: we should have a precise estimate of the flux of DM particles, which depends both on the local density distribution and on the velocity distribution of DM. The only way to get a detailed prediction is to compare some ansatz for these functions, which depend on some unspecified parameters, with the result of numerical simulations and with phenomenological inputs from astrophysics and cosmology. For example all the density profiles for DM that have been proposed display the common behaviour $\rho \propto r^{-2}$, i. e. a density proportional to inverse of the square of the radial distance from the center of the galaxy, for r of the order of the galactic visible disk dimension.

- *Experimental and Particle Physics* input: a careful choice of the material of the detector must be done. Indeed, depending on the nuclear mass and spin of the nucleus, the event rate is increased respectively for spin-independent and spin-dependent cross sections with DM, i. e. cross sections that do not depend (or do) on the spin of the nucleons. Furthermore, in order to maximise the cross section of the interaction, it is better to choose a material with high density. Finally, also the cost of the experiment must be taken into account. Just to mention some relevant examples for the spin-independent searches, the chosen material in some current experiments are xenon (e. g. XENON100, LUX, ZEPLIN), germanium

(CDMS, EDELWEISS, CoGeNT), calcium tungstate (CRESST), sodium iodide (DAMA).

We now discuss the estimate of the event rate in direct experiments from a more quantitative point of view [1, 21, 22].

First of all, we can neglect the scattering of DM with the electrons bound to the nucleus: indeed, since the incoming DM particle is not relativistic, in the interaction the nucleus is seen as a bound state (there is not sufficient energy to resolve its costituents), whose geometric cross section is by far larger than the one with an electron.

The rate R of nuclear recoils due to DM scatterings (event rate) is usually calculated as a differential rate with respect to the recoil energy $E_R \equiv m_X(v_{\rm out}^2 - v_{\rm in}^2)/2$, where m_X is the DM mass, and $v_{\rm in}$ and $v_{\rm out}$ are the incoming and outcoming speed of the DM particle in the detector frame (in this section, all quantities will be understood in the detector frame, unless we specify otherwise). This is the amount of kinetic energy left by the incoming DM particle in the detector after the interaction. The scattering between DM and nucleus, given the non-relativistic speed of DM (of order 10^{-3}), is in the elastic regime.

The rate of expected events per unit of time and volume follows from the definition of differential cross section:

$$\frac{{\rm d}^2 R}{{\rm d}v\,{\rm d}E_{\rm R}} = \frac{{\rm d}^2\sigma_{XN}}{{\rm d}v\,{\rm d}E_{\rm R}}\Big(v, E_{\rm R}\Big)\, n_0\, n_{\rm det}\, v\,, \tag{2.1}$$

where v is the DM speed, n_0 and $n_{\rm det}$ are respectively the local density of DM and the number density of nuclei in the detector, and ${\rm d}^2\sigma_{XN}/{\rm d}v\,{\rm d}E_{\rm R}$ is the differential cross section for the elastic interaction between the DM particle X and the nucleus N.

We now integrate over the DM velocity, by introducing a suitable velocity distribution: this is the main astrophysical input, together with n_0, and must be deduced from the comparison of observations and numerical simulations. The usual ansatz for the velocity distribution is the Maxwell distribution[1] with two modifications. First, we must consider that an upper limit for v is given by the so-called *escape velocity* $v_{\rm esc}$, above which a DM particle is not gravitationally bound to the Milky Way. A standard value is $v_{\rm esc} \approx 650$ km/s, but recent analyses suggest $v_{\rm esc} \approx 544$ km/s (see references in [21]). Secondly, the WIMP speed distribution in the detector frame is obtained through a time-dependent Galilean transformation $\vec{v} \to \vec{v} + \vec{v}_E(t)$, where $\vec{v}_E(t)$ is the velocity of the Earth in the galaxy rest frame, equal to the sum of the Sun's peculiar motion $\vec{v}_\odot$, with $|\vec{v}_\odot| \approx 220$ km/s, and the revolution velocity $\vec{v}_E^{\rm orb}$ of the Earth around the Sun. This vectorial sum can be approximate to $|\vec{v}_E(t)| = |\vec{v}_\odot| + V_\oplus \cos(2\pi t)$, where t is measured in years (starting from the 1$^{\rm st}$ June), and $V_\oplus \approx 30$ km/s.

Therefore, the distribution function with respect to the vector velocity $\vec{v}$ of DM is given by (we understand a normalisation factor)

$$\widetilde{f}(\vec{v}) \propto \exp\left(-\frac{|\vec{v} + \vec{v}_E(t)|^2}{2\sigma^2}\right)\Theta(|\vec{v}| - v_{\rm esc})\,,$$

where $\Theta(x)$ is the Heaviside function, and σ is a parameter usually taken in the range 220 km/s $< \sigma <$ 270 km/s. This distribution can be integrated with respect to the angular variables, leading to a speed distribution depending only on $v = |\vec{v}|$, that we will denote by $f(v)$. In first approximation, the main component of the relative speed of DM particles is the rotation velocity of the Solar System around the center of the Milky Way, which is of the order of 220 km/s; the peculiar motion of the Sun and the rotation velocity are corrections to this value, which in turn are by far larger than the peculiar speed of DM particles, which are assumed follow a Maxwell distribution that today is peaked at velocities around 50 m/s (according

[1] This is an isotropic distribution, but this assumption does not hold for all the models proposed for the DM velocity distribution.

to the CDM paradigm) [23], since the ratio T/m scales as a^-2 for a non-relativistic and non-interacting species.

Returning to eq. (2.1), we can write the differential rate per unit of time and mass (of the target inside the detector) dividing by the density of the detector material $\rho_{\rm det}$, then we integrate over v to get

$$\frac{\mathrm{d}R}{\mathrm{d}E_{\rm R}} = \frac{\rho_0}{m_X}\frac{n_{\rm det}}{\rho_{\rm det}}\int_{v_{\rm min}}^{v_{\rm max}} v f(v)\,\frac{\mathrm{d}^2\sigma_{XN}}{\mathrm{d}v\,\mathrm{d}E_{\rm R}}\Big(v, E_{\rm R}\Big)\,\mathrm{d}v\,, \tag{2.2}$$

where ρ_0 is the local DM density, usually taken equal to $0.3\,\mathrm{GeV/cm^3}$, $n_{\rm det}/\rho_{\rm det}$ gives the inverse of the mass m_N of a nucleus of the detector, $v_{\rm max}$ is determined by $v_{\rm esc}$ and $\vec{v}_E(t)$, and $v_{\rm min}$ is the minimum DM speed which can cause a recoil of energy $E_{\rm R}$, which turns out to be $v_{\rm min} = \sqrt{(m_N E_{\rm R})/2\mu_N^2}$, where $\mu_N = m_X m_N/(m_X + m_N)$ is the reduced mass of X and the nucleus. This formula follows from this alternative expression for $E_{\rm R}$, which can be derived from kinematical considerations:

$$E_{\rm R} = \left(\frac{1}{2}m_X v_{\rm in}^2\right)\frac{4\mu_N}{m_X + m_N}\left(\frac{1-\cos\theta^*}{2}\right),$$

where θ^* is the recoil angle in the center-of-mass frame. We notice that $E_{\rm R}$ is maximum for a value of m_X equal to m_N: if we recall that the detector is sensitive to the recoil energy $E_{\rm R}$, we can understand why the limits on the cross sections coming from direct detection experiments are stronger in the range $m_X \approx 10 \div 100$ GeV, near to the mass of the nuclei of the target material of the experiment. Moreover, from eq. (2.2), we can understand the qualitative behaviour of the sensitivity of direct detection for high values of m_X: indeed, the cross section in first approximation will be proportional to the a parameter with mass dimension (the cut-off scale Λ, that will be introduced in eq. (2.3)) raised to the power (-4), thus for dimensional reasons it will be also proportional to the reduced mass μ_N, that for m_X much greater than m_N tends to the smaller of the two, i. e. m_N. Thus the cross section tends to a constant for $m_X > m_N$, but the number density of dark matter, which is the first multiplicative factor in eq. 2.2, can be written as ρ_0/m_X, where ρ_0 is basically fixed by the observed energy density of dark matter. Therefore, this factor $1/m_X$ mildly reduces the sensitivity of direct detection for masses $m_X > m_N$.

At this point, in eq. (2.2) the only quantity to be discussed is the cross section σ_{XN} for the elastic scattering between X and the nucleus. This cross section can be derived from the microscopic theory through three steps.

First, we can compute the differential cross section for the scattering between a parton (a quark or a gluon) and X from the microscopic theory: this can be done in a specific model by using a complete theory (also called ultraviolet or UV theory), or by using an effective field theory (EFT) approach. In an effective Lagrangian, one considers all the possible effective non-renormalisable operators $\mathcal{O}_i^{(d)}$ of mass dimension d between two quarks (or gluons) and two X fields, each of them with an unknown coefficient $c_i^{(d)}$,

$$\mathcal{L}_{\rm EFT} = \sum_{d\geq 5}\sum_i \frac{c_i^{(d)}}{\Lambda^{d-4}}\,\mathcal{O}_i^{(d)}\,, \tag{2.3}$$

where Λ is the *cutoff scale*, which allows to quantify the goodness of the truncation up to a certain dimension $\bar{d}$. Indeed, depending on the energy scale E of the interaction and the value of Λ, one can approximate eq. (2.3) by truncating the first sum up to a dimension $\bar{d}$ such that $(E/\Lambda)^{\bar{d}} \ll 1$. One think about the Lagrangian (2.3) from the Wilsonian point of view, in which all the degrees of freedom of a renormalisable theory with energy higher than Λ have been integrated out, and therefore in the resulting Lagrangian the operators of dimension $d \geq 5$

listed in eq. (2.3) appear. From this perspective, we can be more precise about the condition $(E/\Lambda)^{\overline{d}} \ll 1$: in fact, we can relate the cut-off scale Λ to the masses and the couplings of heavy fields which have been integrated out in the Wilsonian Lagrangian. A more detailed discussion of the EFTs describing the interactions between DM and SM particles will be given at the beginning of the next chapter.

Returning to our discussion about the event rate for direct searches, we must now convert the microscopic cross section for the parton-DM interaction to a cross section between a nucleon (a neutron or a proton) and X. This is done by using the hadronic matrix elements, i. e. the matrix elements for the operators containing quark or gluon fields, which introduce the *form factors*, functions depending on the momentum exchanged in the interaction that must be measured experimentally and represent the main source of uncertainty in the overall estimate of the event rate. To mention some possibilities, if some of the effective operators $\mathcal{O}_i^{(d)}$ contain the term $\bar{q}\gamma_\mu\gamma_5 q$ or $\bar{q}\gamma_\mu q$, where q is some quark field and γ_μ, γ_5 are the 4×4 Dirac matrices, then we should compute respectively $\mathbf{M}_\mathrm{a} = \langle n|\bar{q}\gamma_\mu\gamma_5 q|n\rangle$, where n is a neutron or a proton, and $\mathbf{M}_\mathrm{v} = \langle n|\bar{q}\gamma_\mu q|n\rangle$. We have cited this couple of examples (respectively, a vector-axial coupling and a vector coupling) because the final result can depend (as for $\mathbf{M}_\mathrm{a}$) or not (as for $\mathbf{M}_\mathrm{v}$) on the spin of the nucleon. This point is very important from the experimental point of view, because in order to probe spin-dependent interactions it is necessary to use a target with nuclei with a non-vanishing total spin (in other words, the spin-dependent interaction is a coherent interaction with all the nucleons, therefore the interference effects can strongly decrease the cross section). This is why only some experiments are sufficiently sensitive to spin-dependent interactions, and the exclusion limits for that case are weaker.

Eventually, the quantity σ_{XN} can be obtained from the cross section between X and a nucleon through nuclear physics considerations. Thanks to the use of nuclear wavefunctions, we can get an approximation of the cross section with a nucleus by introducing parameters which are measured experimentally by nuclear physicists (for further details, see [21] and references therein).

In fig. 2.2 we report the current limits (fig. 2.2a) on the spin-independent cross section of nucleon and dark matter from various experiments, together with the claims of detection from some other competitor ones (fig. 2.2b). In fig. 2.3 we report the corresponding limits for spin-dependent direct searches.

Fig. 2.2b shows the strong tension between the positive results of some experiments and the exclusion limits of other ones. There is still a high pitched debate about the interpretation of these results. Among the reasons why the various experimental collaborations do not find an agreement in their conclusions, there are the difficulty of understanding all the possible backgrounds that contaminate the signal (only a few experiments have a preferred signal region with nearly zero expected events), and the problems in comparing the results of different experiments, which are due to the different materials and DM-SM interactions which are peculiar to each of them. Moreover, as we explained before, there are various theoretical uncertainties with respect to astrophysical and particle physics inputs, which are sometimes faced differently by the experiments. Eventually, it must be said that the current aptitude among both experimentalists and theorists is usually rather skeptical, mainly because of the smaller number of positive results with respect to the negative ones, that put exclusion limits in the signal regions singled out by positive claims. Anyway it is fair to say that there is still room for proposals about the nature of DM and its interactions which are compatible with both classes of results. A couple of possibilities that have been explored is that the events observed in positive detections are due to an *inelastic* scattering X SM $\to$ X' SM, where X' is another new particle slightly heavier than X, or to channeling, a condensed matter effect that lowers the threshold for cristalline detectors (see references in [3]). If these indications were correct,

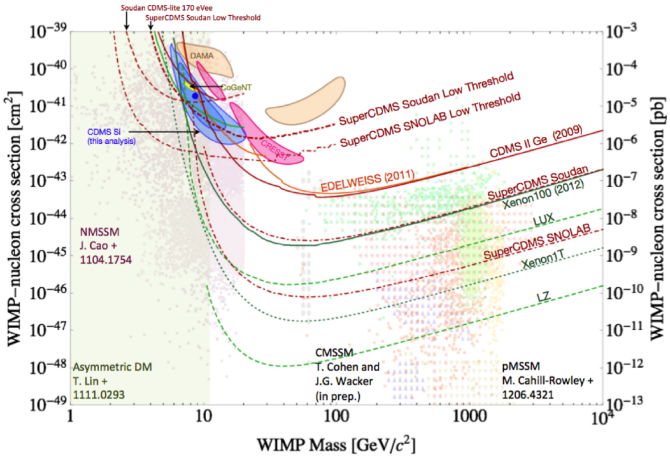

(a) Recent upper bounds at 90% confidence level (CL) from direct searches on the cross section between a WIMP and a nucleon, as a function of the mass. The solid lines represent the upper bounds coming from CDMS II (red), EDELWEISS II (orange), XENON 100 (green). The dashed lines refer to projected sensitivities for some future upgrades of the experiments, and the point distributions refer to possible theoretical predictions from supersymmetric models. The filled regions in the upper left corner represent claims of detections, which are discussed in fig. 2.2b (from [24]).

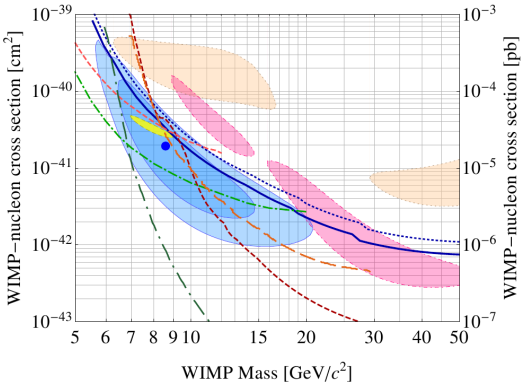

(b) Claims of positive detections from various experiments, compared with the exclusion limits coming from competitor ones. The blue and red lines refer to CDMS II limits, the orange one reports EDELWEISS limit and the green ones the XENON limit. The filled region identify possible signal regions (at 90% CL or higher) from CoGeNT (yellow), DAMA/LIBRA (light orange), CRESST (pink). The overall signal region from these claims is represented by the blue dot and contours (68% and 90% CL, for dark and light blue respectively) (from [25]).

Figure 2.2: Limits from direct searches on spin-independent cross sections for the scattering of DM (which in the labels on the axes is identified with the WIMP, since this is the DM candidate relevant for these searches).

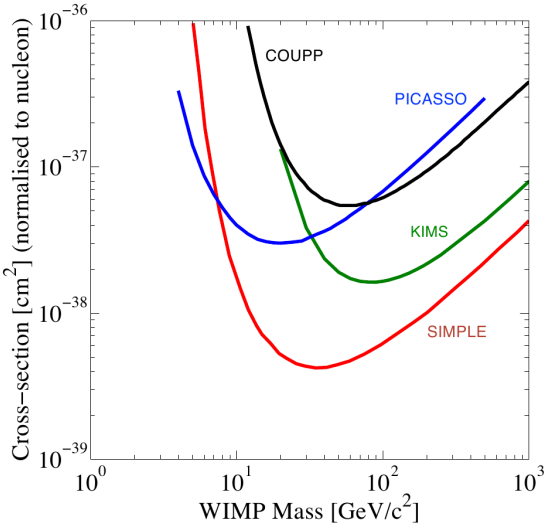

Figure 2.3: Limits from direct searches on spin-dependent cross sections for the scattering of DM (which in the labels on the horizontal axis is identified with the WIMP, since this is the most relevant DM candidate for these searches) (from [1]).

the favoured parameters would be $m_X \approx 1 \div 10$ GeV and a spin-independent cross section $\sigma_{\mathrm{SI}} \approx 10^{-41} \div 10^{-39}$ cm^2.

2.1.2 Indirect searches

Indirect techniques are based on the search of radiation produced in dark matter annihilations, as sketched in the second diagram of fig. 2.1 [2, 3]. Indeed, the reactions which produced dark matter in the early Universe are now inefficient (the thermally averaged cross section times the DM density is much lower than the Hubble rate) and their impact on the DM relic density is negligible, but dark matter annihilation continues and may be observable.

The flux of the radiation produced by these annihilations is proportional to the annihilation rate Γ_{ann}, which in turn depends on the square of the DM density, $\Gamma_{\text{ann}} \propto \rho^2_{\text{DM}}$. Therefore the most promising directions to look at, in order to maximise the probability of detecting the products of these interactions, are the regions where dark matter accumulates, which are also called in this context *amplifiers*. Dense regions of the galactic halo, as the galactic center, are therefore the target of many astrophysical searches, but also the Sun or the Earth could act as amplifiers for dark matter annihilations, since DM could lose energy through the scattering with nucleons inside these objects.

In the following, we will discuss the main types of indirect searches, and eventually we will briefly discuss two current experimental anomalies which might be related to DM.

As already mentioned, one of the most interesting regions for the indirect detection of DM is the galactic center, where, according to the results of numerical simulations, the dark matter density profile is expected to grow as a power law $\rho(r) \propto r^{-\alpha}$ with α greater than 2, which is the exponent for the outer region of the galaxy. A consequence of this steep density profile is that the annihilation rate can strongly increase with α. The products of these annihilations that could be detected experimentally are photons, with energies ranging from the keV (X-rays) to the GeV (γ rays), neutrinos, electrons and positrons, and protons and antiprotons. The latter, being electrically charged, are deviated by the electric or magnetic fields present along the line of sight (the line departing along the direction of observation of the experiment), and therefore their spatial distribution is random and does not keep track of the original source. This fact complicates the probe of dark matter annihilation into electrically charged final products, because the correlation of these particles with their source is crucial in order to prove that they are indeed the products of DM annihilations.

Another possibility is to look for the annihilations coming from the Earth or the Sun: because of the high density of these bodies, DM in the solar system should cumulate towards their centre because of their gravitational attraction and the loss of energy in elastic scatterings with nuclei. Among the products of annihilation of DM, neutrinos are the only particles that could escape from the center of the Earth or the Sun and be detected by experiments. Hence, a possible search consists in looking for unexpected fluxes of neutrinos coming from the center of the Earth or the Sun. The best possibilities for this detection come from high energy neutrinos: indeed, in the case of a Cherenkov detector, neutrinos of higher energy are more likely to produce (through a weak charged interaction) a muon, which leaves a track (identified by the Cherenkov cone) much straighter than the one of an electron, since its energy loss is lower. Therefore, muon tracks remain more aligned with the direction of the original neutrino, allowing to map the positions of the sources of most energetic neutrinos. A final remark about this type of searches is that the cross section for production of neutrinos from DM annihilations is strongly model dependent: for example, for a neutralino candidate (see sec. 2.2.1) there is a non negligible branching ratio for the production of neutrinos only if its mass is higher than the W or Z boson mass, while for Kaluza-Klein DM (sec. 2.2.2) the expected flux of very energetic neutrinos is higher [2].

We now discuss two anomalies observed in the e^+, e^- cosmic rays and in X-rays, and their possible interpretation as signals of DM annihilations.

The first one is confirmed by many satellite-based experiments dedicated to the observa-

tion of cosmic rays, among which the latest one (AMS) gives the most precise measurement (see fig. 2.4): in an energy range above some GeV, the number of observed positrons is higher than expected. The positron fraction is expected to be decreasing above this threshold, while experimentally, up to some hundreds of GeV, is increasing. The origin of this behaviour is still under debate, and could very well be of astrophysical origin: our modelling of the background of cosmic rays could miss some astrophysical phenomenon which increases the number of observed positrons in that energy range. Despite this possibility, one may explore the hypothesis that this excess of positrons comes from DM annihilations. The problem with this proposal is that the required cross section should be two or three orders of magnitude greater than the one expected from the freeze out mechanism in order to get the observed relic density. Then the cross section for this process should be enhanced today with respect to the freeze out time: a possible way out could be given by the so-called *Sommerfeld enhancement*, an increase in the non relativistic limit in the cross section for a process with a massless mediator[2] of a factor

$$S = \frac{\pi \alpha_X / v}{1 - e^{-\pi \alpha_X / v}},$$

where v is the relative speed of the colliding DM particles, and α_X is the fine structure constant for the interaction that allows the annihilation [3]. Since v was typically around $1/3$ at the freeze out, while today is of order 10^{-3}, in principle this mechanism could seem to accommodate the prediction. This unfortunately is not true anyway, because the relic density of DM constrains α_X (and then S) from above. There are some other proposed dark matter explanations, but these seem more elaborate than the astrophysical ones [3].

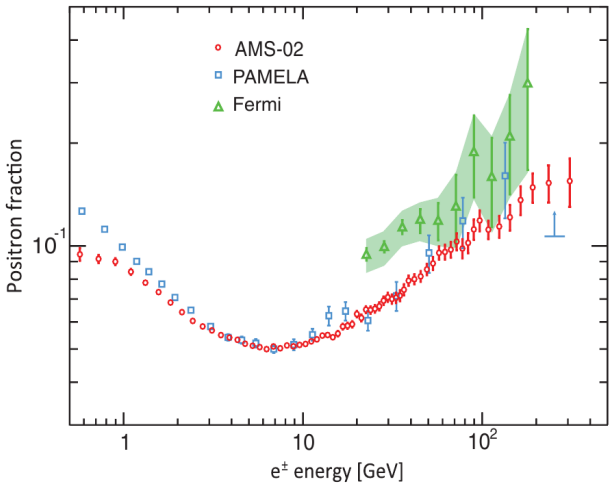

Figure 2.4: Measurement of the positron fraction, defined as $N_{e^+}/(N_{e^-} + N_{e^+})$ where N_i is the number of observed particles of type i, from the experiments of AMS-02, PAMELA and Fermi-LAT, which are three satellite-based experiment dedicated to the detection of cosmic rays (from [26]).

Another anomaly, recently claimed in [27] and (with a larger data sample) in [28], consists in the observation of an unidentified spectral line in the X-ray spectrum from various galaxies. These analyses consider the spectrum of many galaxy clusters, each of them shifted of an energy equal to the opposite of the redshift of that object, in order to be able to directly compare and sum the various spectra. This operation has also the effect of disentangling the final result from the systematic errors (such as background lines or instrumental response artefacts) which

[2] In the case of a massive light mediator with mass M_*, S has approximately the same tendence until $S \approx \alpha_X m_X / m_M$, which acts as a cutoff.

have a defined energy: indeed, since these effects occur in the detector frame, the "average" of spectra of galaxies at different redshifts[3] smears out these errors and amplifies intrinsic (though weak) spectral lines. The result of the two analyses that we have cited is the observation of an unidentified very weak line at the energy of 3.57 ± 0.03 keV, which is argued not to correspond to any atomic transition in the galactic plasma. Both collaborations support the hypothesis that this line is the result of the decay of a sterile neutrino N (sec. 1.4.3) into a left-handed neutrino ν_{L} and a photon (fig. 1.7). Neglecting the tiny mass of ν_{L}, the decay products share each an energy equal to half of the neutrino mass m_N (in the rest frame of N), and indeed the photon should be monoenergetic[4]. This observation would imply $m_N \approx 7.1$ keV. Furthermore, the two papers give an estimate of the dark matter density along the line of sight, which, together with the observed flux of X-rays at that energy, allows to infer the lifetime of this DM candidate. Specialising this formula to the case of a decaying sterile neutrino, the decay width constrains the mixing angle θ between left-handed and right-handed neutrinos, and it turns out to have $\sin^2(2\theta) \approx 7 \times 10^{-11}$. Even if the analysis exposed in [27] seems rather accurate, and finds a spatial distribution for these X-rays which is peaked towards the centre of the galaxies (as expected in the case of decaying dark matter), these claims need further confirmations from upcoming analyses, and also alternative explanations must be considered.

2.1.3 Collider searches

The last diagram of fig. 2.1 suggests another option to investigate the origin of dark matter, in the hypothesis that some (weak) non-gravitational interaction with the SM occurs: the possible production of dark matter at colliders.

Because of the extremely weak interaction with ordinary matter, DM is expected not to leave any track in the detectors and to escape from them undetected: therefore, its experimental signature is a rather large amount of missing energy[5] ($\not{E}_{\mathrm{T}}$). However, some additional trigger requirement must be chosen, therefore the usual analysis for DM searches involves the search of a single jet (from quark or gluon initial state radiation) plus $\not{E}_{\mathrm{T}}$ [29, 30, 31, 32] or a single photon (from electromagnetic initial state radiation) plus $\not{E}_{\mathrm{T}}$ [33, 34]. The main SM background for this type of searches comes from the events where a Z boson is produced[6] and decays in two neutrinos (which escape from the detectors too) with an initial state radiation (ISR) of a jet or a photon. This background could be reduced in principle in an e^+-e^- collider, where the total energy of the collision can be tuned far from the resonant production of the Z and the colliding particles could be polarised (in order to suppress the cross sections for the weak interactions); this cannot be done unfortunately in a hadronic collider as the LHC, where the initial energy and polarisation of the colliding partons cannot be constrained [3].

A usual requirement about the DM candidate is that it respects a discrete $\mathbb{Z}_2$ parity, and therefore it should be produced only in pairs. This is a completely reasonable assumption, indeed the stability of DM on cosmological scales, and the hypothesis that it has some kind of non-gravitational interaction with the observable sector, makes it very unlikely that in any typical model there are not decay channels (at higher order in loops) for DM, unless some discrete symmetry which gives a different quantum number to the observable and the dark

[3] In [27], for example, the 73 galaxies considered in the sample range in redshift from $z = 0.01$ to $z = 0.35$.

[4] We point out that the observation of a monoenergetic photon, if this is the product of a decay, implies a two-body decay of some particle X' into two photons or a photon plus an invisible particle. The latter case includes $\nu_{\mathrm{L}}\gamma$ or $X''\gamma$, where X'' is a stable particle of the dark sector: but then the decaying particle X' was not the lightest one in the dark sector, and its relic density should be too low to account for the observed flux of these photons.

[5] This quantity is defined as $\not{E}_{\mathrm{T}} \equiv |\vec{\not{p}}_{\mathrm{T}}|$, where $\vec{\not{p}}_{\mathrm{T}}$ is the opposite of the sum, over all the reconstructed particles, of their momenta projected onto the plane orthogonal to the beam direction.

[6] Another relevant background is given by $W \to \ell\nu$ events in which the lepton is misidentified as a jet, or it is not isolated, or it is emitted out of the geometric acceptance region [29].

sector is preserved. In that case, the lightest particle with a given quantum number for that symmetry is absolutely stable. This is what naturally happens for example in supersymmetry and extra-dimension models (sec. 2.2.1, 2.2.2). Hence the relevant Feynman diagrams for the search of DM at colliders are those of fig. 2.5.

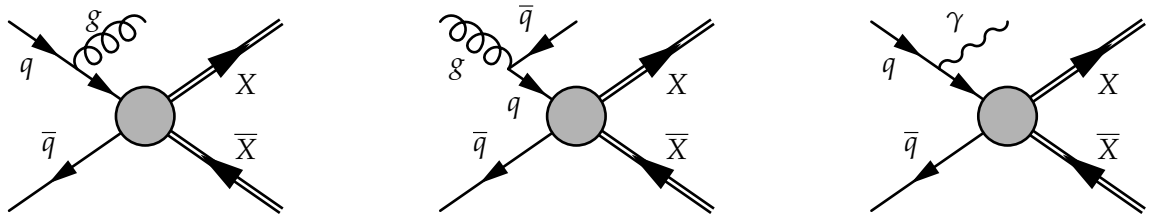

Figure 2.5: Feynman diagrams for the production of DM at LHC with an additional jet or photon in the final state (we understand the symmetric diagrams in which the final jet or photon is radiated from the other incoming parton). The DM final states are drawn with a double straight line, in order not to assume implicitly a given spin for the DM candidate (in the case of a real scalar field or a Majorana fermion X, in the final state there are two X particles instead of $X\overline{X}$). The cross section for the second diagram is further suppressed if X is heavy, because of the low value of the gluonic parton distribution function for high energy fractions.

We must make an additional remark about this type of search. The observation of missing particles at colliders simply reveals that some particles weakly interacting with the SM were produced, but it is far from a compelling evidence that this can be the DM candidate. In case of a positive detection by the experimental collaborations, further studies (or even further collider experiments) are needed to understand the mass and the lifetime of that particle, and possibly the branching ratios for its decays. Then, on the basis of these data, one should compute the thermal relic density and check that the result is consistent with cosmological observations. Therefore only further analyses and complementary studies of a discovered "invisible" particle with different experimental approaches can convince that this is indeed the DM candidate: this consideration is very relevant for collider searches [3].

We now turn to a more detailed discussion of the experimental results. We focus on the monojet search [29, 30, 31, 32], which at hadron colliders gives stronger limits with respect to the monophoton search.

In table 2.1 we present the selection cuts imposed on the data sample by the two experiments CMS and ATLAS. Apart from some minor differences, the common goal of their selection is to select events with a large amount of $\not{E}_{\mathrm{T}}$ and an energetic jet, by suppressing QCD dijet events and rejecting events with isolated leptons coming from the hard scattering.

The estimates of the two main backgrounds that we have already mentioned, the $Z(\to \nu\nu) + j$ and $W(\to \ell\nu) + j$ events, are done by using the data sample, while other minor backgrounds are estimated through Montecarlo (MC) simulation. Both analyses find a number of events in the data passing the selection cuts compatible with the SM expectations, and are therefore able to put the exclusion limits reported in table 2.2 (for CMS) and figure 2.6 (for ATLAS).

These exclusion limits can be interpreted also in terms of an effective field theory description, as we have outlined in sec. 2.1.1. We can choose a subset (or all) of the effective operators of mass dimension $\leq \overline{d}$, and assume that the corresponding EFT description can be used to predict the number of events generated at the collider, by computing the corresponding cross section. This assumption is very delicate when we are dealing with the energy regimes of colliders [35, 36, 37], because the energy Q exchanged during the parton interaction is very high and could even reach the energy scale of the mass M_* of the mediator of the interaction between DM and SM: the nearer is Q to M_*, the poorer is the prediction of the EFT about the

	CMS [31]	ATLAS [32]
Cut on $\not{E}_T$	$\not{E}_T > 250, 300, 350, 400$ 450, 500, 550 GeV	$\not{E}_T > E_i$, where E_i, depending on the signal region, is equal to 120, 220, 350 or 500 GeV
Jets requirement	$p_T(j_1) > 110$ GeV $\lvert\eta(j_1)\rvert < 2.4$ $\Delta\phi\left(\vec{p}_T(j_1), \vec{p}_T(j_2)\right) < 2.5$ No more than 2 jets with $\lvert\vec{p}_T\rvert > 30$ GeV and $\lvert\eta\rvert < 4.5$	$p_T(j_1) > E_i$ $\lvert\eta(j_1)\rvert < 2.0$ $\Delta\phi\left(\not{\vec{p}}_T, \vec{p}_T(j_1)\right) > 0.5$ No more than 2 jets with $\lvert\vec{p}_T\rvert > 30$ GeV and $\lvert\eta\rvert < 4.5$
Lepton veto	No isolated μ, e with $\lvert\vec{p}_T\rvert > 10$ GeV	No e with $\lvert\vec{p}_T\rvert > 20$ GeV, $\lvert\eta\rvert < 2.47$ No μ with $\lvert\vec{p}_T\rvert > 7$ GeV, $\lvert\eta\rvert < 2.5$

Table 2.1: Main selection cuts imposed by CMS (luminosity of 19.5 fb^{-1} of 2012 data at a collision energy of $\sqrt{s} = 8$ TeV) and ATLAS (luminosity of 10 fb^{-1} of 2012 data at a collision energy of $\sqrt{s} = 8$ TeV) in the monojet search. We denote the jets of the event as j_i and we order them by decreasing $|\vec{p}_T|$. If we use polar coordinates and denote by θ the angle between a particle track and the beam axis, and by ϕ the angle in the transverse plane with respect to the plane of the collider, we can define the pseudorapidity as $\eta \equiv -\ln\tan(\theta/2)$.

$\not{E}_T$ (GeV) $\rightarrow$	≥ 250	≥ 300	≥ 350	≥ 400	≥ 450	≥ 500	≥ 550
Total SM	49154 ± 1663	18506 ± 690	7875 ± 341	3663 ± 196	1931 ± 131	949 ± 83	501 ± 59
Data	50419	19108	8056	3677	1772	894	508
Expected	3580	1500	773	424	229	165	125
Observed	4695	2035	882	434	157	135	131

Table 2.2: Exclusion limits reported by CMS (luminosity of 19.5 fb^{-1} of 2012 data at a collision energy of $\sqrt{s} = 8$ TeV) in the monojet search, given as upper limits (at 95% CL) on the number of non-SM events that could pass the selection cuts, normalised to the luminosity of the data sample [31].

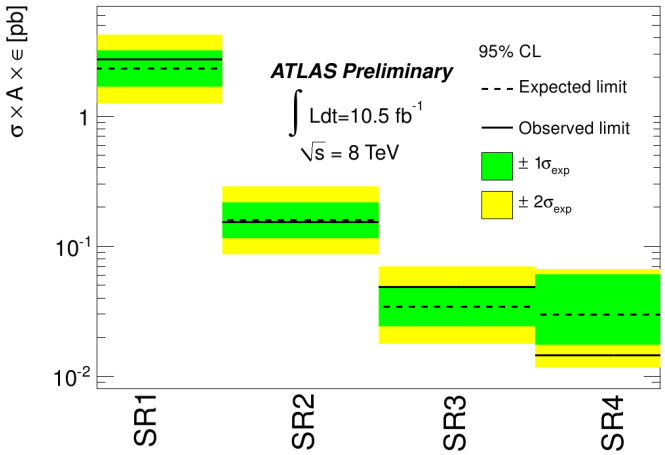

Figure 2.6: Exclusion limits reported by ATLAS (luminosity of 10 fb^{-1} of 2012 data at a collision energy of $\sqrt{s} = 8$ TeV) in the monojet search, given as upper limits on the *visible* cross section, which is equal to the absolute cross section multiplied by the event acceptance and the identification efficiency [32].

process. In particular, when the collision energy is sufficient for a resonant production of the mediator, the cross section in the complete theory receives an enhancement that the EFT cannot

predict, thus the limit predicted by the effective theory underestimates the true limit.

This is the approach used in [32] to deduce exclusion limits on the cutoff scale Λ of the EFT description, on the basis of the exclusion limits from the collider experiments. In fig. 2.7 we report the result obtained in [32] for the lower limit of Λ as a function of the DM mass m_X. The procedure to obtain these limits is the following: one computes the cross section of an EFT including only a chosen operator, for the production of $X\overline{X} + j$, which will be a function of the two parameters m_X, Λ. Then, for each value of m_X, one can convert the experimental upper limit on the cross section for that process (obtained from the ATLAS experiment) into a lower limit on the cut-off scale Λ. In fig. 2.7 we report the results for the three possible effective operators for the interaction between two partons and two DM particles, which are listed in table 2.3. All these operators assume that the DM particle X is a Dirac fermion.

Name	Initial state	Lorentz structure	Operator	Mass dimension
D5	q, $\overline{q}$	vector-vector	$\frac{1}{\Lambda^2}\overline{X}\gamma^\mu X\,\overline{q}\gamma_\mu q$	6
D8	q, $\overline{q}$	pseudovector-pseudovector	$\frac{1}{\Lambda^2}\overline{X}\gamma^\mu\gamma_5 X\,\overline{q}\gamma_\mu\gamma_5 q$	6
D11	g, g	scalar	$\frac{\alpha_S}{4\Lambda^3}\overline{X}X\,(G^a_{\mu\nu})^2$	7

Table 2.3: List of possible EFT operators for the interaction between two SM particles (indicated in the column "Initial state") and two DM particles, in the hypothesis that the latter is a fermion. These are the operators used in [32] to get lower limits on Λ.We notice that the definition of D11 includes the strong coupling constant α_S because this operator typically arises at one loop in the UV theory.

We can see that the lower limits on the cut-off scale are very different, depending on the operator under exam. In particular, we see that the limits for the operators D5 and D8 are very similar, while the limit for D9 is stronger and the one for D11 is much weaker.

2.2 WIMP candidates for dark matter

In this section we review a class of DM candidates that was postponed in the discussion of sec. 1.4, the WIMPs, which are the best candidates within our current experimental reach, in particular at colliders. We discuss three categories of WIMPs: the first is the Lightest Supersymmetric Particle (LSP), which is surely one of the most motivated from the point of view of particle physics, then we discuss the Lightest Kaluza-Klein Particle (LKP) that arises in theories with extra dimensions, and finally we sketch some possibilities along another possible scenario, in which one tries to get a viable DM candidate by adding the least number of ingredients to the SM.

2.2.1 Candidates from supersymmetry

The first studies of supersymmetry (SUSY in the following) date back to the beginning of the '70s in two dimensional string theories; then Wess and Zumino discussed the first SUSY model by focusing on the properties implied by a transformation that links scalar and fermionic fields, and some years later the SUSY algebra turned out to be the only extension of the Poincaré algebra consistent with a non trivial S-matrix (Haag-Lopuszanski-Sohnius theorem) (for a pedagogical review see [38] and references therein).

It is quite impressive that some of the most critical problems of the SM, as the hierarchy problem, or dark matter, or the inclusion of quantum gravity, found only later in SUSY, respec-

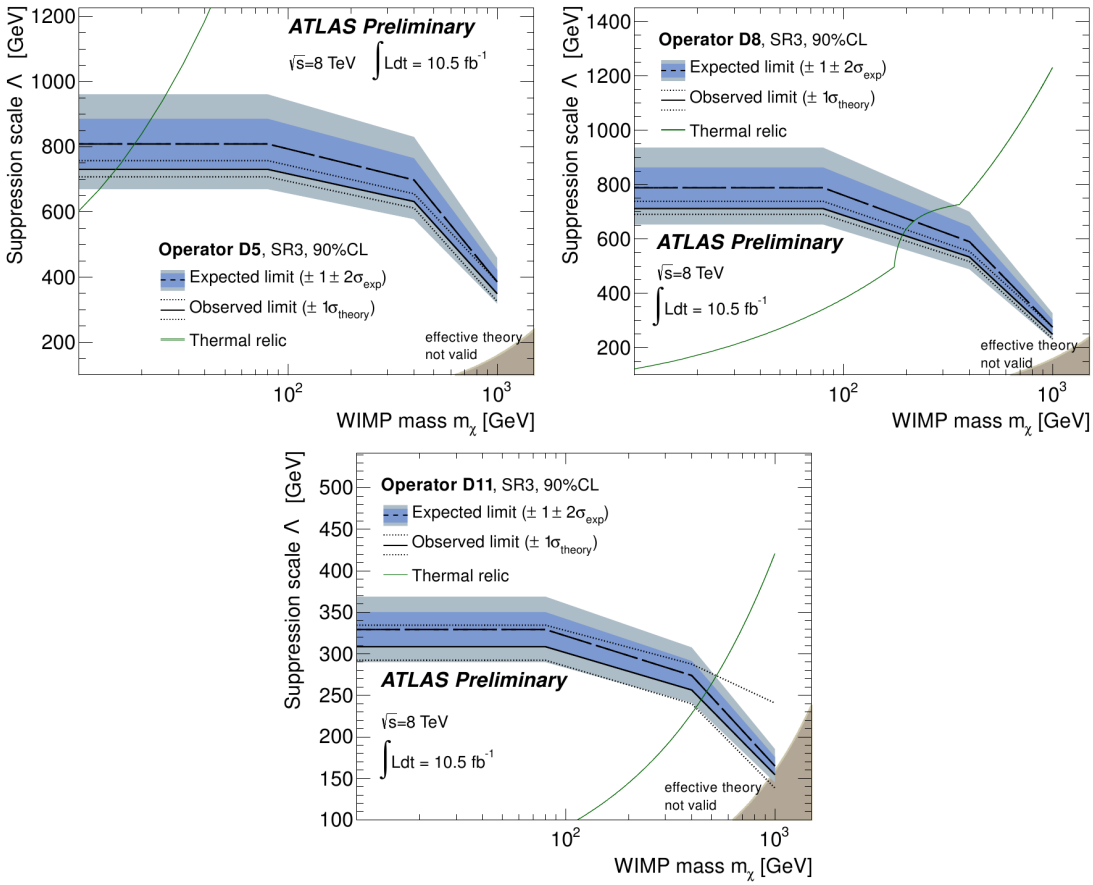

Figure 2.7: ATLAS lower limits at 90% CL on the cutoff scale Λ as a function of the mass m_χ, each of them obtained by assuming that the DM-SM interaction proceeds only with the operator indicated in the legend. The uncertainties around the expected limit (blue $\pm 1\sigma$ and $\pm 2\sigma$ band) include the variation expected from statistical fluctuations and experimental systematic uncertainties on SM and signal processes. The thin dotted lines around the observed limit show the impact of theoretical uncertainties. The green line shows the value of Λ which would give the correct cross section in order to yield the observed relic abundance, in the hypotheses that the production mechanism is the freeze out and that the corresponding operator is the only contribution to the DM-SM interaction. The light grey areas in the lower right corner indicate the region where $\Lambda > m_X/(2\pi)$, where the EFT approach must break down because the kinematics imposes a momentum transfer greater than M_* (in the hypothesis that the couplings of the mediator to DM and SM remain in the perturbative regime g_q, $g_X < 4\pi$).

tively, a coherent explanation (or at least a mitigation of the problem), a WIMP candidate, and the hint of a possible path to the solution (supergravity and superstring theories).

In this thesis, we will not provide a detailed introduction to SUSY and to the simplest supersymmetric extension of the SM, the so-called Minimal Supersymmetric Standard Model (MSSM), we refer to [38] for this. We mention only the basic facts that are needed to introduce the DM candidates from SUSY.

We begin by summarising in table 2.4 the supersymmetric multiplets contained in the MSSM, in order to fix the notation and to introduce the fields contained in this model. The supersymmetry transformations relate each of these fields to the other fields contained in that supermultiplet.

A part of the MSSM Lagrangian describes the kinetic terms and the usual gauge interactions for each of the scalar and spinor fields, with the addition of the "supersymmetrised versions" of the interactions [38], i. e., for each interaction vertex, there is also an interaction where two

Names		spin 0	spin $\frac{1}{2}$	spin 1	$(SU(3)_C, SU(2)_L, U(1)_Y)$
squarks, quarks	Q	$(\widetilde{u}_L\ \widetilde{d}_L)^T$	$(u_L\ d_L)^T$		$(\mathbf{3}, \mathbf{2}, \frac{1}{6})$
	U^c	$\widetilde{u}_R^*$	$(u_R)^c$		$(\overline{\mathbf{3}}, \mathbf{1}, -\frac{2}{3})$
($\times$3 families)	D^c	$\widetilde{d}_R^*$	$(d_R)^c$		$(\overline{\mathbf{3}}, \mathbf{1}, \frac{1}{3})$
sleptons, leptons	L	$(\widetilde{\nu}_L\ \widetilde{e}_L)^T$	$(\nu_L\ e_L)^T$		$(\mathbf{1}, \mathbf{2}, -\frac{1}{2})$
($\times$3 families)	E^c	$\widetilde{e}_R^*$	$(e_R)^c$		$(\mathbf{1}, \mathbf{1}, 1)$
Higgs, higgsinos	H_u	$(H_u^+\ H_u^0)^T$	$(\widetilde{H}_u^+\ \widetilde{H}_u^0)^T$		$(\mathbf{1}, \mathbf{2}, \frac{1}{2})$
	H_d	$(H_d^0\ H_d^-)^T$	$(\widetilde{H}_d^0\ \widetilde{H}_d^-)^T$		$(\mathbf{1}, \mathbf{2}, -\frac{1}{2})$
gluino, gluon ($a = 1, \ldots, 8$)			$\widetilde{G}^a$	G^a	$(\mathbf{8}, \mathbf{1}, 0)$
winos, W bosons			$\widetilde{W}^\pm\ \widetilde{W}^0$	$W^\pm\ W^0$	$(\mathbf{1}, \mathbf{3}, 0)$
bino, B boson			$\widetilde{B}$	B	$(\mathbf{1}, \mathbf{1}, 0)$

Table 2.4: Field content of the MSSM.

among the interacting fields are replaced by their supersymmetric partners, and the others are left unchanged. One of such vertices that will be cited in the following (to discuss the mass of the DM candidate) is the interaction between the neutral Higgs field H_i^0 (where i denotes u or d), the neutral Higgsino $\widetilde{H}_i^0$ and one gaugino between $\widetilde{W}^0$ and $\widetilde{B}$.

In addition to this part of the Lagrangian, there is also a contribution from the so-called *superpotential* W. This is defined as a function of the superfields (that we generically denote Φ^i), and its contribution to the resulting Lagrangian in terms of the component fields (among which we denote by ϕ^i and ψ^i the corresponding scalar and fermion field, respectively) is given by

$$\left.\frac{\partial^2 W}{\partial\Phi^i\partial\Phi^j}\right|_{\Phi^i\to\phi^i}\overline{\psi}^i P_L\psi^j + \left|\left.\frac{\partial^2 W}{\partial\Phi^i}\right|_{\Phi^i\to\phi^i}\right|^2,$$

where the subscript $\Phi^i \to \phi^i$ means that, after the derivative calculation, the superfields must be replaced by their scalar components. For the MSSM, the superpotential is

$$W_{\rm MSSM} = U^c\mathbf{Y}_u Q H_u - D^c\mathbf{Y}_d Q H_d - E^c\mathbf{Y}_e L H_d + \mu H_u H_d\,, \tag{2.4}$$

where $\mathbf{Y}_i$ ($i = u$, d or e) are the 3×3 Yukawa matrices in the flavour space, and μ is a real constant with the dimension of a mass.

Since L and H_d have exactly the same quantum numbers under the SM gauge group (see table 2.4), we could also add to the superpotential the terms where the H_d multiplet is replaced by L, and also a term of the form $U^cD^cD^c$. The problem with these terms is that they would violate the baryonic (B) and/or leptonic (L) number, which are extremely constrained by the experiments. These quantum numbers are defined for the various multiplets as follows: $B = +1/3$ for Q, $B = -1/3$ for U^c and D^c, and $B = 0$ for the others; $L = +1$ for L, $L = -1$ for E^c and 0 for the others.

The way to forbid these term in the superpotential (and therefore to avoid strong unmotivated fine tuning) is to impose that a discrete $\mathbb{Z}_2$ symmetry is preserved, the so-called matter parity. This quantum number is defined on the superfields as $(-1)^{3B-L}$, and imposing that each term of $W_{\rm MSSM}$ must have a matter parity number equal to +1 forbids the unwanted terms to appear. This symmetry (which commutes which the supersymmetry transformations) can be equivalently rephrased in term of the R-parity, which is defined on the component fields

as $(-1)^{3B-L+2s}$, where s is the spin of each field in a supermultiplet[7]. We can now justify the choice of the notation for the fields in table 2.4: in fact, we have denoted with a tilde all the fields with R-parity equal to -1, which are the superpartners of the SM particles (including in this case an extended Higgs sector).

R-parity has important physical consequences, and the most relevant is directly linked to what we have discussed in sec. 2.1.3: the lightest particle with R-parity equal to -1 cannot decay into lighter particles because otherwise it would violate R-parity, therefore it is absolutely stable. This is exactly the type of discrete symmetry that could make the DM candidate stable on cosmological scales. Therefore, the MSSM predicts a DM candidate if the lightest supersymmetric particle (LSP) is electrically neutral.

The remaining part of the MSSM Lagrangian is denoted by $\mathcal{L}_{\text{soft}}$ and includes the soft supersymmetry breaking terms: $\mathcal{L}_{\text{soft}}$ arises when supersymmetry is spontaneously broken and some heavy sector describing spontaneous supersymmetry breaking is integrated out. Indeed, exact supersymmetry implies that all the fields belonging to the same supermultiplet have the same mass: since this is evidently far from what happens in Nature, supersymmetry, if present at a higher scale, must be spontaneously broken at the electroweak scale. For the MSSM, $\mathcal{L}_{\text{soft}}$ is

$$\begin{aligned}\mathcal{L}_{\text{soft}} = &-\frac{1}{2}\Big(M_3\widetilde{G}^a\widetilde{G}^a + M_2\widetilde{W}^i\widetilde{W}^i + M_1\widetilde{B}\widetilde{B} + \text{c.c.}\Big)\\ &-\Big(\widetilde{u}^*_{\text{R}}\mathbf{A}_u\widetilde{Q}H_u - \widetilde{d}^*_{\text{R}}\mathbf{A}_d\widetilde{Q}H_d - \widetilde{e}^*_{\text{R}}\mathbf{A}_e\widetilde{L}H_d + \text{c.c.}\Big)\\ &-\widetilde{Q}^*\mathbf{m}^2_{\text{Q}}\widetilde{Q} - \widetilde{L}^*\mathbf{m}^2_{\widetilde{L}}\widetilde{L} - \widetilde{u}^*_{\text{R}}\mathbf{m}^2_{u}\widetilde{u}_{\text{R}} - \widetilde{d}^*_{\text{R}}\mathbf{m}^2_{d}\widetilde{d}_{\text{R}} - \widetilde{e}^*_{\text{R}}\mathbf{m}^2_{e}\widetilde{e}_{\text{R}}\\ &-m^2_{H_u}H^*_uH_u - m^2_{H_d}H^*_dH_d - (bH_uH_d + \text{c.c.})\,,\end{aligned} \tag{2.5}$$

where the indices a and i run respectively on $1,\dots,8$ and $1,2,3$, and $\mathbf{A}_u$, $\mathbf{A}_d$, $\mathbf{A}_e$, $\mathbf{m}^2_{\text{Q}}$, $\mathbf{m}^2_{\widetilde{L}}$, $\mathbf{m}^2_{u}$, $\mathbf{m}^2_{d}$, $\mathbf{m}^2_{e}$ are complex 3×3 matrices in the flavour space. The parameters M_1, M_2, M_3 and b can be complex, but are taken to be real in many phenomenological analyses, for simplicity and to avoid strong constraints from CP-violation.

We can now discuss the possible LSP candidates in supersymmetric theories.

- *Neutralino*: this is the name given to each of the mass eigenstates which arise as a mixing of the four neutral fermion fields $\widetilde{B}$, $\widetilde{W}^0$, $\widetilde{H}^0_d$ and $\widetilde{H}^0_u$. These fields have the same quantum numbers, therefore the mass eigenstates (that we will denote by $\widetilde{\chi}^0_i$, $i=1,\dots,4$) will be a mixing among them; a similar diagonalisation must occur in the $(\widetilde{H}^\pm_u,\,\widetilde{W}^\pm)$ space, and the corresponding Dirac eigenstates are called *charginos*. After the electroweak symmetry breaking (EWSB), the expectation values of the neutral Higgs bosons are $\langle H^0_u\rangle = v_u$, $\langle H^0_d\rangle = v_d$. Then the mass matrix in the MSSM in the $(\widetilde{B},\,\widetilde{W}^0,\,\widetilde{H}^0_d,\,\widetilde{H}^0_u)$ space is

$$\mathbf{M}_{\widetilde{\chi}^0} = \begin{pmatrix} M_1 & 0 & -g'v_d/\sqrt{2} & g'v_u/\sqrt{2}\\ 0 & M_2 & gv_d/\sqrt{2} & -gv_u/\sqrt{2}\\ -g'v_d/\sqrt{2} & gv_d/\sqrt{2} & 0 & -\mu\\ g'v_u/\sqrt{2} & -gv_u/\sqrt{2} & -\mu & 0\end{pmatrix}, \tag{2.6}$$

  where the terms M_1, M_2 appear in $\mathcal{L}_{\text{soft}}$, μ comes from the so-called μ-term of the superpotential (eq. (2.4)), and the other mass terms come from the higgsino-gaugino-Higgs boson gauge interaction vertex after EWSB. The eigenvalues of this matrix are the masses of the neutralinos. The lightest among them can be the LSP, depending on the overall

[7] R-parity is equivalent to matter parity, because for each interaction vertex of the MSSM the product of $(-1)^{2s}$ for the correponding fields is equal to $+1$.

mass spectrum of the model which is determined by the values of the coefficients of $\mathcal{L}_{\text{soft}}$ and the expectation values v_u, v_d.

- *Sneutrino*: this scalar superpartner of the neutrino is potentially a viable DM candidate because it is a colour singlet and is electrically neutral. Today, however, the searches performed at colliders (in particular at LEP) and in direct searches have nearly ruled out this candidate in the MSSM. Indeed, since the sneutrino interacts via the Z boson, it would have been already detected in direct searches if it was the DM particle, and sneutrino masses below $m_Z/2$ are ruled out by the agreement of the invisible width of the Z boson measured at LEP with the value predicted by the SM. Extended models with right-handed or sterile neutrinos may reopen the possibility of sneutrino dark matter by lowering the interaction cross section.

- *R-hadrons*: this is the name given to condensates of squarks and gluinos which are singlets of the strong interaction $SU(3)_C$. They can be seen as "supersymmetrised" versions of the hadrons of the SM: they could be DM candidates, since they are electrically neutral. They are a candidate of Strongly Interacting Massive Particle (also called SIMP). Today they basically ruled out by the strong constraint from the Earth heat flow: when the dark matter capture rate in Earth is efficient, the rate of energy deposition by dark matter self-annihilation products would grossly exceed the measured heat flow of Earth. The limits from this constraint exclude a nucleon-DM cross section higher than around $10^{-34} \div 10^{-33}$ cm^2, severely restricting the chances that this could be the DM candidate [39, 40].

- *Gravitino*: this is the spin-3/2 superpartner of the graviton in supergravity theories. Its mass is related to the the supersymmetry breaking scale F (of the dimension of a mass squared) by $m_{\widetilde{G}} = F/(\sqrt{3}M_{\text{P}})$, where $M_{\text{P}} = 1/\sqrt{8\pi G}$ is the reduced Planck mass. There is no theoretical reason to expect the gravitino to be heavier or lighter than the lightest SM superpartner, thus the gravitino has the same chances of the neutralino to be the LSP. As discussed in section 1.4.2, the gravitino is likely to be a SuperWIMP candidate, i. e. a very weakly interacting candidate that decoupled from the thermal bath in the early universe through the mechanism of the freeze out and decay (sec. 1.3.2).

2.2.2 Lightest Kaluza-Klein particle

Another important class of DM candidates is given by the so-called Lightest Kaluza-Klein particles, which arise in models with extra dimensions with respect to the usual four spacetime dimensions ([41] and references therein).

The ancestor of these models is the well known proposal put forward by T. Kaluza in 1919 (his article was published in 1921), and improved by O. Klein in 1926. With the intention to unify gravity and electromagnetism, Kaluza proposed a theory with a five dimensional spacetime, in which the metric $G_{AB}(X)$, with $A, B = 0, 1, 2, 3, 5$, $X = (x^\mu, y)$, does not depend on the fifth extra spatial coordinate y. In his model, the four vector $G_{\mu 5}$ is associated with the electromagnetic potential, and the Einstein's equations $R_{AB} - \frac{1}{2}G_{AB}R = \kappa^2 T_{AB}$ bring to the 10 usual equations for general relativity for $A, B = 0, \ldots, 3$, while for $A = 0, \ldots, 3, B = 5$ they yield Maxwell equations after a suitable identification of the charge. Moreover, Klein pointed out that the periodicity of the fifth direction had to do with quantization, since the momentum in the fifth direction had to be an integer multiple of $\frac{1}{\ell}$, where $2\pi\ell$ m is the period in the y direction. Even if this theory turned out to be inconsistent, many of its features are common to many successive higher dimensional theories.

Extradimensional models returned to be amply studied at the end of the 90's with more emphasis on phenomenology. An important paper by Arkani-Hamed, Dimopoulos and Dvali

in 1998 in the contezt of supergravity and superstring theories suggested that spacetime can have more than 4 dimensions and all the SM particles are confined to a four-dimensional subvariety, referred to as a "3-brane". The only fundamental force whose interactions spread in the extra dimensions is gravity, and they postulate that in the higher dimensional spacetime general relativity holds, and deduce the consequences for our world on the 3-brane. They observe that the limit on the size of the extra dimensions would then be fixed by the experimental tests on Newton's law of gravitation, which are now probing the μm scale. In their proposal, the weakness of gravitational forces is due to the leak of gravity into the extra dimensions, and the hierarchy problem is translated into the problem of the discrepancy between the large size of the extra dimensions and the value of the Planck length.

Among the various subsequent proposals, the Randall-Sundrum (RS) set-up is one of the most promising. They propose that the SM particles are confined on a 3-dimensional brane living in a 5-dimensional anti de Sitter space time, where only gravity can propagate. In their model, the weak scale is generated from the Planck scale through an exponential hierarchy, arising from the background metric: in this way, only a modest fine-tuning is required with respect to what is needed in ADD model.

These proposals encouraged many phenomenological investigations of models of extra dimensions, also called Kaluza-Klein (KK) models. Their common feature is the presence of "towers" of discrete levels of excited states with respect to the ordinary SM particles, due to the quantisation of the momentum of the fields (gravitons, or in some cases also the SM particles) along the extra dimensions. The first level of excited states can be produced at energies of the order of $1/R$, where R is the radius of compactification of the extra dimension, which ranges from the order of the meV^{-1} ($\approx$ mm) in ADD models, to the TeV^{-1} ($\approx 10^{-18}$ m) when ordinary particles can propagate in extra dimension, or even to $M_{\rm P}^{-1}$.

The excited KK states are in general not stable, since they can decay to states of lower energy. The discrete $\mathbb{Z}_2$ symmetry that insures the stability of the Lighest KK Particle (LKP) is the so-called Kaluza-Klein parity, a discrete symmetry related to the conservation of momentum along the extra dimension, which remains unbroken in a some specific class of models named Universal Extra Dimensions (UED). This symmetry allows for the LKP, if it is electrically neutral with interactions of a strength comparable to that of the electroweak force, and if the extra dimension has a size of the order of the TeV^{-1} , to be the DM candidate.

Among the relevant possibilities for the LKP that arise in various extra dimensional models, we cite the following:

- *KK graviton*: in the original ADD proposal, it is the only field that can propagate in the extra dimension. This is a SuperWIMP candidate, and would be produced in the early Universe analogously to the gravitino in supergravity theories. In some scenario, without some fine tuning it tends to have parameters that overclose the universe (i. e. that brings to an energy density higher than the critical one corresponding to a flat universe);

- *KK gauge boson*: the lightest neutral mass eigenstate among the excited states of the electroweak bosons (the equivalent of the photon, that in KK modes is mainly composed by the excited state B^1 of the B boson), could the a WIMP candidate for DM. In some scenarios, also the Z^1 or H^1 (the excited states of the Z and H bosons) can be the LKP;

- *KK neutrino*: also the excited state of the left-handed neutrino could be the dark matter candidate;

- *KK radion*: it is the scalar degree of freedom related to the size of the extra dimension. It has typically the same mass and coupling of the KK graviton, and it is also affected by an overclosure problem in some models;

- *KK branon*: these excited states corresponds to brane fluctuations, in models where the SM particles are confined on a brane. They can be thought as the Goldstone bosons arising from spontaneous symmetry breaking of translational invariance in the presence of the branes.

We do not discuss thoroughly the various classes of extra dimensional models, which display also remarkable differences between them; we have mentioned some relevant examples just to show the variety of DM candidates provided by this class of theories.

2.2.3 Minimal dark matter

The two classes of model that we have discussed in the previous two sections have a strong motivation in the solution of the gauge hierarchy problem. The "little hierarchy problem" that arose after LEP (and is confirmed by the present results of the LHC), i. e. the agreement of the predictions of the SM with the results of the collider searches, which points to a mild fine tuning in the Higgs boson mass if the scale of new physics is around or above the TeV scale.

An alternative approach, motivated also by the little hierarchy problem, is to give up solving the hierarchy problem, and to consider the DM problem as the starting one for model building. Within this approach, we review the main features of the so-called *minimal dark matter* (MDM) proposal [42].

This approach, proposed by Cirelli and Strumia, consists in adding to the SM the minimal set of ingredients for DM: only one electroweak multiplet $\mathcal{X}$ (which can be a complex scalar or a Dirac fermion field), singlet under $SU(3)_C$ in light of the exclusion limits from the Earth's heat flow mentioned when discussing R-hadron candidates. Moreover, to minimise the assumptions, no discrete symmetry is introduced to make the DM stable: only the electroweak multiplets that do not allow for interactions that would lead to a rapid decay of DM are considered. Therefore, in the absence of interactions with the SM particles apart from the gauge interactions, the only parameter of MDM is the mass M of the electrically neutral component of $\mathcal{X}$.

If we denote by (n, Y) the quantum numbers under $SU(2)_L \times U(1)_Y$, n must be lower or equal to 5 (for fermionic $\mathcal{X}$) or 8 (for scalar $\mathcal{X}$) in order not to accelerate too much the running of the coupling constant of $SU(2)_L$, bringing to non-perturbative values at the Planck scale, and by requiring a value of Y such that there is an electrically neutral component of $\mathcal{X}$. Now, direct detection constraints for a DM particle interacting with the exchange of a Z boson require Y to be 0. Furthermore, by excluding the choices of n that allow for operators that can bring to the decay of $\mathcal{X}^0$, only two possibilities are left: a fermionic 5-plet and a scalar 7-plet. The scalar option would leave room for a non-minimal quartic interaction with the H boson (the so-called Higgs portal), thus Cirelli and Strumia consider only the 5-plet option. It is clear that such high-dimensional $SU(2)_L$ representation cannot bring to an interaction with the SM fermions that is renormalisable and singlet under the SM gauge group: thus the stability of DM comes out as an accidental property of the model, and is not gained through additional discrete symmetries.

Once the multiplet is fixed, the only parameter M is constrained by the requirement of the correct relic abundance through the freeze out mechanism. The calculation of the relic density for the DM candidate requires taking into account the Sommerfeld enhancement, discussed in sec. 2.1.2, since the weak interaction bosons turn out to be much lighter (of two order of magnitude) than $\mathcal{X}^0$. This effect increases the cross section, and implies a value for M of 9.6 TeV. This WIMP candidate has a higher mass than the typical ones (below the TeV) because of the Sommerfeld enhancement and the coannihilations with its charged partners, which have very similar masses: in particular, the mass of the $\mathcal{X}^{\pm}$ is only 166 MeV higher than M.

At colliders, the searches for this candidate are nearly hopeless: indeed, a clear signature could come from the production $\mathcal{X}^{\pm}$ rather than from $\mathcal{X}^0$, but the energy needed to produce $\mathcal{X}^+\mathcal{X}^-$ is much higher than the one reachable by the LHC. Apart from that, the $\mathcal{X}^{\pm}$ particles would decay into $\mathcal{X}^0\pi^{\pm}$ within an average distance $\tau = 1.8$ cm because of the small mass splitting, that also implies a rather low energy for the pion: a similar track represent a difficult signal for triggers.

Direct searches have better chances to detect the MDM candidate, because its interaction cross section with nucleons is around 10^{-44} cm^2, which is within the reach of future experiments. On the other hand, indirect searches are even more likely to detect a signal of $\mathcal{X}^0$ annihilations, which would produce W^+W^- pairs that in turn decay to all particles: e^+, $\overline{p}$, γ, ν. Furthermore, the cross section would still be increased by the Sommerfeld enhancement, thanks to the large difference between M and the mass of the gauge bosons. For a more complete discussion about the possibilities of detection through the various indirect searches, see [42].

CHAPTER 3

Discussion of two simplified models for DM

3.1 From effective theories to simplified models

As we have seen in the previous two chapters, there is plenty of DM candidates in many extensions of the SM. Even by restricting to the candidates that have the best options to be seen at colliders or in direct searches, the WIMP candidates, described in sec. 2.2, within each of the scenarios we have introduced there are different specific models, each with its own peculiarities. To derive and discuss the constraints from experiments, it is clear that it is not practical to take each of the possible models and derive the exclusion limits on its specific parameters. It would be a burdensome task, and rather meaningless because by changing slightly the characteristics of the model we could change the exclusion limits. Furthermore, in some of the experimental set-ups the energy of the interaction could be below the threshold needed to appreciate the details of a complete theory: in other words, an experiment cannot excite the degrees of freedom of energy higher than its energy scale. Thus, in such a situation, there is no need to specify the whole theory, and the effective theory can sometimes take into account all the physical phenomena relevant to the experiment.

This type of considerations motivated the study of the exclusion limits coming from various searches in terms of the effective operators describing the interaction of DM with SM particles: some of the first papers that introduced an EFT analysis for the collider limits are [40, 43]. This approach became even more motivated after direct and collider searches began to rule out appreciable regions of the parameter space, motivating a more agnostic approach in the search of DM. A valuable advantage of the use of effective theories for the parametrisation of DM interactions is that, once one fixes a maximum mass dimension for the operators of the EFT, their number is limited, and one can parametrise virtually *any* complete model through a finite number of coefficients. The fragile side of this approach is that the approximate equality between the predictions of the complete theory and those of its effective description breaks down around the cut-off energy scale, which depends in general on the details of the microscopic completion of the theory. Recently, this has been the subject of many studies, which pointed out that at the energy regimes of collider searches the EFT is usually not applicable: the consequence is that, with the increase in the energy of the interaction, the predictions of the complete theory begin to deviate from those of a given complete theory.

This problem clearly requires an overcoming of the naïf EFT approach, especially in sight

of the higher energy collisions expected in the next runs of the LHC or of the next planned colliders. The most sensible option is to identify benchmark renormalisable theories that allow a control over the validity of the corresponding effective theory ([35, 36, 37, 44] and references therein). These models are usually called *simplified models*, since they can be seen as a simplification of existing theories beyond the Standard Model, where one specifies a renormalisable theory that introduces a minimal set of new fields, usually only the DM particle and the mediator of its interactions with the SM. However, the meaning of these models is deeper than a mere depletion of more complete and sophisticated theories: indeed, simplified models capture essential features of more extended theories, thus share with effective theories a degree of generality that makes them very useful as a tool to parametrise different models. Simplified models are broad enough to include the features of classes of models, but on the other hand allow a precise control of the range of validity of the corresponding EFT. In this sense, they capture the main advantages of both the effective theory approach (because of their generality: a few simplified models can include many of the possible scenarios for particle DM) and complete UV theories such as for example the MSSM or the Kaluza-Klein set-up (because they allow a control over the limits of validity of the effective theory approach).

3.2 Our simplified models

In this thesis we will consider two simplified models, described in sections 3.2.1 and 3.2.2. In both models, DM is a fermion neutral under SM gauge groups, and interacts via a particle mediator with the quark sector of the SM: the main difference will be in the mediator of the DM-SM interaction.

We choose to restrict the interaction to the quark sector, leaving aside the leptonic one to avoid the limits from e^+-e^- colliders and electroweak precision tests. Our choice leads to comparable limits from direct detection and collider searches. Indeed, in direct searches (where the kinematic regime is non-relativistic) the cross section of the interaction of DM with the whole nucleus is by far larger than the cross section with a bound electron. Thus, for DM interacting only with leptons the interaction with nuclei would arise at one-loop, yielding looser limits.

3.2.1 Model A: vector mediator

In this model we consider a massive vector mediator Z' that makes the DM candidate X interact with the quarks. We assume that X is a Dirac fermion, and that in the interaction Lagrangian the field Z'_μ is coupled to a *axial vector* current built out of X and the quarks: this is the only renormalisable interaction (together with the vector one) between a fermion and a vector boson that preserves Lorentz invariance.

Therefore the Lagrangian for this model is

$$\begin{aligned}
\mathcal{L}_{\text{Model A}} &= \mathcal{L}_{\text{SM}} + \mathcal{L}_{Z'} + \mathcal{L}_X + \mathcal{L}_{\text{int}}\,, \\
\mathcal{L}_{Z'} &= -\frac{1}{4} Z'_{\mu\nu} Z'^{\mu\nu} + \frac{1}{2} m^2_{Z'} Z'_\mu Z'^\mu\,, \quad Z_{\mu\nu} = \partial_\mu Z'_\nu - \partial_\nu Z'_\mu\,, \\
\mathcal{L}_X &= i\overline{X}\gamma^\mu \partial_\mu X - m_X \overline{X} X\,, \\
\mathcal{L}_{\text{int}} &= Z'_\mu J^\mu_{Z'} = Z'_\mu \Big(g_q \sum_{\text{flavours}} \bar{q}\gamma^\mu\gamma^5 q + g_X \overline{X}\gamma^\mu\gamma^5 X \Big)\,,
\end{aligned} \tag{3.1}$$

where the sum is understood to be over all the six quark flavours, $\mathcal{L}_{\text{SM}}$ is the SM Lagrangian and the four real parameters[1] of the model are g_q, g_X, $m_{Z'}$, m_X.

[1]The couplings g_q, g_X must be real so that the Lagrangian is real. On the other hand their relative sign is not

We could see the interaction of this model as a mimicry of a $U(1)$ gauge interaction: indeed a possible high energy scenario that motivates this model is the spontaneous breaking of a Grand Unified Theory (GUT) to the SM gauge group, leaving this $U(1)$ as a remnant subgroup.

The choice of an axial vector interaction instead of a vector one is very relevant: indeed, this implies that, at the leading order, the interactions between DM and the nuclei in direct searches are spin dependent, and thus the constraints from these experiments on the parameters of the model are much looser.

Another important choice involves the quark couplings to Z': in eq. (3.1) we have assumed a diagonal coupling matrix $G_{ij} = g\mathbf{1}_3$ in the quark family space, for both up- and down-type quarks. Indeed, writing a non-diagonal mass matrix would introduce flavour changing neutral currents that are strongly constrained by experimental limits. The most natural assumption is then that the three couplings are equal, so that $G = g\mathbf{1}_3$ and the quarks can be rotated in any basis without changing the interaction with the Z'. The only degree of freedom left is the possibility to assign two different couplings to down-type and up-type quarks: for simplicity, we assume that these two couplings are equal. This choice would correspond to gauging an "axial baryon number"[2]; it also allows to write the sum over the quark flavours in eq. (3.1) in a $SU(2)_L$ invariant way.

We now derive the effective Lagrangian associated to eq. (3.1). In the limit in which the Z' boson is much heavier than the energy scale of the interaction, we can neglect the terms containing $\partial_\mu Z'$ with respect to the mass term for Z'. Then the approximate equations of motion for Z' are

$$Z'^\mu = -\frac{1}{m_{Z'}^2} J^\mu_{Z'} \,,$$

and if we substitute them into eq. (3.1) we get

$$\mathcal{L}^{\mathrm{A}}_{\mathrm{EFT}} \approx \frac{g_X^2}{2m_{Z'}^2}(\overline{X}\gamma^\mu\gamma^5 X)(\overline{X}\gamma_\mu\gamma^5 X) \tag{3.2a}$$

$$-\frac{g_q^2}{2m_{Z'}^2}\sum_{\text{flavours}}(\overline{q}\gamma^\mu\gamma^5 q)\sum_{\text{flavours}}(\overline{q}\gamma_\mu\gamma^5 q) \tag{3.2b}$$

$$-\frac{g_q g_X}{m_{Z'}^2}(\overline{X}\gamma^\mu\gamma^5 X)\sum_{\text{flavours}}(\overline{q}\gamma_\mu\gamma^5 q)\,. \tag{3.2c}$$

The effective interaction term (3.2a) could be constrained by the limits on DM self-interaction, (3.2b) is constrained by the di-jet searches at hadronic colliders such as the LHC, and the DM-quark effective interaction (3.2c) is the one of interest for the calculation of the DM relic abundance and the direct and collider searches.

3.2.2 Model B: scalar mediator

In our second simplified model we assume as mediator particle is a scalar boson charged under the SM gauge group, which mediates the interaction with a Majorana fermion χ that is the DM candidate.

This scenario is strongly motivated by supersymmetry. Indeed, in the MSSM the most plausible DM candidate (together with the gravitino in supergravity theories) is the neutralino

constrained: if we think to this interaction as a gauge one (explicitly broken in this Lagrangian by the Z' mass), their signs depend on the "charges" of the quarks and X under the $U(1)$ interaction. We assume for simplicity that both g_q and g_X are positive, since for the cases of interest to us their sign will not be relevant.

[2]For simplicity, and in the spirit of simplified models, we will ignore the additional degrees of freedom and/or interactions required by the mechanism of anomaly-cancellation, as well as the possible kinetic and/or mass mixing between the Z' and the Z.

(a Majorana fermion), which interacts (among the others) with all the particles charged under the electroweak interactions because of its $\widetilde{B}$, $\widetilde{W}^0$ components. Thus it interacts with quarks in a vertex with the squarks, the supersymmetric partners of quarks, which are coloured scalars.

These considerations should not induce to think that model B is simply a parametrisation of the MSSM or of one of its extensions. As we have discussed before, the goal of simplified models is to capture some features that could be common to many more complete models, without the limitation of selecting a specific one, which could have for example fixed coupling constants or peculiar decay channels. This is the reason why, in our model, we only make the hypothesis of a Majorana fermion DM with a scalar mediator, leaving the coupling constants free and discussing the remaining issues without referring to a specific extension of the SM such as the MSSM.

We now discuss our model. The renormalisable (and Lorentz scalar) interaction term between a quark q, the DM particle χ and a generic scalar mediator ϕ is a term of the type $\bar{q}\chi\phi$.

If we assume that χ is a singlet of the SM gauge group, then ϕ should have the same quantum numbers of the quark q: in particular, it will transform in the fundamental representation of $SU(3)_C$, and its $SU(2)_L \times U(1)_Y$ quantum numbers will be $(\mathbf{2}, 1/6)$, $(\mathbf{1}, 2/3)$ $(\mathbf{1}, -1/3)$ depending on whether q is the left-handed doublet Q_L, the right-handed up-quark u_R or the right-handed down-quark d_R. We choose to consider the second case mentioned above, and we denote the scalar mediator as $\widetilde{u}_\mathrm{R}$, the usual notation of the MSSM, to recall the substantial analogies between these two particles. Indeed, limits on squark searches can be recast into limits on our scalar mediator.

As for model A, we must now discuss the flavour issue for this model. The most elegant and natural solution to avoid the problems with the constraints from flavour-changing neutral currents is to introduce three scalar mediators $\widetilde{u}^i_\mathrm{R}$ $(i = 1, 2, 3)$ that couple each to the respective quark u^i_R with a universal coupling constant, with the $\widetilde{u}^i_\mathrm{R}$ degenerate in mass. In this way we are free to rotate the three scalars with the same matrix used for the quarks, leaving the Lagrangian invariant. This is our assumption for model B. Then, whenever we write u_R, $\widetilde{u}_\mathrm{R}$, we understand that the same relation holds for all the three generations. Another option, discussed in [45], is to assume that there is only one scalar, coupling only to the up quark (in the mass basis) at some energy scale. In [45] it is shown that the renormalisation group (RG) equations do not ruin very much this situation, i. e. that starting from three couplings $g_{u^i} \approx (1, 0, 0)$ at high energies, the RG-induced coupling of $\widetilde{u}_\mathrm{R}$ to the charm quark is still below the limits coming from $D - \overline{D}$ oscillations.

After these preliminary considerations, we write down the complete Lagrangian of model B:

$$
\begin{aligned}
\mathcal{L}_{\text{Model B}} &= \mathcal{L}_\mathrm{SM} + \mathcal{L}_{\widetilde{u}_\mathrm{R}} + \mathcal{L}_\chi + \mathcal{L}_\mathrm{int}\,, \\
\mathcal{L}_{\widetilde{u}_\mathrm{R}} &= (D_\mu \widetilde{u}_\mathrm{R})^\dagger (D^\mu \widetilde{u}_\mathrm{R}) - m^2_{\widetilde{u}_\mathrm{R}} \widetilde{u}^\dagger_\mathrm{R} \widetilde{u}_\mathrm{R}\,, \quad D_\mu = \partial_\mu - i g_\mathrm{S} G^a_\mu T^a - i g \frac{2}{3} B_\mu\,, \\
\mathcal{L}_\chi &= \frac{1}{2} i \overline{\chi} \gamma^\mu \partial_\mu \chi - \frac{1}{2} m_\chi \overline{\chi} \chi\,, \\
\mathcal{L}_\mathrm{int} &= -g_\mathrm{DM}\, \widetilde{u}_\mathrm{R}\, \overline{u_\mathrm{R}}\, \chi + \text{h. c.}\,,
\end{aligned}
\tag{3.3}
$$

where the covariant derivative D_μ acting on $\widetilde{u}_\mathrm{R}$ contains the strong coupling constant g_S, the gluon fields G^a_μ, $(a = 1, \ldots, 8)$, the generators T^a of $\mathfrak{su}(3)$ in the fundamental representation, the gauge field B_μ of $U(1)_Y$ and its coupling constant g. The coupling constant g_DM is a priori complex, but can be chosen real and positive by absorbing its phase into a redefinition of the $\widetilde{u}_\mathrm{R}$ field.

Similarly to what we have done for model A, the EFT (reliable as long as the energy scale of the interaction is lower than $m_{\widetilde{u}_\mathrm{R}}$) can be obtained by neglecting the terms containing $\widetilde{u}_\mathrm{R}$ or its derivatives with respect to the mass term for $\widetilde{u}_\mathrm{R}$. The corresponding equation of motion for

$\widetilde{u}_{\mathrm{R}}$ is

$$\widetilde{u}_{\mathrm{R}} = -\frac{g_{\mathrm{DM}}}{m^2_{\widetilde{u}_{\mathrm{R}}}}\overline{\chi}u_{\mathrm{R}}\,,$$

which after substitution into eq. (3.3) yields

$$\begin{aligned}\mathcal{L}^{\mathrm{B}}_{\mathrm{EFT}} &\approx \frac{g^2_{\mathrm{DM}}}{m^2_{\widetilde{u}_{\mathrm{R}}}}\Big(\overline{\chi}u_{\mathrm{R}}\Big)\Big(\overline{u_{\mathrm{R}}}\chi\Big)\\ &= -\frac{g^2_{\mathrm{DM}}}{8m^2_{\widetilde{u}_{\mathrm{R}}}}\Big(\overline{\chi}\gamma^{\mu}\gamma^5\chi\Big)\Big(\overline{u}\gamma_{\mu}u\Big) \qquad (3.4a)\\ &\quad -\frac{g^2_{\mathrm{DM}}}{8m^2_{\widetilde{u}_{\mathrm{R}}}}\Big(\overline{\chi}\gamma^{\mu}\gamma^5\chi\Big)\Big(\overline{u}\gamma_{\mu}\gamma^5u\Big)\,, \qquad (3.4b)\end{aligned}$$

where in the second equality we have used the Fierz transformation (eq. (A.7)).

We conclude this section by observing that models A and B, even if arising from very different set-ups, bring to an effective interaction between quarks and DM parametrised by similar effective operators. In particular, the operator (3.2c) is the same as (3.4b): this interaction is formed by two axial-vector Lorentz bilinears built out of DM and quarks. The complete effective interaction of model B then includes also the operator (3.4a). This is a concrete example of the power of EFT approach in parametrising a very large set of theories; but we must keep in mind that the expressions (3.2) and (3.4) are sensible approximations only at sufficiently low energy scales, and the advantage of picking up a simplified model is that one can control the theory even at the energy scales of collider experiments, without completely spoiling the generality of the approach.

3.3 Relic density of DM

The first constraint of interest for a DM model is that the relic abundance of the DM candidate today should be equal to (or at least lower than, if one conservatively assumes that other species contribute to the DM relic density) the one observed today. The most precise measurement of $\Omega_{\mathrm{DM}}h^2$ (where $h = H/(100\ \mathrm{km/s/Mpc})$) currently comes from the Planck satellite [4], which gives $\Omega_{\mathrm{DM}}h^2 = 0.1199 \pm 0.0027$.

In our models, we assume that the relic density arises through the usual freeze out mechanism. In appendix B we review the Boltzmann equation, which allows to calculate the relic density on the basis of the thermally averaged cross section $\langle\sigma v\rangle$; we derive for $\langle\sigma v\rangle$ an exact expression (eq. (B.7)), and the following approximate one,

$$\langle\sigma v\rangle \approx \frac{1}{4g^2m^2}\left(a + \frac{3(16b-a)}{8x}\right), \qquad (B.10)$$

obtained by performing a low-velocity expansion in the limit of low temperature. The coefficients a and b defined by

$$(\sigma_{\mathrm{ann}}\widetilde{F}) \approx a + bv^2\,, \qquad (B.9)$$

and can be calculated from the microscopic theory They allow us to compute the approximate value of the relic density on the basis of eq. (B.19) and (B.20).

In this section we compute these coefficients in models A and B. Before, we must introduce some notation and other formulæ that are useful for the evaluation of the moduli squared of the matrix elements we are going to calculate in this chapter.

3.3.1 Notation, and useful formulæ

Before discussing the specific cases of models A and B, we introduce the notation and other useful formulæ for the calculation of the Mandelstam variables in the center-of-mass frame.

Once we compute the Feynman amplitude $\mathcal{M}$ for given particle helicities (in our case, we will have two fermions in the initial state and two other fermions in the final one, and we will denote their helicities by r_1, r_2 for the ingoing particles and s_1, s_2 for the outgoing ones), we must compute the unpolarised modulus squared $\overline{|\mathcal{M}^2|}$ by summing over the helicity and the colour configurations of the final states and by averaging over those of the initial state.

Then, the differential cross section in the center-of-mass frame for the scattering of two particles into two other ones is given by (the quantity $(\sigma_{\text{ann}}\widetilde{F})$ that appears in the first equality is defined in eq. (B.4))

$$\sigma_{\text{ann}} = \frac{(\sigma_{\text{ann}}\widetilde{F})}{4g^2F} = \frac{1}{4g^2F}\frac{1}{16\pi^2}\frac{|\vec{k}|}{\sqrt{s}}\int \overline{|\mathcal{M}^2|}\mathrm{d}\Omega = \frac{1}{64\pi^2}\frac{|\vec{k}|}{|\vec{p}|}\frac{1}{s}\int \overline{|\mathcal{M}^2|}\mathrm{d}\Omega\,, \tag{3.5}$$

where $F = \sqrt{(p_1\cdot p_2)^2 - m^4} = |\vec{p}|\sqrt{s}$ is the flux factor, s is the Mandelstam variable $(p_1+p_2)^2$, and $\vec{p}$ and $\vec{k}$ are respectively the incoming and outgoing 3-momenta in the center-of-mass frame (see fig. 3.1).

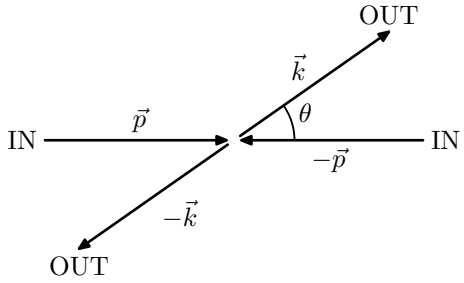

Figure 3.1: Notation about the momenta of the scattering particles in the center-of-mass frame.

The Mandelstam variables t, u can be evaluated in center-of-mass frame as follows: denoting by p_1, p_2, k_1, k_2 respectively the incoming and outgoing 4-momenta of a scattering between two initial particles of mass m and two final particles of mass m' , we have

$$p_1 = (\sqrt{s}/2, 0, 0, |\vec{p}|)\,,\ p_2 = (\sqrt{s}/2, 0, 0, -|\vec{p}|)\,,$$
$$k_1 = (\sqrt{s}/2, |\vec{k}|\sin\theta, 0, |\vec{k}|\cos\theta)\,,\ k_2 = (\sqrt{s}/2, -|\vec{k}|\sin\theta, 0, -|\vec{k}|\cos\theta)\,,$$

where

$$|\vec{p}| = \sqrt{s/4 - m^2}\,, \qquad |\vec{k}| = \sqrt{s/4 - m'^2}\,. \tag{3.6}$$

Thus we obtain

$$t = (p_1 - k_1)^2 = -s/2 + m^2 + m'^2 + 2\cos\theta|\vec{p}||\vec{k}|\,, \tag{3.7}$$
$$u = (p_1 - k_2)^2 = -s/2 + m^2 + m'^2 - 2\cos\theta|\vec{p}||\vec{k}|\,. \tag{3.8}$$

A quantity that will often appear in the calculations of the following cross sections is

$$\frac{t^2+u^2}{2} = \frac{s^2}{4} + \left(m^2+m'^2\right)^2 - s\left(m^2+m'^2\right) + \cos^2\theta\left[\frac{s^2}{4} - s(m^2+m'^2) + 4m^2m'^2\right]. \tag{3.9}$$

3.3.2 Model A: calculation of the thermal relic density

We will now calculate the cross section for the process $q\overline{q} \to X\overline{X}$, in the full theory, for model A.

The Feynman diagram for this process is displayed in fig. 3.2.

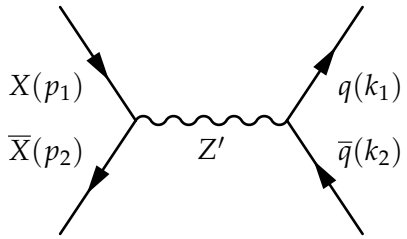

Figure 3.2: Feynman diagram for the process $X\overline{X} \to q\overline{q}$ in model A.

Before writing the amplitude for this process, we must calculate the decay width of the Z' boson as a function of the masses and couplings of the model. The allowed decay channels for the Z' are into $X\overline{X}$ and $q\overline{q}$, if $m_{Z'} > 2m_X, 2m_{\text{top}}$. Thus we can calculate the amplitude for a Feynman diagram in which Z' decays into two generic fermions (fig. 3.3).

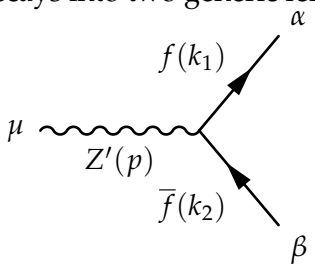

Figure 3.3: Feynman diagram for the decay $Z' \to f\overline{f}$ in model A.

The amplitude for the diagram of fig. 3.3 is

$$\mathcal{M} = ig_f \left(\overline{u}(k_1)\gamma^\mu\gamma^5 v(k_2)\right)_{\alpha\beta} \varepsilon_\mu^{(\lambda)} ,$$

where $\varepsilon_\mu^{(\lambda)}$, $\lambda = 1, 2, 3$, is the polarisation vector of the Z' boson. The modulus squared of the amplitude, summed over the final fermion polarisations and averaged over the three polarisations of the Z', gives

$$\begin{aligned}\overline{|\mathcal{M}^2|} &= \frac{c_f}{3} g_f^2 \left[\sum_\lambda \varepsilon_\mu^{(\lambda)} \varepsilon_\nu^{(\lambda)}\right] tr\Big((\not{k}_1 + m_f)\gamma^\mu\gamma^5(\not{k}_2 - m_f)\gamma^\nu\gamma^5\Big) = \\ &= \frac{4c_f}{3} g_f^2 \, m_{Z'}^2 \left(1 - \frac{4m_f^2}{m_{Z'}^2}\right) ,\end{aligned}$$

where c_f is the colour multiplicity ($c_X = 1$, $c_q = 3$). The phase space and the flux factor for the decay into two particles give

$$\frac{d\Gamma_{Z'}}{d\Omega} = \sum_f \frac{1}{64\pi^2} \frac{1}{m_{Z'}} \sqrt{1 - \frac{4m_f^2}{m_{Z'}^2}} \overline{|\mathcal{M}^2|} ,$$

that after the integration over the angular variables gives the total decay width

$$\Gamma_{Z'} = \frac{m_{Z'}}{12\pi} \left[g_X^2 \left(1 - \frac{4m_X^2}{m_{Z'}^2}\right)^{\frac{3}{2}} + \sum_q 3g_q^2 \left(1 - \frac{4m_q^2}{m_{Z'}^2}\right)^{\frac{3}{2}} \right] . \tag{3.10}$$

We can now write down the Feynman amplitude for the annihilation process $X\overline{X} \to q\bar{q}$ (fig. 3.2):

$$\mathcal{M} = \overline{v}(p_2)(ig_X\gamma^\mu\gamma^5)u(p_1)\,(-i)\left(\eta_{\mu\nu} - \frac{q_\mu q_\nu}{m_{Z'}^2}\right)\frac{1}{q^2 - m_{Z'}^2 + i\Gamma_{Z'}m_{Z'}}\overline{u}(k_1)(ig_q\gamma^\nu\gamma^5)v(k_2)\,, \tag{3.11}$$

where $q = p_1 + p_2$. Before taking the modulus squared of eq. (3.11), it is useful to simplify it with the equations of motion of the spinors: the term $q_\mu q_\nu / m_{Z'}^2$ can be contracted with the Lorentz bilinears, and by using

$$\begin{aligned}\overline{v}(p_2)\not{q}\gamma^5 u(p_1) &= \overline{v}(p_2)\not{p}_2\gamma^5 u(p_1) - \overline{v}(p_2)\gamma^5\not{p}_1 u(p_1) = -2m_X\overline{v}(p_2)\gamma^5 u(p_1)\,,\\ \overline{u}(k_1)\not{q}\gamma^5 v(k_2) &= \overline{u}(k_1)\not{k}_1\gamma^5 v(k_2) - \overline{u}(k_1)\gamma^5\not{k}_2 v(k_2) = 2m_q\overline{u}(k_1)\gamma^5 v(k_2)\,,\end{aligned}$$

we get

$$\begin{aligned}\mathcal{M} = {} & i\frac{g_q g_X}{q^2 - m_{Z'}^2 + i\Gamma_{Z'}m_{Z'}}\cdot\\ \cdot & \left[\Big(\overline{v}(p_2)\gamma^\mu\gamma^5 u(p_1)\Big)\Big(\overline{u}(k_1)\gamma_\mu\gamma^5 v(k_2)\Big) + \frac{4m_X m_q}{m_{Z'}^2}\Big(\overline{v}(p_2)\gamma^5 u(p_1)\Big)\Big(\overline{u}(k_1)\gamma^5 v(k_2)\Big)\right].\end{aligned} \tag{3.12}$$

From this expression, we must now compute the sum over all the fermion polarisations of $\overline{|\mathcal{M}^2|}$, including a factor 3 due to the admissible colour configurations in the final state, and we do not have to include the factor $g^2 = 4$ due to the average over the initial states that is cancelled in the expression of $(\sigma_{\text{ann}}\widetilde{F})$. The result is

$$\overline{|\mathcal{M}^2|} = \frac{48\,g_q^2 g_X^2}{(s - m_{Z'}^2)^2 + \Gamma_{Z'}^2 m_{Z'}^2}\left[\frac{t^2+u^2}{2} - m_X^4 - m_q^4 + 6m_X^2 m_q^2 - 8m_q^2 m_X^2\frac{s}{m_{Z'}^2} + 4m_q^2 m_X^2\frac{s^2}{m_{Z'}^4}\right]. \tag{3.13}$$

From the expression for $\overline{|\mathcal{M}^2|}$, we can obtain $(\sigma_{\text{ann}}\widetilde{F})$ by following eq. (3.5): we must perform an integral over the angular variables that appear in $(t^2+u^2)/2$ (eq. 3.9), and the final result is

$$\begin{aligned}(\sigma_{\text{ann}}\widetilde{F}) &= \frac{1}{16\pi^2}\frac{|\vec{k}|}{\sqrt{s}}\int\overline{|\mathcal{M}^2|}\,\mathrm{d}\Omega\\ &= \frac{2}{\pi}\frac{g_q^2 g_X^2}{(s - m_{Z'}^2)^2 + \Gamma_{Z'}^2 m_{Z'}^2}\sqrt{1 - \frac{4m_q^2}{s}}\cdot &\text{(3.14a)}\\ &\quad\cdot\left[s^2 - 4s(m_x^2 + m_q^2) + 28m_X^2 m_q^2 - 24m_X^2 m_q^2\frac{s}{m_{Z'}^2} + 12m_q^2 m_X^2\frac{s^2}{m_{Z'}^4}\right]. &\text{(3.14b)}\end{aligned}$$

This is an exact formula for $(\sigma_{\text{ann}}\widetilde{F})$ into a couple of quarks; the total annihilation cross section must be summed over the quark flavours. Following the procedure discussed in appendix B, we now expand this expression in powers of v, the modulus of the relative velocity between the incoming DM particles, to identify the coefficients a and b that appear in eq. (B.9). Thus we expand $s \approx m_X^2(4 + v^2)$: to make the formulæ more readable, we define $\alpha = m_q/m_X$, $\beta = m_X/m_{Z'}$. The terms inside eq. (3.14) can be expanded as

$$(3.14a) \approx \frac{2}{\pi}\frac{g_q^2 g_X^2}{m_X^4}\frac{\beta^4\sqrt{1-\alpha^2}}{(4\beta^2-1)^2 + \Gamma_{Z'}^2/m_{Z'}^2}\left(1 + \frac{\alpha^2}{8(1-\alpha^2)}v^2\right)\left(1 - \frac{2(4\beta^2-1)\beta^2}{(4\beta^2-1)^2 + \Gamma_{Z'}^2/m_{Z'}^2}v^2\right),$$

$$(3.14b) \approx 4m_X^4\Big[3\alpha^2(1 - 8\beta^2 + 16\beta^4) + \Big(1 - \alpha^2(1 + 6\beta^2 - 24\beta^4)\Big)v^2\Big].$$

Some caution is needed in this expansion: indeed, the term inside the first squared brackets in the first line comes from the expansion of the squared root (coming from the phase space integration) in eq. (3.14a). In the limit $\alpha \to 1$, i. e. for m_X tending to the mass of a quark, the square root is expanded around zero, where it is not an analytical function. This is why the expression inside the square brackets diverges for $\alpha \to 1$. On the other hand, as it can be seen in figure 3.4, this expansion does not affect very much the final results: in the plot, it is clear that the deviation from the exact formula due to the non-analiticity of this expansion ceases for m_X just a few GeV over the top quark mass [46].
From the previous equations we can finally calculate a, b in model A (we understand a sum over the 6 quark flavours whose mass is below m_X):

$$\begin{cases} a = \dfrac{8}{\pi} g_q^2 g_X^2 \dfrac{\beta^4\sqrt{1-\alpha^2}}{(4\beta^2-1)^2+\Gamma_{Z'}^2/m_{Z'}^2} \cdot 3\alpha^2(1-8\beta^2+16\beta^4)\,, \\ b = \dfrac{8}{\pi} g_q^2 g_X^2 \dfrac{\beta^4\sqrt{1-\alpha^2}}{(4\beta^2-1)^2+\Gamma_{Z'}^2/m_{Z'}^2} \\ \quad \times \left[\left(\dfrac{-6\alpha^2\beta^2(4\beta^2-1)}{(4\beta^2-1)^2+\Gamma_{Z'}^2/m_{Z'}^2} + \dfrac{3\alpha^4}{8(1-\alpha^2)} \right)(1-8\beta^2+16\beta^4) + \left(1-\alpha^2(1+6\beta^2-24\beta^4)\right) \right]. \end{cases} \tag{3.15}$$

These formulæ allow a more precise estimate of the relic density with respect to what is available in the literature: in [47], that considers the model of a Z' mediator with DM, it is stated that, in the limit of $\beta \ll 1$ and zero velocity,

$$\langle \sigma v \rangle = \frac{1}{16 m_X^2} \frac{8 g_q^2 g_X^2}{\pi} \beta^4 \sqrt{1-\alpha^2}\, 3\alpha^2\,,$$

but from the comparison with eq. (B.11) we see that the previous formula neglects also the second order of $\langle \sigma v \rangle$ in $1/x_f$, and assumes $\Gamma_{Z'} \ll m_{Z'}$. Both assumptions, as we will see in the following, are rather extreme for this specific model.

An important point to notice is that a, the leading order term for $v \to 0$, is proportional to α: then, it vanishes in the limity of massless quarks. This is called *helicity suppression*, and is due to the vector-axial coupling that we have imposed. A way to understand this phenomenon is to express the matrix element of eq. (3.12) in the limit of massless quarks, and non relativistic dark matter: then, only the first term inside the squared brackets of eq. (3.12) survives. The DM spinors can be written in the Weyl basis as

$$u(p_1) = \sqrt{m_X} \begin{pmatrix} \xi \\ \xi \end{pmatrix}, \qquad v(p_2) = \sqrt{m_X} \begin{pmatrix} \xi' \\ -\xi' \end{pmatrix},$$

where ξ, ξ' are two Weyl spinors. The Lorentz bilinear can be written in terms of these two-components spinors as (see formulæ in appendix B)

$$\begin{aligned} \overline{v}(p_2)\gamma^\mu\gamma^5 u(p_1) &= m \begin{pmatrix} \xi'^\dagger & -\xi'^\dagger \end{pmatrix} \begin{pmatrix} & \mathbf{1}_2 \\ \mathbf{1}_2 & \end{pmatrix} \begin{pmatrix} & \sigma^\mu \\ \overline{\sigma}^\mu & \end{pmatrix} \begin{pmatrix} -\mathbf{1}_2 & \\ & \mathbf{1}_2 \end{pmatrix} \begin{pmatrix} \xi \\ \xi \end{pmatrix} = \\ &= -m(\xi'^\dagger \overline{\sigma}^\mu \xi + \xi'^\dagger \sigma^\mu \xi) = \begin{cases} -2m\xi'^\dagger\xi & \mu = 0\,, \\ 0 & \mu = 1,2,3\,. \end{cases} \end{aligned}$$

Then, the non-relativistic expansion of the DM current selects the temporal component of the Lorentz product with the quark current. This can be rewritten as follows: first, we decompose into left-handed and right-handed spinors with

$$\overline{q}\gamma^\mu\gamma^5 q = \overline{q}_{\mathrm{R}}\gamma^\mu q_{\mathrm{R}} - \overline{q}_{\mathrm{L}}\gamma^\mu q_{\mathrm{L}}\,.$$

Each of these has a vanishing $\mu = 0$ component: we are going to show this fact for the right-handed quarks. The corresponding spinors in the Weyl basis are

$$u(k_1) = \sqrt{2E}\begin{pmatrix}0\\0\\1\\0\end{pmatrix}, \qquad v(k_2) = \sqrt{2E}\begin{pmatrix}0\\0\\0\\-1\end{pmatrix},$$

then the temporal component of the Lorentz bilinears reads

$$\overline{u}_{\mathrm{R}}(k_1)\gamma^0 v_{\mathrm{R}}(k_2) = 2E\begin{pmatrix}0 & 0 & 1 & 0\end{pmatrix}\begin{pmatrix}-\overline{\sigma}^0 & \\ & \sigma^0\end{pmatrix}\begin{pmatrix}0\\0\\0\\-1\end{pmatrix} = 2E\begin{pmatrix}1 & 0\end{pmatrix}\sigma^0\begin{pmatrix}0\\-1\end{pmatrix} = 0\,.$$

This argumentation shows that in the limit of massless quarks, and non-relativistic dark matter, the amplitude of the annihilation $X\overline{X} \to q\bar{q}$ vanishes.

Returning back to the goal of this section, we can compute the thermal relic density by using the equations (3.15) and (B.19). In fig. 3.4 we show the effects in model A of the two approximations introduced in the derivation of eq. (B.10) for the thermally averaged cross section $\langle\sigma v\rangle$ presented in appendix B. The first approximation consists in the expansion of the Bessel function in the integral in eq. (B.7). The analytical result of this approximation is drawn with a brown line, which basically coincides with the blue line (corresponding to the exact solution): this means that the approximation of the Bessel function is perfectly allowed. The second approximation comes from the expansion of $(\sigma_{\mathrm{ann}}\widetilde{F})$ of eq. (B.9) (purple line): the two distortions induced by this approximation are discussed in the caption of fig. 3.4.

At this point, we have an expression for the relic density of X in terms of four parameters: $m_X, m_{Z'}, g_q, g_X$. By imposing that the corresponding relic density is equal to the value measured by Planck ($\Omega_{\mathrm{DM}} = 0.1199$), we can remove one degree of freedom. The resulting constraints are discussed in the next section.

3.3.3 Constraints on model A from the relic density

We begin the discussion of the constraints arising on model A from the requirement of the correct relic density by checking the limit that one could have obtained by use of the effective field theory (Lagrangian (3.2)). That regime is obtained by imposing $m_{Z'} \gg \Gamma_{Z'}$ and $m_{Z'} \gg m_X$. The corresponding limit is the one shown in figure 3.5: the annihilation cross section, in the EFT limit, depends on g_q, g_X, $m_{Z'}$ only through the combination $\Lambda = m_{Z'}/\sqrt{g_q g_x}$, which is then directly constrained once m_X is fixed.

In the following, we are going to show some limitations and distortions of the picture of the EFT. First, we notice from the form of the coefficients a and b (eq. (3.15)), which appear in the relic abundance through eq. (B.19, B.11), that, in the complete theory, the annihilation cross section $\langle\sigma v\rangle$ depends on the overall coefficient $1/\Lambda^4 = g_q^2 g_x^2/m_{Z'}^4$, on $\Gamma_{Z'}/m_{Z'}$ that appears in the denominator of a and b, and then subleadingly on the value of $\beta = m_X/m_{Z'}$, through various terms of higher order in β. Thus, the behaviour of the relic density as a function of the parameters of the model is not easily predictable through a completely analytical approach. In order to derive the bounds on the parameters of the model, we generated a sample of values of $(g_q,\, g_X,\, m_X,\, m_{Z'})$ (with $g_q,\, g_X \in [0.1,\, 4\pi]$, $m_X \in [10,\, 1000]$ GeV) that yield $\Omega_{\mathrm{DM}}h^2 = 0.1199$, and we have analysed their distribution in the parameters space.

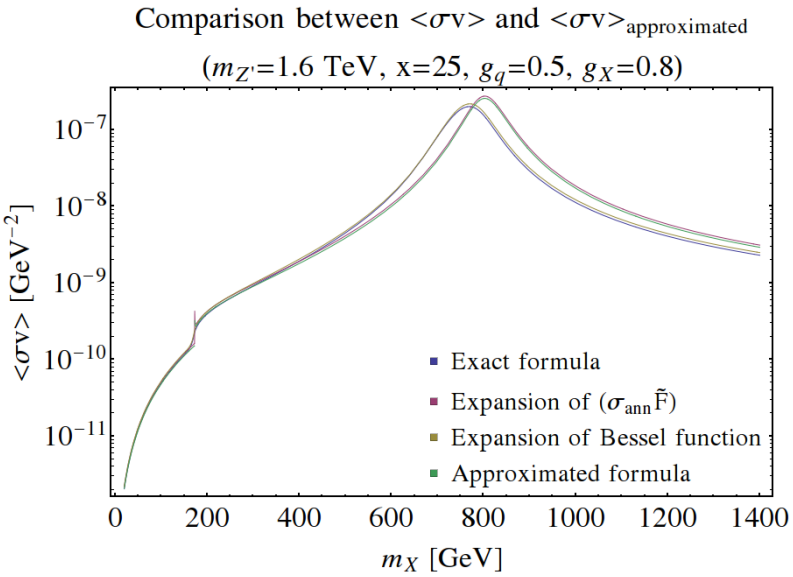

Figure 3.4: Comparison between eq. (B.7) and (B.10), in the case of model A. The bump around 172.9 GeV is due to addition of the $t\bar{t}$ annihilation channel, and is enhanced in the approximation of $(\sigma_{\text{ann}}\tilde{F})$ in the limit $v \to 0$ because near that threshold the espansion of the factor $\sqrt{1-4m_q^2/s}$ coming from the phase space integration is not analytical. On the other hand, the difference between the two around the resonance $m_X \sim m_{Z'}/2$ is due to the fact that there, the expansion of the denominator $(s-m_{Z'}^2)^2 + \Gamma_{Z'}^2 m_{Z'}^2$ for $v \to 0$ should not be truncated because the term of higher order in v^2 allow a better tracking of the resonance in the s-channel.

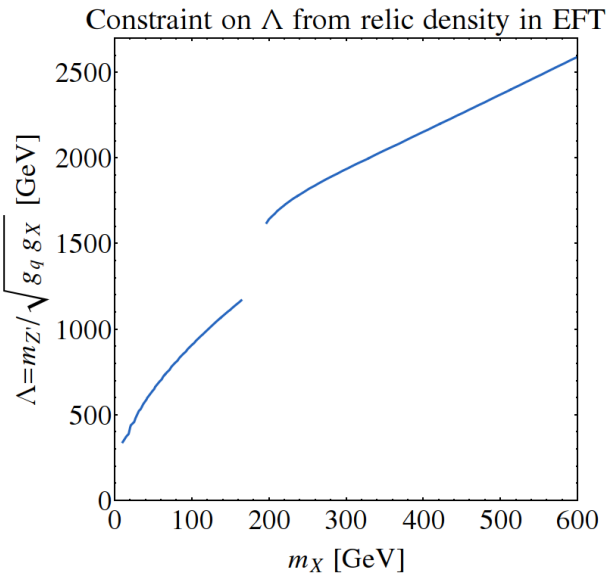

Figure 3.5: Constraint on the coefficient of the effective operator (3.2c) in the effective field theory (obtained in the limit $m_{Z'} \gg \Gamma_{Z'}$ and $m_{Z'} \gg m_X$) from the observed relic density. The curve disappears in a small window around the top mass, where the low velocity limit used to derive $\Omega_{\text{DM}}h^2$ is not a valid approximation. This plot is a substantial improvement over the naïf estimate presented in [47], where it is stated that, for m_X greater than the top mass, the relic density constrains Λ to be approximately 1500 GeV: this turns out to be the correct value only for $m_X \approx m_{\text{top}}$.

The most important fact that comes out from this check is that there are various regions of

the parameter space that are not allowed by the relic density constraint because of the non-perturbativity of the couplings: this behaviour is not captured at all by the EFT approach. The most representative plot in this sense is the one shown in figure 3.6, which shows the constraint in the (m_X, g_X) plane for fixed $m_{Z'}$, g_q. If we follow the curves from higher to lower values of m_X, we see that g_X is slightly increasing until the top quark mass; below that threshold, the annihilation channel $X\overline{X} \to t\bar{t}$ disappears and the cross section strongly decreases, thus the coupling should increase in order to keep the same value of $\langle\sigma v\rangle$. The crucial point is that the higher is g_X, the bigger the decay width $\Gamma_{Z'}$ (eq. (3.10)) gets. In this region, $\Gamma_{Z'}$ rises up to non-perturbative values (of the same order or even higher than $m_{Z'}$), and then suppresses the annihilation cross section because of its appearance in the denominator of (3.15). Since both $(\Gamma_{Z'}/m_{Z'})^2$ (once we neglect the quark decay contribution) and the overall coefficient $1/\Lambda^4$ are proportional to g_X^2, the two compensate and the annihilation cross section can never grow to the needed value. Thus, the region of low m_X in figure 3.6 is not allowed. In all the following plots, we do not show the points for which $\Gamma_{Z'}/m_{Z'} > 1$: we take this as the (conventional) limit between perturbative and non-perturbative regime.

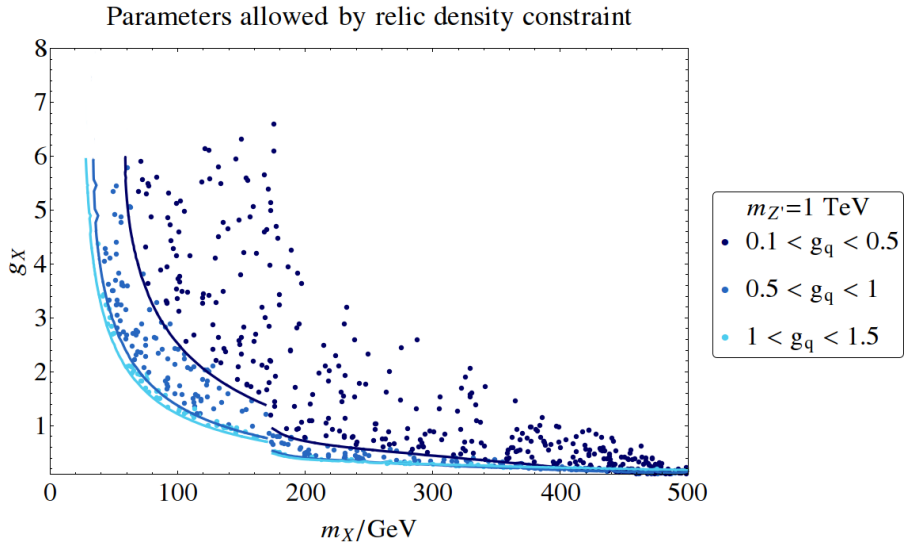

Figure 3.6: Relic density constraint on g_X as a function of m_X, for fixed $m_{Z'} \simeq 1$ TeV (within 5%) and different regions of g_q, shown with different shades of blue. Analytical contour lines for the corresponding values of g_q are superimposed on the plot with the same colour. Only the points for which $\Gamma_{Z'}/m_{Z'} < 1$ are shown.

As a second point of discussion, we focus now on the dependence of $\langle\sigma v\rangle$ on the parameters of the model. As we have already mentioned, it is proportional to the overall coefficient $1/\Lambda^4 = g_q^2 g_x^2/m_{Z'}^4$, it is strongly affected by $\Gamma_{Z'}/m_{Z'}$ when it reaches non-perturbative values, and further depends on $\beta = m_X/m_{Z'}$. We can observe from eq. (3.15) that, in the limit of low β, the dependence of a, b on β is very mild. This is indeed what happens in the large majority of the cases: figure 3.7 shows that, within the allowed region in the $(m_X, m_{Z'})$ plane, β is nearly always smaller than 0.5 once we impose $\Gamma_{Z'}/m_{Z'} < 1$. This can be rephrased as the implication that $\beta > 0.5$ forces the width to be large: this can be understood by noticing that the resonance production is no more possible for $\beta > 0.5$, then the cross section must be enhanced (in order to track the required value for the annihilation cross section) by enlarging the couplings, which in turn increase the width up to non-perturbative values.

This remark allows us to focus on the relevance of the width $\Gamma_{Z'}/m_{Z'}$ on $\langle\sigma v\rangle$. We can have a

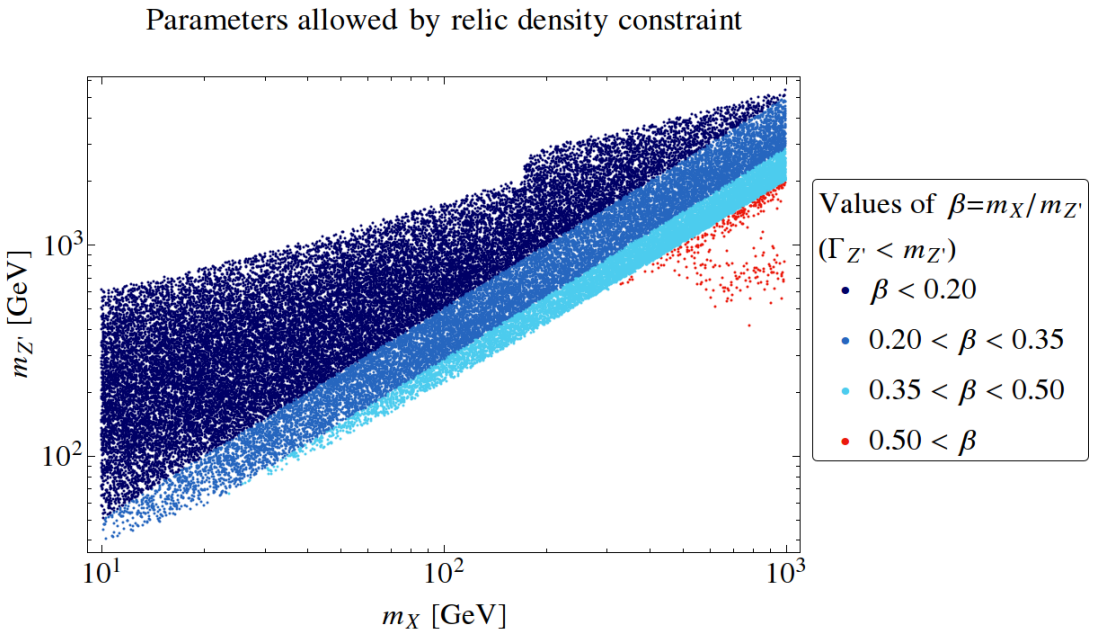

Figure 3.7: Distribution in $(m_X, m_{Z'})$ of the sample of parameter values allowed by the relic density constraint. Regions of fixed $\beta = m_X/m_{Z'}$ are shown with different colours.

better understanding of what we have discussed in figure 3.6 by observing the plot in figure 3.8. This plot shows the distribution of the allowed values in the $(m_X, \Lambda = m_{Z'}/\sqrt{g_q g_X})$ plane. By observing fig. 3.8, two important considerations can be made: first, we notice that a relevant portion within this region is occupied by points where $\Gamma_{Z'}/m_{Z'}$ is larger than 0.25, i. e. by points which tend to a non-perturbative regime. In the remaining portion, if we restrict to the points with a low ratio $\beta = m_X/m_{Z'}$, we see that the remaining region (in dark blue) is very thin, and for a fixed value of m_X there is substantially only one allowed value for Λ. Thus, we have a computational cross-check of what we could guess from the analytic expression, i. e. that for low β (which happens often), the annihilation cross section $\langle\sigma v\rangle$ mainly depends on $1/\Lambda^2$ and $\Gamma_{Z'}/m_{Z'}$, and that the latter is often relevant because it can reach non-perturbative values. This peculiar behaviour is in turn a consequence of the helicity suppression of the annihilation cross section, which requires the coupling to grow to high values in order to track the correct relic abundance of DM. But the most important point that we get from this plot is that the use of the EFT hides a large portion of the allowed parameter space: in particular, if we fix a given Λ, the value predicted by the EFT (the dark blue zone) should be replaced by a considerably larger interval (the light blue area) in which the correct relic density can still be obtained. In this sense, fig. 3.8 is a clear illustration of the limited reliability of the EFT in regimes that are far from being extreme, in this case the region $m_X > 0.2\, m_{Z'}$.

3.3.4 Model B: calculation of the thermal relic density

In this section, we will derive the annihilation cross section $(\sigma_{\text{ann}}\widetilde{F})$ needed to compute the relic density in model B.

The Feynman diagrams contributing to this process are those of fig. 3.9. The arrows in these diagrams display the conservation of the colour charge, or equivalently the conservation of the particle number (i. e. the difference between particles and antiparticles, which is the conserved charge associated to the $U(1)$ invariance for complex fields). This explains why the χ lines do not carry any arrow.

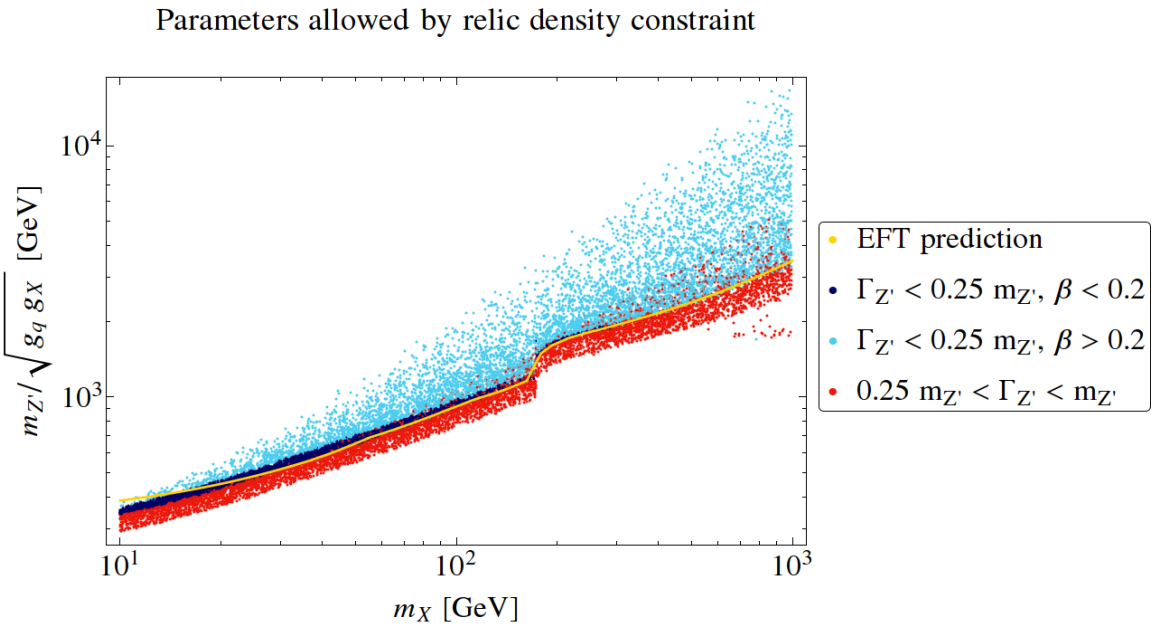

Figure 3.8: Distribution in (m_X, Λ) of the sample of parameter values allowed by the relic density constraint. The points for which $\Gamma_{Z'}/m_{Z'} > 0.25$ are shown in red: these correspond to a strong coupling regime. In the remaining region, light and dark blue differentiate between β higher or lower than 0.2. The thin yellow line shows the limit on Λ that we get from the effective theory (fig.3.5): it falls within the region of low β (dark blue dots), as expected.

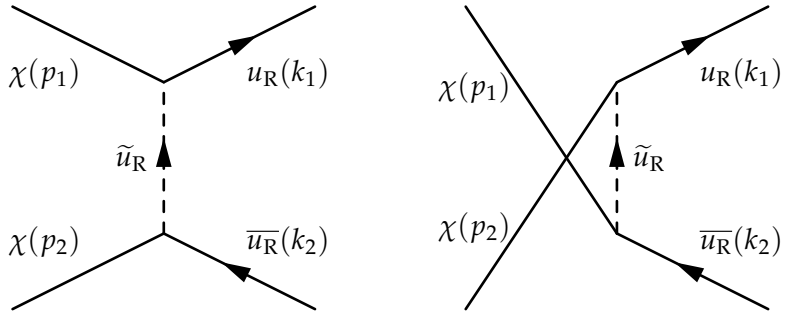

Figure 3.9: Feynman diagrams for the process $\chi\overline{\chi} \to u_R\overline{u_R}$ in model B; the two diagrams have an opposite sign, because of the anticommutation that one must impose on the Majorana fermions.

To write the amplitude of a Feynman diagram with Majorana fermions, the best way of writing the correct spinors associated to the external legs is to explicitly calculate the matrix element associated to that diagram (see appendix A). The result, with the use of eq. (A.9), gives

$$\begin{aligned}\mathcal{M} = i g_{\mathrm{DM}}^2 \Bigg[& \frac{1}{t - m_{\widetilde{u}_R}^2} \Big(\overline{v}(p_2) P_R v(k_2)\Big) \Big(\overline{u}(k_1) P_L u(p_1)\Big) \\ & - \frac{1}{u - m_{\widetilde{u}_R}^2} \Big(\overline{v}(p_1) P_R v(k_2)\Big) \Big(\overline{u}(k_1) P_L u(p_2)\Big) \Bigg] .\end{aligned} \tag{3.16}$$

As discussed in appendix B, the relative minus sign arises because of the anticommutation that we must impose on the two Majorana spinors to contract their fields with the creation operators from the initial state.

In the calculation of the modulus squared of this matrix element, some attention must be paid when contracting the spinor indices (to get the traces over gamma matrices) in the inter-

ference terms. Indeed, as explained also in [48], in the interference terms it is necessary to use the sum rules (eq. (A.11)), which require to transpose some of the matrices resulting from the contraction of the spinors. In the following equation, we write explicitly the resulting traces:

$$\overline{|\mathcal{M}^2|} = \frac{3}{4} g_{\mathrm{DM}}^4 \Bigg\{ \frac{\mathrm{tr}\Big[(\not{p}_2 - m_\chi) P_R (\not{k}_2 - m_q) P_L\Big] \mathrm{tr}\Big[(\not{k}_1 + m_q) P_L (\not{p}_1 + m_\chi) P_R\Big]}{(t - m^2_{\widetilde{u}_\mathrm{R}})^2} \tag{3.17a}$$

$$+ \frac{\mathrm{tr}\Big[(\not{p}_1 - m_\chi) P_R (\not{k}_2 - m_q) P_L\Big] \mathrm{tr}\Big[(\not{k}_1 + m_q) P_L (\not{p}_2 + m_\chi) P_R\Big]}{(u - m^2_{\widetilde{u}_\mathrm{R}})^2} \tag{3.17b}$$

$$- \frac{\mathrm{tr}\Big[P_R (\not{k}_2 - m_q) P_L (\not{p}_1 - m_\chi) C^\mathrm{T} P_L^\mathrm{T} (\not{k}_1 + m_q)^\mathrm{T} P_R^\mathrm{T} C^{-1} (\not{p}_2 - m_\chi)\Big]}{(t - m^2_{\widetilde{u}_\mathrm{R}})(u - m^2_{\widetilde{u}_\mathrm{R}})} \tag{3.17c}$$

$$- \frac{\mathrm{tr}\Big[P_R (\not{k}_2 - m_q) P_L (\not{p}_2 - m_\chi) C^\mathrm{T} P_L^\mathrm{T} (\not{k}_1 + m_q)^\mathrm{T} P_R^\mathrm{T} C^{-1} (\not{p}_1 - m_\chi)\Big]}{(t - m^2_{\widetilde{u}_\mathrm{R}})(u - m^2_{\widetilde{u}_\mathrm{R}})} \Bigg\} \tag{3.17d}$$

The first two terms in eq. (3.17) are the modulus squared of the diagrams corresponding to the t and u channel respectively, while (3.17c) and (3.17d) come from the interference term. In order to compute the traces, the following formulæ are useful to simplify the projection operators:

$$P_R(\not{p} \pm m) P_L = \not{p} P_L\,, \quad P_R(\not{p} \pm m) P_R = \pm m P_R\,,$$
$$P_L(\not{p} \pm m) P_R = \not{p} P_R\,, \quad P_L(\not{p} \pm m) P_L = \pm m P_L\,.$$

The first two traces in eq. (3.17) can then be computed straightforwardly, and give

$$(3.17a) = \frac{4\, k_1 \cdot p_1\; k_2 \cdot p_2}{(t - m^2_{\widetilde{u}_\mathrm{R}})^2} = \frac{(m_\chi^2 + m_q^2 - t)^2}{(t - m^2_{\widetilde{u}_\mathrm{R}})^2}\,,$$
$$(3.17b) = \frac{4\, k_2 \cdot p_1\; k_1 \cdot p_2}{(u - m^2_{\widetilde{u}_\mathrm{R}})^2} = \frac{(m_\chi^2 + m_q^2 - u)^2}{(u - m^2_{\widetilde{u}_\mathrm{R}})^2}\,.$$

The last two traces in (3.17c) and (3.17c) must be simplified with the formulæ (A.4), together with the formula for the transposed gamma matrices, $\gamma^\mathrm{T} = -C^{-1}\gamma^\mu C$, which imply [48]

$$C^\mathrm{T} P_L^\mathrm{T} (\not{k}_1 + m_q)^\mathrm{T} P_R^\mathrm{T} C^{-1} = P_L(\not{k}_1 - m_q) P_R = \not{k}_1 P_R\,.$$

With the use of this equation, the traces of the numerators in (3.17c) and (3.17d) give the same result (notice that they are simply related by the switch of p_1 and p_2),

$$m_\chi^2\, 2\, k_1 \cdot k_2 = m_\chi^2 (s - 2m_q^2)\,.$$

The final result for the annihilation cross section times $\widetilde{F}$ (eq. (3.5)) is

$$\frac{\mathrm{d}(\sigma_\mathrm{ann}\widetilde{F})}{\mathrm{d}(\cos\theta)} = \frac{1}{16\pi}\sqrt{1 - \frac{4m_q^2}{s}}\,\frac{3}{4} g_{\mathrm{DM}}^4 \cdot$$
$$\cdot \left[\frac{(m_\chi^2 + m_q^2 - t)^2}{(t - m^2_{\widetilde{u}_\mathrm{R}})^2} + \frac{(m_\chi^2 + m_q^2 - u)^2}{(u - m^2_{\widetilde{u}_\mathrm{R}})^2} + \frac{4m_q^2 m_\chi^2 - 2s m_\chi^2}{(t - m^2_{\widetilde{u}_\mathrm{R}})(u - m^2_{\widetilde{u}_\mathrm{R}})} \right]. \tag{3.18}$$

The $\cos\theta$ integral in eq. (3.18) is a cumbersome one: the dependence of t, u on $\cos\theta$ can be found in eq. (3.7), (3.8). Thus, to derive the coefficients a, b of the expansion for low velocities,

defined in eq. (B.9), we use the software *Mathematica* to expand eq. (3.18) up to the second order in v and to perform the integral in $\cos\theta$. The result can be written in a more compact form by defining, analogously to model A, $\alpha = m_q/m_\chi$, $\beta = m_\chi/m_{\widetilde{u}_R}$ (we understand a sum over the up-type quark flavours whose mass is below m_χ):

$$\begin{cases} a = \dfrac{3}{8\pi} g_{\rm DM}^4 \dfrac{\beta^4\sqrt{1-\alpha^2}}{(1+\beta^2-\alpha^2\beta^2)^2}\,\alpha^2\,, \\ b = \dfrac{3}{64\pi} g_{\rm DM}^4 \dfrac{\beta^4\sqrt{1-\alpha^2}}{(1+\beta^2-\alpha^2\beta^2)^2}\cdot \\ \qquad \cdot\left[16-7\alpha^2+\dfrac{3\alpha^2}{1-\alpha^2}-\beta^2\alpha^2(16-7\alpha^2)+\beta^4(1-\alpha^2)(14-4\alpha^2+7\alpha^4)\right]. \end{cases} \tag{3.19}$$

With these expression, we are able to apply the formulæ derived in appendix B to calculate the relic density of χ after the freeze out.

To understand the results of the plots obtained by imposing the correct relic density, we must discuss the limit in which the EFT is valid. First of all, we write down the result for $(\sigma_{\rm ann}\widetilde{F})$ in the effective theory: the amplitude for the process $\chi\chi \to q\bar{q}$ is analogous to the one for the complete theory (eq. (3.16)), with the important difference that the two propagators are replaced by $m^2_{\widetilde{u}_R}$. Thus the modulus squared of the amplitude requires the calculation of the same traces of eq. (3.17), with the replacement of the denominators by $m^4_{\widetilde{u}_R}$. The result can be then simplified in

$$\begin{aligned} \overline{|\mathcal{M}^2|} &= \frac{3g_{\rm DM}^4}{4m^4_{\widetilde{u}_R}}\left[(m_\chi^2+m_q^2-t)^2+(m_\chi^2+m_q^2-u)^2+4m_q^2m_\chi^2-2sm_\chi^2\right] \\ &= \frac{3g_{\rm DM}^4}{2m^4_{\widetilde{u}_R}}\left[\frac{t^2+u^2}{2}-m_\chi^4-m_q^4+sm_q^2\right]. \end{aligned} \tag{3.20}$$

From the comparison between this formula and eq. (3.18), or directly from the Feynman amplitudes for the full theory and the effective one, it is easy to understand that the limit in which the EFT gives reliable predictions is when $(m^2_{\widetilde{u}_R}-t) \approx m^2_{\widetilde{u}_R}$, $(m^2_{\widetilde{u}_R}-u) \approx m^2_{\widetilde{u}_R}$. Now, in the annihilation process, t and u are negative: if we recall the definitions (3.6) and the expressions (3.7) and (3.8), we can rewrite t and u as (for each $\pm$ or $\mp$ factor, the upper one refers to t and the other to u)

$$-(|\vec{k}|-|\vec{p}|)^2-2|\vec{k}|\,|\vec{p}| \pm 2\cos\theta|\vec{k}|\,|\vec{p}| = -(|\vec{k}|-|\vec{p}|)^2-2(1\mp\cos\theta)|\vec{k}|\,|\vec{p}| < -(|\vec{k}|-|\vec{p}|)^2\,,$$

which is negative. With a similar calculation, the lower limit on t, u turns out to be

$$t,\,u > -(|\vec{k}|+|\vec{p}|)^2\,.$$

Thus we can neglect t and u in the denominators of eq. (3.18) if

$$m_{\widetilde{u}_R} \gg (|\vec{k}|+|\vec{p}|)^2 = \left(\sqrt{\frac{s}{4}-m_q^2}+\sqrt{\frac{s}{4}-m_\chi^2}\right)^2 \underset{v\to 0}{\to} (m_\chi^2-m_q^2)\,,$$

that is always a positive quantity since χ can only annihilate to lighter quarks. Thus the condition of validity for the predictions of the effective theory for the relic density is

$$\beta = m_\chi/m_{\widetilde{u}_R} \ll 1\,.$$

We notice that in the limit of zero velocity the annihilation cross section displays the *helicity suppression*, as it happened in model A. Indeed, for $m_q = 0$ and $v = 0$, t and u are equal

to $-m_\chi^2$, and the expression inside squared brackets in eq. (3.18) vanishes. This can be explained with the same calculation performed for model A (sec. 3.3.2), which showed that in the limit of non-relativistic dark matter and relativistic quarks, with an axial-vector coupling, the Lorentz bilinear vanishes. In this case, we can explain this phenomenon also by invoking the conservation of angular momentum [46, 49]. Indeed, the incoming χ particles, in the limit of zero velocity, annihilate in s-wave, i. e. the leading component in the expansion of the overall wavefunction in spherical harmonics is the one corresponding to $\ell = 0$ (corresponding to zero orbital angular momentum). Since they are identical fermions (while in model A the particles X and $\overline{X}$ are distinguishable), they cannot share all the same quantum numbers, then their total wavefunction must have spin 0 (otherwise their spin should be aligned). Therefore, the overall angular momentum in the initial state is 0. On the other hand, in the final state the two quarks are massless, thus their helicities cohincide with the chiralities of the corresponding spinors. Since the quark current is a Lorentz axial vector, the current couples spinors with the same chirality, and thus the corresponding quark and antiquark have opposite helicities; hence, since they have opposite velocities, their spins are aligned. Therefore, the total angular momentum of the final state is 1, and is different from the angular momentum of the initial state.

The helicity suppression reduces significatively the annihilation cross section for this process. As we have seen also in model A, this implies that in order to yield the correct relic abundance the coupling will be rather strong, and the limits from direct and indirect searches (that we are going to discuss in the following sections) will be by far less constraining.

3.3.5 Constraints on model B from the relic density

In this section, we show the results obtained by imposing the correct relic density of dark matter through the freeze out mechanism. We use the formulæ derived in appendix B to calculate the relic density from the knowledge of the coefficients a and b.

We will analyse only the region of the parameter space where $m_{\widetilde{u}_\mathrm{R}}$ is higher than m_χ. Indeed, when the two masses are comparable the analysis of the freeze out for the two species cannot be done for each of them independently, because the process $\chi\chi \to q\bar{q}$ has a rate comparable to $\widetilde{u}_\mathrm{R}\widetilde{u}_\mathrm{R}^* \to q\bar{q}$, and the two species χ and $\widetilde{u}_\mathrm{R}$, which interact via the exchange of a quark, decouple together. In this situation, the two Boltzmann equations describing the evolution of their number densities cannot be disentagled, and they must be solved simultaneously through a numerical procedure. This regime is also called *coannihilation*. In order to avoid the complications related to this issue, we will assume from now on that $m_{\widetilde{u}_\mathrm{R}}$ is not of the same order of m_χ. The constraints from various kind of searches for models analogous or equivalent to our model B have been recently discussed in the literature [50, 51, 52], and [45] studies the case when the two masses are comparable. In the following, we fix $\beta = m_\chi / m_{\widetilde{u}_\mathrm{R}} = 0.9$ as the maximum value for this ratio, analogously to what is done e. g. in [50]. In this work, we will focus only on the region where the two masses are not comparable, in order to discuss more carefully the limits of the predictions of the effective theory with respect to the complete one.

We observe that the only quarks with which DM is interacting are the up-type ones (u, c, t flavours), then for m_χ below the top quark mass the allowed annihilation channels are only two, with respect to the five channels available in model A. Recalling the effect of helicity suppression (i. e. the coefficient a in the expansion of $(\sigma_\mathrm{ann}\widetilde{F})$ is negligible for low values of the quark masses), this implies that, in the region $m_\chi < m_t$, the required values of the couplings will be higher, and the mass of the mediator lower, with respect to what we have seen for model A.

We now turn to the discussion of the plots resulting from the requirement that the relic density is the correct one. In model B, the free parameters of the model are three (g_DM, $m_{\widetilde{u}_\mathrm{R}}$, m_χ), and the requirement of the correct relic abundance leaves only two degrees of freedom.

We begin by showing the limit obtained in the EFT: this limit can be achieved from the formulæ for the full theory by choosing a very high value for $m_{\tilde{u}_R}$. In that limit $m_{\tilde{u}_R}$ appears only in the scale $\Lambda = m_{\tilde{u}_R}/g_{DM}$ that factorises from the cross section through a factor Λ^{-4}, thus we can easily rescale the energy scale Λ with the value of $m_{\tilde{u}_R}$ that we have imposed, obtaining the plot in fig. 3.10. We will see in the following how this plot changes in the full theory.

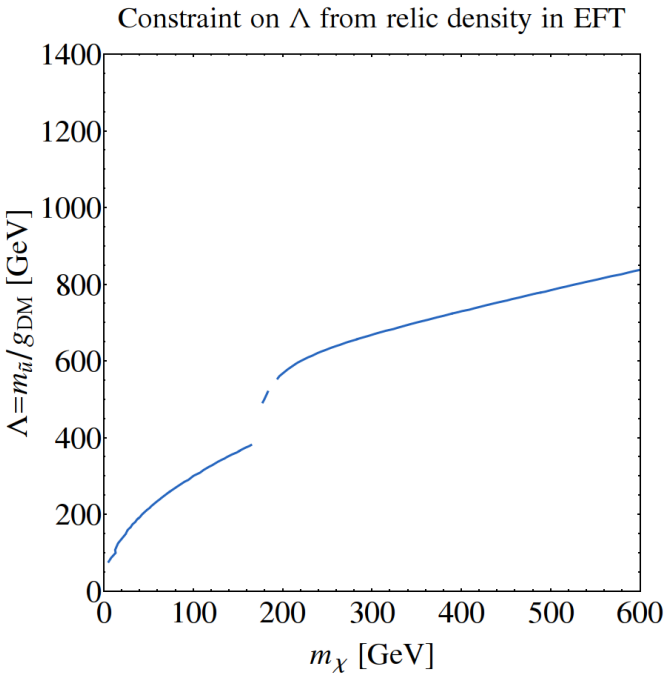

Figure 3.10: Value of the scale $\Lambda = m_{\tilde{u}_R}/g_{DM}$ in the EFT for model B that give the correct relic density, as a function of m_χ. As discussed in the text, the cutoff scale sharply decreases for m_χ below m_t because the annihilation channels reduce from three to two. The plot is discontinuous in a small region around m_t because there the factor b is singular (because of the expansion around zero of the square root factor which comes from the phase space integration).

The plot in fig. 3.11, which displays the contour lines for g_{DM} that yield the correct relic density as a function of m_χ (at fixed $m_{\tilde{u}_R}$), shows the relevant difference with respect to what happens in model A, where, for given mass parameters, the rise of the couplings brings $\Gamma_{Z'}$ to very high values that suppress the cross-section and forbid the relic abundance to track the correct one. This phenomenon is a consequence of the exchange of the mediator in the s-channel, and is not a feature of model B: figure 3.11 shows that, for a fixed mediator mass $m_{\tilde{u}_R}$, there is always a couple of values (m_χ, g_{DM}) that brings to the correct relic abundance. We recall the difference with respect to figure 3.6, where the contour lines for g_X could not go below a given threshold in m_X.

We now build a sample of allowed values for the triplet of parameters $(g_{DM}, m_\chi, m_{\tilde{u}_R})$ by choosing randomly $g_{DM} \in [0.1, 4\pi]$, $m_\chi \in [5, 1000]$ GeV (with a uniform distribution on the logarithm of these quantities), and by calculating $m_{\tilde{u}_R}$ by requiring that it brings the correct relic density. We reject the resulting triplet of parameters if $m_\chi > 0.9\, m_{\tilde{u}_R}$. Then we study the distribution of the points of our sample in the parameter space. We begin by discussing the parameter that is relevant for the validity of the EFT: the ratio $\beta = m_\chi/m_{\tilde{u}_R}$. As observed in the previous section, the condition to assure that t, $u \ll m^2_{\tilde{u}_R}$ is that $\beta \ll 1$. The distribution of the allowed points in the $(m_\chi, m_{\tilde{u}_R})$ plane is shown in fig. 3.12: we can see that, similarly to what happened in model A, a large amount of them lies within the region of $\beta < 0.2$ (we recall that

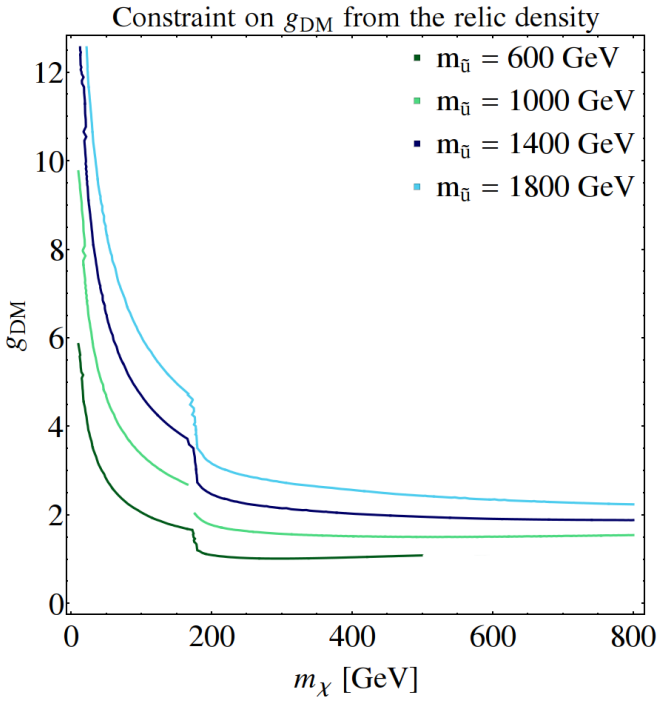

Figure 3.11: Contour lines in the (m_χ, g_{DM}) plane for fixed mediator masses. The required value for g_{DM} rises sharply for m_χ below the threshold of the top mass, because of the disappearance of that annihilation channel, and the consequent decrease of the total annihilation cross section.

it is a logarithmic plot, thus the surface of the upper regions looks smaller than it actually is).

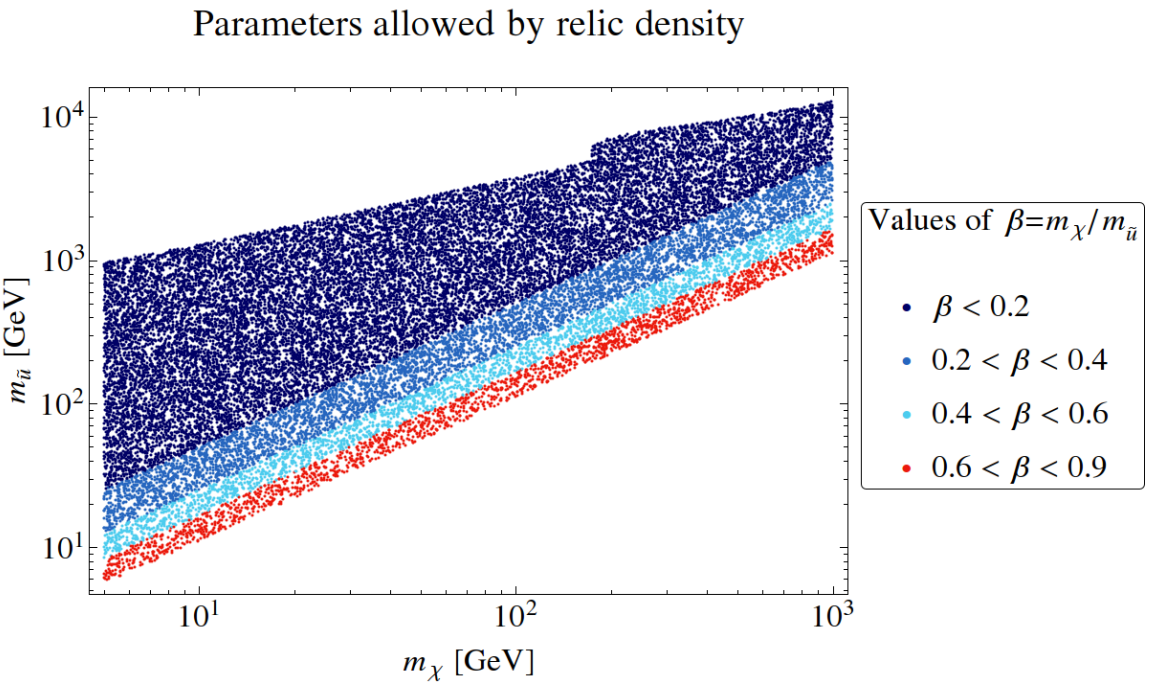

Figure 3.12: Distribution of the points of the sample in the $(m_\chi, m_{\tilde{u}_R})$ plane. The colour of the points depends on the corresponding ratio $\beta = m_\chi / m_{\tilde{u}_R}$.

We can now inspect how the plot obtained in the EFT for the limit on the cut-off scale Λ

(fig. 3.10) changes in the complete theory. We can guess that, since the EFT is valid in the limit $\beta \ll 1$, deviations from that curve will arise for higher β, i. e. for smaller $m_{\tilde{u}_R}$ (once we fix a value of m_χ on the horizontal axis). The denominators in eq. (3.18) are higher than $m^4_{\tilde{u}_R}$: thus the deviations from the EFT will show up in a shift downwards of the line of fig. 3.10, because the scale Λ must be smaller if the denominators change (increase) from the expression (3.20) to (3.18). In fig. 3.13 we can see a confirmation of this guess. We can also see that the overall effect of considering the complete theory with respect to EFT broadens the expected curve for Λ by roughly 30% of its value, thus it a rather relevant effect, even if it is not as crucial as in model A where in the complete theory the mediator could be resonantly produced.

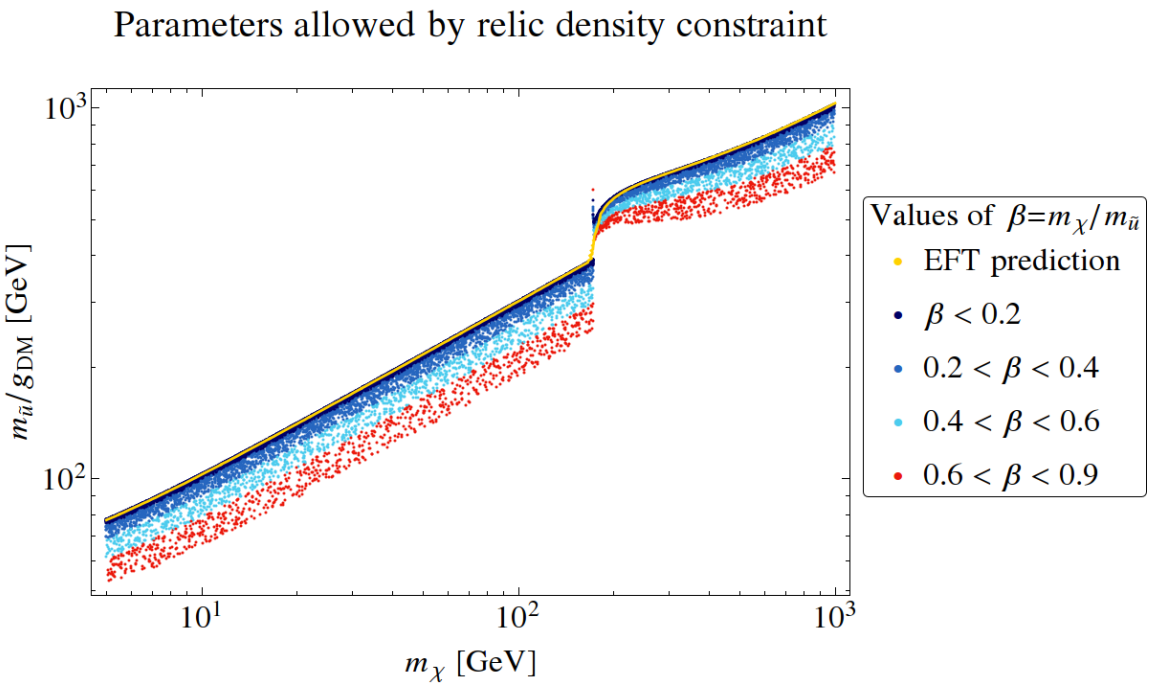

Figure 3.13: Distribution of the points of the sample in (m_χ, Λ) plane. The different colours correspond to different values of β. The thin yellow line corresponds to the prediction of the EFT: we can see that its prediction cohincides with that of the full theory for $\beta \ll 1$, and that the allowed range for Λ spans around the 30% of the value predicted by EFT.

From figure 3.13 we can infer the behaviour of the coupling constant for each of those points. Indeed, while the colours of the dots show that, for fixed m_χ, $m_{\tilde{u}_R}$ decreases (in the red region) of an order of magnitude, the scale $m_{\tilde{u}_R}/g_{DM}$ has a much lower excursion. Thus we expect that the coupling constant will scale like $m_{\tilde{u}_R}$: thus the upper region corresponds to higher values of g_{DM}. What is not predicted by the effective theory is the absolute value of the coupling g_{DM} in that region: the overall scale Λ of the EFT is sensitive only to the ratio $m_{\tilde{u}_R}/g_{DM}$, and not to the absolute value of g_{DM}, which is of crucial importance for discussing the validity of the perturbative description for the full theory. The plot in figure 3.14 shows that the region of validity of the EFT corresponds to a coupling even higher than 4 (red points). This phenomenon can be eventually attributed to the helicity suppression, which decreases the annihilation cross section and requires the coupling to grow larger. It is interesting however to notice that the limit that we recover from the effective theory turns out to correspond to a non-perturbative regime of the microscopic theory.

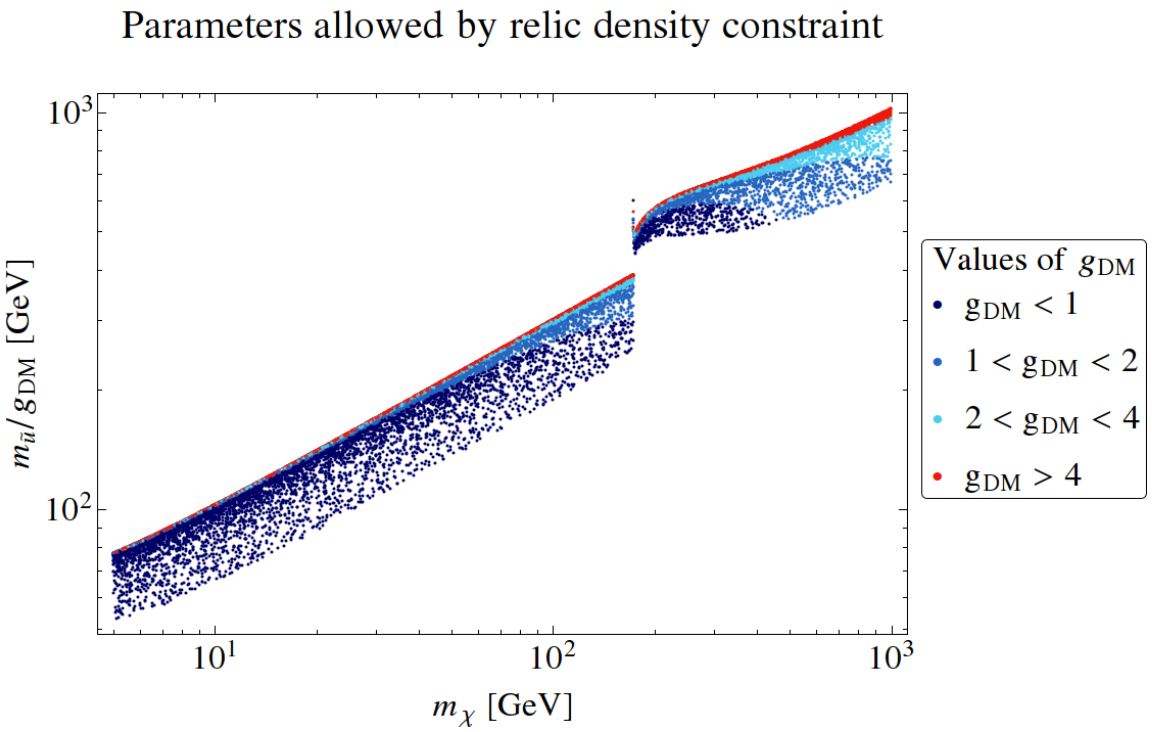

Figure 3.14: Distribution of the points of the sample in the (m_χ, Λ) plane. The various colours correspond to different values of the coupling constant $g_{\rm DM}$. The upper strip of red and light blue dots, which is the one predicted by the effective theory (we know from fig. 3.13 that it corresponds to low values of β), correspond to points with $g_{\rm DM} > 2$, thus to a strongly coupled regime of the microscopic theory.

3.4 Limits from direct detection

In this section, we discuss the limits from direct search experiments on the two models we consider. We have already discussed the main points of the procedure to calculate the event rate for a given experiment, starting from the microscopic theory, in section 2.1.1. In order to derive the exclusion limits on our models, we use the tools provided by Cirelli et al. in [22]: they supply a set of functions that allow to derive, through a straightforward recipe, the constraints on any EFT for the interaction between DM and quarks or gluons. In the following, we briefly review their procedure.

As we have already explained in 2.1.1, the starting point is an EFT at the microscopic level, which involves some among the 10 effective operators $\mathcal{O}_k^q$ of lowest dimension between quarks and DM, and the 4 effective operators $\mathcal{O}_k^g$ between quarks and gluons (for a complete list of them, see [53]). Therefore the interaction Lagrangian of the EFT reads

$$\mathcal{L}_{\rm eff}^{{\rm DM}-q,g} = \sum_{k=1}^{10} \sum_q c_k^q \mathcal{O}_k^q + \sum_{k=1}^{4} c_k^g \mathcal{O}_k^g \,. \tag{3.21}$$

As we mentioned in section 2.1.1, this Lagrangian is transposed to the nucleon level with the introduction of *form factors*, i. e. the expectation values of the operators $\mathcal{O}_k^q$, $\mathcal{O}_k^g$ on a nucleon ($N = n,\ p$, where n and p stand respectively for neutron and proton) state:

$$\mathcal{L}_{\rm eff}^{{\rm DM}\text{-}n,p} = \sum_{k=1}^{10} \sum_{N=n,\,p} c_k^N \mathcal{O}_k^N \,, \tag{3.22}$$

and the relations between the coefficients $c_k^{q,g}$ and c_k^N are given in [22]. This is the step that introduces the main uncertainties: indeed, the determination of the nucleon form factors through experiments and lattice QCD simulations is still subject to relevant uncertainties.

The following step consists in rewriting the previous operators in the non-relativistic limit. The resulting operators can be functions only of the exchanged momentum $\vec{q}$, the relative velocity $\vec{v}$ between DM and the nucleus, and the respective spins $\vec{s}_{\rm DM}$, $\vec{s}_N$. Among these operators, the 11 most relevant ones are listed in [22], together with the relations between the coefficients c_k^N and $\mathfrak{c}_i^N$ that appear in

$$\mathcal{L}_{\rm eff,\,NR}^{{\rm DM}-n,p} = \sum_{i=1}^{11} \mathfrak{c}_i^N(\lambda,\, m_X)\mathcal{O}_i^{\rm NR}\,, \tag{3.23}$$

where the $\mathfrak{c}_i^N$ are a function of the DM mass m_X and the undetermined coefficients of the model, denoted collectively by λ.

Then, we have to take into account the following series of steps, as we mentioned also in sec. 2.1.1:

- sum over the contributions from all the nucleons inside the nucleus, for each component T of the target, and taking the modulus squared of the amplitude, obtaining

$$\overline{|\mathcal{M}^2|}_{\rm T} = \frac{m_T^2}{m_N^2}\sum_{i,j=1}^{11}\sum_{N,N'=n,p}\mathfrak{c}_i^N(\lambda,\, m_X)\mathfrak{c}_j^{N'}(\lambda,\, m_X)F_{i,j}^{(N,N')}(v,\, E_R,\, T)\,, \tag{3.24}$$

  where m_T is the mass of the target nucleus and m_N is the mass of a nucleon (we can neglect the small difference between m_p and m_n), and $F_{i,j}^{(N,N')}$ are form factors that depend on specific target;

- deduce the differential cross section $\mathrm{d}\sigma/\mathrm{d}E_R$ with respect to the recoil energy;

- calculate the differential event rate $\mathrm{d}R_T/\mathrm{d}E_R$ with respect to the recoil energy: this step takes into account the DM velocity distribution and density;

- introduce suitable factors, specific to each experiment, to model the response of the detector to the signal. These include the response function, i. e. the probability that in an event with recoil energy E_R the measure gives an energy E', and the efficiency of the measurement as a function of the recoil energy;

- deduce the expected number of events observed by a given experiment, for each energy bin.

The crucial point of the procedure developed in [22] is that all the previous steps are *linear* with respect to the form factors $F_{i,j}^{(N,N')}$ introduced in eq. (3.24). This means that we can perform all the steps of the previous list on the form factors, to get *integrated form factors* $\widetilde{\mathcal{F}}_{i,j}^{(N,N')}$, and write the final result in a very simple form:

$$N^{\rm exp} = X\sum_{i,j=1}^{11}\sum_{N,N'=n,p}\mathfrak{c}_i^N(\lambda,\, m_X)\mathfrak{c}_j^{N'}(\lambda,\, m_X)\widetilde{\mathcal{F}}_{i,j}^{(N,N')}\,, \tag{3.25}$$

where $N^{\rm exp}$ is the total number of expected event and X is a fixed coefficient, function of the masses and the DM density. This consideration is crucial for our final result. Indeed, in order to derive a constraint on the parameters λ of the model (from the experiments that give a negative result), [22] introduces the likelihood ratio test statistic, i. e. the logarithm of the ratio

between the likelihood functions $\mathscr{L}$ of obtaining the experimentally observed data $\vec{N}^{\rm obs} = \vec{N}^{\rm exp} + \vec{N}^{\rm bkg}$ (with the vector notation we denote a histogram over the energy bins, and $\vec{N}^{\rm bkg}$ are the background events), over the likelihood function for obtaining the background only:

$$\mathrm{TS}(\lambda,\, m_X) = -2\ln\left(\frac{\mathscr{L}(\vec{N}^{\rm obs}|\lambda)}{\mathscr{L}(\vec{N}^{\rm bkg})}\right).$$

This quantity has an approximate χ^2 distribution, with a number of degrees of freedom equal to the number of free parameters λ of the model. Therefore, given a certain confidence level (CL), we can infer the limit on the parameters by solving $\mathrm{TS}(\lambda,\, m_X) = \chi^2_{\rm CL}$, i. e. the χ^2 value corresponding to the desired CL for a given number of free parameters.

The last step of the procedure of [22] is the following: once we fix a bound on the parameter $\lambda_{\rm B}(m_X)$ of a simple benchmark model (they consider λ_B as the cut-off scale of the effective operator corresponding to a scalar coupling of DM with protons), we can get the limit on another model by imposing $\mathrm{TS}(\lambda_{\rm B}(m_X),\, m_X) = \mathrm{TS}(\lambda,\, m_X)$, which can be shown to be solved by

$$\begin{gathered}\sum_{i,j=1}^{11}\sum_{N,N'=n,p} \mathfrak{c}_i^N(\lambda,\, m_X)\mathfrak{c}_j^{N'}(\lambda,\, m_X)\widetilde{\mathcal{F}}_{i,j}^{(N,N')}(m_X) = [\lambda_{\rm B}(m_X)]^2\widetilde{\mathcal{F}}_{1,1}^{(p,p)}(m_X) \quad \Longrightarrow \\ \sum_{i,j=1}^{11}\sum_{N,N'=n,p} \mathfrak{c}_i^N(\lambda,\, m_X)\mathfrak{c}_j^{N'}(\lambda,\, m_X)\mathcal{Y}_{i,j}^{(N,N')}(m_X) = [\lambda_{\rm B}(m_X)]^2\,, \qquad (3.26) \\ \mathcal{Y}_{i,j}^{(N,N')} \equiv \mathcal{F}_{i,j}^{(N,N')}\Big/\mathcal{F}_{1,1}^{(p,p)}\,.\end{gathered}$$

In conclusion, the linearity of the event rate with respect to the form factors brings to eq. (3.26), which can be solved numerically rather easily, and allows to infer, with a few steps, the constraint on the parameters of any EFT for the interaction between DM and quarks or gluons. The overall procedure will be clarified by its application to models A and B.

3.4.1 Constraints on model A from direct searches

First of all, we must understand if the EFT of model A is reliable in the context of direct search experiments.

The Feynman amplitude for the interaction $Xq \to Xq$ at the tree level can be simply obtained by eq. (3.11) through a *crossing symmetry*, by replacing the Mandelstam variable s by t and viceversa. Then the modulus squared of the amplitude immediately follows from eq. (3.13), and reads (we must average over the initial spin configurations, thus we divide by 4)

$$\overline{|\mathcal{M}^2|} = \frac{12\, g_q^2 g_X^2}{(t-m_{Z'}^2)^2+\Gamma_{Z'}^2 m_{Z'}^2}\left[\frac{s^2+u^2}{2} - m_X^4 - m_q^4 + 6m_X^2 m_q^2 - 8m_q^2 m_X^2\frac{t}{m_{Z'}^2} + 4m_q^2 m_X^2\frac{t^2}{m_{Z'}^4}\right].$$

This result, obtained in the complete theory, must be compared with the one we would get from the effective theory, that is

$$\overline{|\mathcal{M}^2|} = \frac{12\, g_q^2 g_X^2}{m_{Z'}^4}\left[\frac{s^2+u^2}{2} - m_X^4 - m_q^4 + 6m_X^2 m_q^2\right].$$

Thus we can safely use the EFT to describe the DM-quark interactions in direct search experiments if the following equations hold:

$$t \ll m_{Z'}\,, \qquad \Gamma_{Z'} \ll m_{Z'}\,. \qquad (3.27)$$

The first condition is always satisfied in the non-relativistic regime. Indeed, the momenta of the incoming and outgoing X particle in the c. o. m. frame are respectively

$$p_1 = (E^*,\, 0,\, 0,\, m_X v^*)\,, \quad k_1 = (E^*,\, m_X v^* \sin\theta,\, 0,\, m_X v^* \cos\theta)\,,$$

where E^* and v^* are the energy and velocity of X in the c. o. m. frame. Since v^* is of order 10^{-3} for the elastic scattering on nuclei, we get

$$t = (p_1 - k_1)^2 = -m_X^2 (v^*)^2 \Big(\sin^2\theta + (1-\cos\theta)^2\Big) = -4 m_X^2 (v^*)^2 \sin^2\frac{\theta}{2} \ll m_X^2,\, m_{Z'}^2\,.$$

We now discuss the second condition of eq. (3.27). If we suppose not to neglect $\Gamma_{Z'}$ with respect to $m_{Z'}$, then the cross section for the DM-quark interaction in the complete theory is proportional to $1/(\widetilde{\Lambda})^4$ with $\widetilde{\Lambda} = m'_Z \sqrt[4]{1+(\Gamma_{Z'}/m_{Z'})^2}/\sqrt{g_q g_x} = \Lambda \sqrt[4]{1+(\Gamma_{Z'}/m_{Z'})^2}$, while the EFT gives an overall coefficient $1/\Lambda^4$. Then, once we fix m_X, the given limit ℓ that we obtain from the experiments should be assigned to $\widetilde{\Lambda}$ instead of Λ: since $\sqrt[4]{1+(\Gamma_{Z'}/m_{Z'})^2} > 1$, the limit ℓ is in general a conservative one, i. e. the true limit on $m'_Z/\sqrt{g_q g_x}$ is lower (of a factor $\sqrt[4]{1+(\Gamma_{Z'}/m_{Z'})^2}$) than the one that we get from the use of the EFT. This correction is always small in the perturbative regime: the factor $\sqrt[4]{1+(\Gamma_{Z'}/m_{Z'})^2}$ brings a 10% correction only for $\Gamma_{Z'}/m_{Z'} > 0.7$.

Thus we can safely proceed with the effective theory for model A, with interaction (3.2c). Using the notation of [22], we have

$$\mathcal{L}_{\text{eff}}^{\text{DM}-q} = \sum_q c_8^q \mathcal{O}_8^q = -\frac{1}{\Lambda^2}(\overline{X}\gamma^\mu\gamma^5 X)\sum_q(\overline{q}\gamma_\mu\gamma^5 q)\,, \quad c_8^q = -\frac{1}{\Lambda^2}.$$

The corresponding DM-nucleon interaction is given by

$$\mathcal{L}_{\text{eff}}^{\text{DM}-N} = \sum_{N=n,p} c_8^N \mathcal{O}_8^N = \sum_{N=n,p} c_8^N (\overline{X}\gamma^\mu\gamma^5 X)(\overline{N}\gamma_\mu\gamma^5 N)\,, \quad c_8^N = \sum_q c_8^q \Delta_q^{(N)} = -\frac{1}{\Lambda^2}\sum_q \Delta_q^{(N)}\,,$$

where $\Delta_q^{(N)}$ is the fraction of nucleon spin carried by the quark q, defined through the hadronic matrix element $\langle N|\overline{q}\gamma_\mu\gamma^5 q|N\rangle$. In general, $\Delta_q^{(n)} = \Delta_q^{(p)}$, and they are negligible for c, b, t quarks. The uncertainty on these coefficients is rather large: if we define $\Delta \equiv \sum_q \Delta_q^{(p)}$, the values of this quantity (according to the references in [22]) can vary up to the 30%. We decide to use the values used by the references [54, 56, 57] of [22], which are used in the software *MicrOMEGA*, and give $\Delta = 0.32$, because they are among the most recent available, and are the ones endowed by most recent papers on direct detection. Therefore,

$$\mathcal{L}_{\text{eff}}^{\text{DM}-N} = -\frac{\Delta}{\Lambda^2}(\mathcal{O}_8^n + \mathcal{O}_8^p)\,.$$

Finally, the non-relativistic limit of this Lagrangian gives

$$_{\text{out}}\langle X,\, N|\mathcal{O}_8^N|X,\, N\rangle_{\text{in}} = -16 m_X m_N \mathcal{O}_4^{\text{NR}}\,, \quad \mathcal{O}_4^{\text{NR}} = \vec{s}_X \cdot \vec{s}_N\,,$$
$$\mathfrak{c}_4^N = 16 m_X m_N \frac{\Delta}{\Lambda^2}\,.$$

In conclusion, in model A eq. (3.26) reads

$$[\lambda_{\text{B}}(m_X)]^2 = \Big[\mathfrak{c}_4^N(\Lambda,\, m_X)\Big]^2 \Big[\mathcal{Y}_{4,4}^{(n,n)}(m_X) + 2\mathcal{Y}_{4,4}^{(n,p)}(m_X) + \mathcal{Y}_{4,4}^{(p,p)}(m_X)\Big]\,,$$

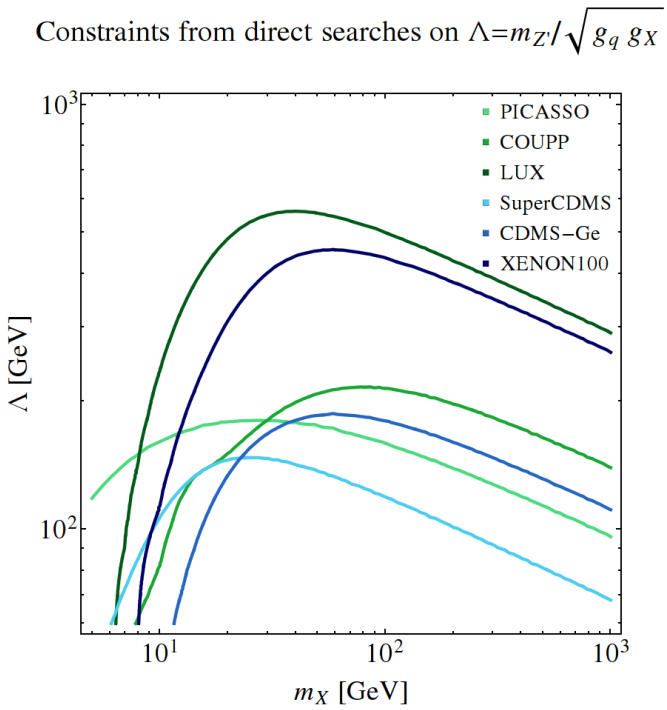

Figure 3.15: Lower limits on the scale $\Lambda = m_{Z'}/\sqrt{g_q g_X}$ as a function of m_X from various direct search experiments.

where we used the fact that $\mathcal{Y}_{i,j}^{(N,N')} = \mathcal{Y}_{j,i}^{(N',N)}$. With the use of the functions $\mathrm{TS}(\lambda_B(m_X), m_X)$ and $\mathcal{Y}_{i,j}^{(N,N')}$ provided by the authors of [22], we can extract then a limit on the parameter Λ from six experiments: the results are shown in figure 3.15.

The strongest constraint comes from the LUX experiment, operating at the Sanford Underground Research Facility in South Dakota. This experiment uses liquid Xenon, which is sensible to spin-dependent cross sections because of the unpaired neutron in the isotopes ^{129}Xe and ^{131}Xe. Since in this model this is the strongest constraint, it is sufficient to use only this experiment to derive the constraints from direct searches. We can see that the constraint from direct searches is stronger for DM masses of the order of the mass of the nuclei used in the experiment, because there the recoil energy is higher for kinematical reasons, and it decreases for increasing m_X, because even if the scattering cross section tends to a constant ($\sigma_{XN} \propto \mu_N^2/\Lambda^4$) there is an additional $1/m_X$ factor in the rate, since $\mathrm{d}R/\mathrm{d}E_R \propto n_{\mathrm{DM}} = \rho_0/m_X$ (see eq. (2.2) and the following comments).

We can now superimpose this plot to the corresponding one obtained from the relic density constraint (fig. 3.8), with the result shown in fig. 3.16.

The exclusion limit from LUX is competitive with the relic density constraint: a large portion of the parameter space in which $\Gamma_{Z'}/m_{Z'}$ must be greater than 0.25 to yield the correct Ω_{DM} is excluded, and in the region $14 < m_X/\mathrm{GeV} < 30$ direct searches and the relic density constraints nearly rule out model A. Very interestingly, that region is not completely excluded by direct searches only thanks to the light blue points, which are not predicted by the EFT (they correspond to $m_X > 0.2 m_{Z'}$). Thus, once again, the difference between the constraints predicted by the effective theory and those obtained in the full theory is appreciable.

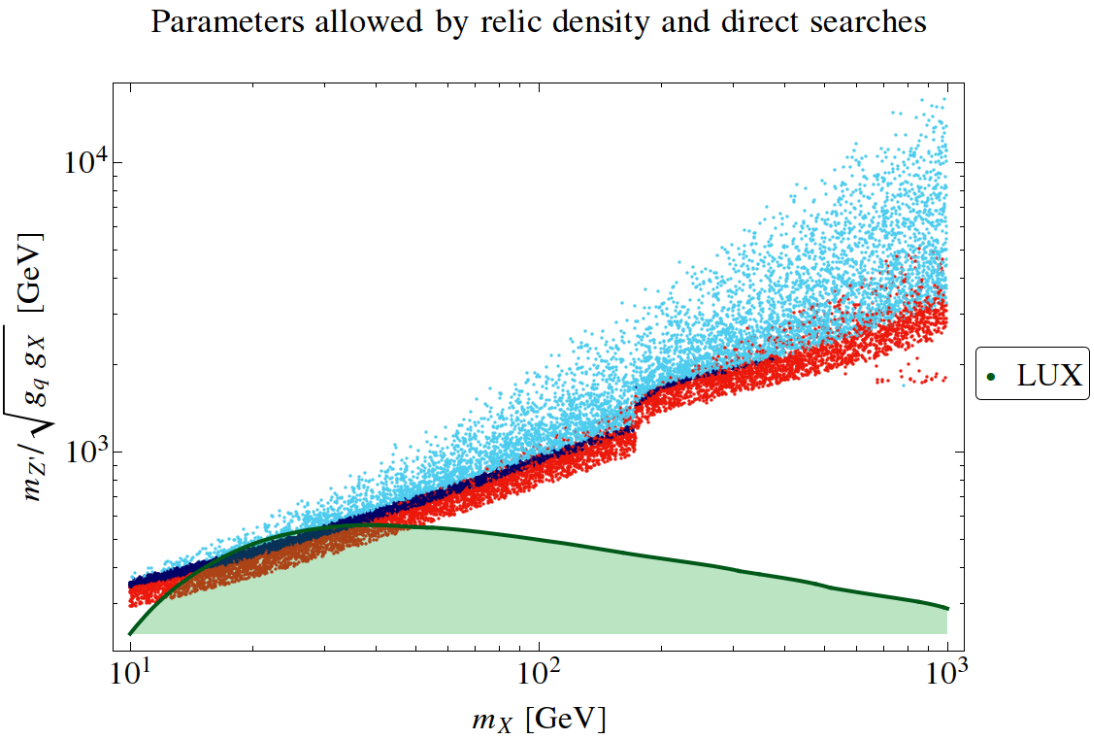

Figure 3.16: Superimposition of the limits from the relic density constraint and the LUX limit on the scale $\Lambda = m_{Z'}/\sqrt{g_q g_X}$ as a function of m_X. The legend for the colours of the dots is the same of fig. 3.8: the red dots correspond to $0.25 < \Gamma_{Z'}/m_{Z'} < 1$, and the remaining ones (with $\Gamma_{Z'}/m_{Z'} < 0.25$) are dark and light blue respectively if $\beta = m_X/m_{Z'} < 0.2$ or $\beta > 0.2$.

3.4.2 Constraints on model B from direct searches

We now discuss the implementation of the bounds from direct searches on model B. First of all, as we have done for model A, we must discuss whether the application of the effective theory is consistent.

As mentioned in the previous section, the modulus squared of the amplitude for the process $\chi q \to \chi q$ can be obtained by the corresponding formula for the process $\chi\chi \to q\bar{q}$ by a crossing symmetry, which exchanges the Mandelstam variables s and t, leaving u unchanged. The crucial point is that in the direct search detection, both s and u are not suppressed by the DM velocity. Indeed, we can write the momenta of the particles involved in the process as (we denote by v^* the speed of the incoming particles in the c. o. m. frame, of order 10^{-3}, and we approximate to 0 the mass of the up quark which is the only relevant one because of PDFs and the interaction of χ with up-type quarks):

$$p_1 = (m_\chi,\, 0,\, 0,\, m_\chi v^*) + \mathcal{O}(v^2)\,, \quad k_1 = (m_\chi,\, m_\chi v^* \sin\theta,\, 0,\, m_X v^* \cos\theta) + \mathcal{O}(v^2)\,,$$
$$p_2 = (m_\chi v^*,\, 0,\, 0,\, -m_\chi v^*) \quad k_2 = (m_\chi v^*,\, -m_X v^* \sin\theta,\, 0,\, -m_\chi v^* \cos\theta)\,,$$
$$s = (p_1 + p_2)^2 = m_\chi^2[1 + (v^*)^2] + \mathcal{O}(v^2)\,,$$
$$u = (p_1 - k_2)^2 = m_\chi^2[1 - 2v^* - (v^*)^2(1 + 2\cos\theta)] + \mathcal{O}(v^2)\,.$$

Thus we see that without the specific assumption $m_\chi \ll m_{\tilde{u}_R}$, it is not possible to assume that t, u are much smaller than $m^2_{\tilde{u}_R}$, thus it is not possible to trust the effective theory, which is valid only if that limit holds. For this reason, we must be cautious about the interpretation of the constraint from direct searches on this limit.

Now we derive the bounds from direct searches on the scale of the effective theory of model B, keeping in mind that they are reliable only in the regime $\beta \ll 1$. Using the notation of [22], the effective Lagrangian (3.4) reads

$$\mathcal{L}_{\text{eff}}^{\text{DM}-q} = \sum_{q=u,c,t} c_6^q \mathcal{O}_6^q + c_8^q \mathcal{O}_8^q\,, \quad c_6^q = c_8^q = -\frac{1}{8\Lambda^2}.$$

The corresponding DM-nucleon interaction is given by

$$\mathcal{L}_{\text{eff}}^{\text{DM}-N} = \sum_{N=n,p} c_6^N \mathcal{O}_6^N + c_8^N \mathcal{O}_8^N = \sum_{N=n,p} c_6^N (\overline{\chi}\gamma^\mu\gamma^5\chi)(\overline{N}\gamma_\mu N) + c_8^N (\overline{\chi}\gamma^\mu\gamma^5\chi)(\overline{N}\gamma_\mu\gamma^5 N)\,,$$

$$c_6^N = \begin{cases} 2c_6^u = -2/8\Lambda^2 & N = p, \\ c_6^u = -1/8\Lambda^2 & N = n, \end{cases} \qquad c_8^N = \sum_{q=u,c,t} c_8^q \Delta_q^{(N)} = -\frac{1}{\Lambda^2}\Delta_u^{(N)}\,,$$

where $\Delta_u^{(N)} \equiv \Delta_u = 0.84$ in the reference we cited in the previous section. The last step brings to the non-relativistic limit of the interaction between DM and nucleon:

$${}_{\text{out}}\langle \chi,\, N|\mathcal{O}_6^N|\chi,\, N\rangle_{\text{in}} = 8m_\chi m_N \mathcal{O}_8^{\text{NR}} + 8m_\chi \mathcal{O}_9^{\text{NR}}\,, \quad \mathcal{O}_8^{\text{NR}} = \vec{s}_\chi \cdot \vec{v}_\perp\,, \quad \mathcal{O}_9^{\text{NR}} = i\vec{s}_\chi \cdot (\vec{s}_N \times \vec{q})\,,$$

$${}_{\text{out}}\langle \chi,\, N|\mathcal{O}_8^N|\chi,\, N\rangle_{\text{in}} = -16 m_\chi m_N \mathcal{O}_4^{\text{NR}}\,, \quad \mathcal{O}_4^{\text{NR}} = \vec{s}_\chi \cdot \vec{s}_N\,,$$

$$\mathfrak{c}_4^N = 2m_\chi m_N \frac{\Delta_u}{\Lambda^2}\,, \quad \mathfrak{c}_8^N = -m_\chi m_N \frac{1}{\Lambda^2}\cdot\eta_N\,, \quad \mathfrak{c}_9^N = -m_\chi \frac{1}{\Lambda^2}\cdot\eta_N\,,$$

where we denote $\eta_N = 2$ for $N = p$, $\eta_N = 1$ for $N = n$. We notice that the coefficients of the NR expressions of $\mathcal{O}_6^N$ (coming from the interaction term (3.4a)) and $\mathcal{O}_8^N$ (coming from (3.4b)) have opposite signs: this means that the interference between the amplitudes corresponding to the two operators is destructive. This interference will decrease the limit from direct searches on the scale Λ.

We are now able to write down the expression (3.26) for model B. By writing explicitly the coefficients $\mathfrak{c}_i^N$, and recalling that $\mathcal{Y}_{i,j}^{(N,N')} = \mathcal{Y}_{j,i}^{(N',N)}$, we obtain the following expression (we understand the argument (m_χ) of the $\mathcal{Y}$ functions)

$$\begin{aligned}
[\lambda_{\text{B}}(m_\chi)]^2 = \frac{1}{\Lambda^4}\Big[& 4m_\chi^2 m_N^2 \Delta_u^2 \Big(\mathcal{Y}_{4,4}^{(n,n)} + 2\mathcal{Y}_{4,4}^{(n,p)} + \mathcal{Y}_{4,4}^{(p,p)}\Big) \\
& + m_\chi^2 m_N^2 \Big(\mathcal{Y}_{8,8}^{(n,n)} + 4\mathcal{Y}_{8,8}^{(n,p)} + 4\mathcal{Y}_{8,8}^{(p,p)}\Big) \\
& + m_\chi^2 \Big(\mathcal{Y}_{9,9}^{(n,n)} + 4\mathcal{Y}_{9,9}^{(n,p)} + 4\mathcal{Y}_{9,9}^{(p,p)}\Big) \\
& - 2m_\chi^2 m_N^2 \Delta_u \Big(2\mathcal{Y}_{4,8}^{(n,n)} + 3\mathcal{Y}_{4,8}^{(n,p)} + 2\mathcal{Y}_{8,4}^{(n,p)} + 4\mathcal{Y}_{4,8}^{(p,p)}\Big) \\
& - 2m_\chi^2 m_N \Delta_u \Big(2\mathcal{Y}_{4,9}^{(n,n)} + 3\mathcal{Y}_{4,9}^{(n,p)} + 2\mathcal{Y}_{9,4}^{(n,p)} + 4\mathcal{Y}_{4,9}^{(p,p)}\Big) \\
& + m_\chi^2 m_N \Big(2\mathcal{Y}_{8,9}^{(n,n)} + 4\mathcal{Y}_{8,9}^{(n,p)} + 4\mathcal{Y}_{9,8}^{(n,p)} + 8\mathcal{Y}_{8,9}^{(p,p)}\Big)\Big]\,.
\end{aligned}$$

With the use of the functions $\mathcal{Y}$ and of the test function provided by [22] we obtain the exclusion plot shown in figure 3.17. In the region of low m_χ, below 8 GeV, the stronger limit comes from the PICASSO experiment, situated at SNOLAB in Ontario, that is sensible also to very low DM masses because it uses a C_4F_10 target, made of very light nuclei.

We can superimpose this exclusion limit from direct searches with the one we have obtained for the constraint from the relic density. The result is shown in figure 3.18.

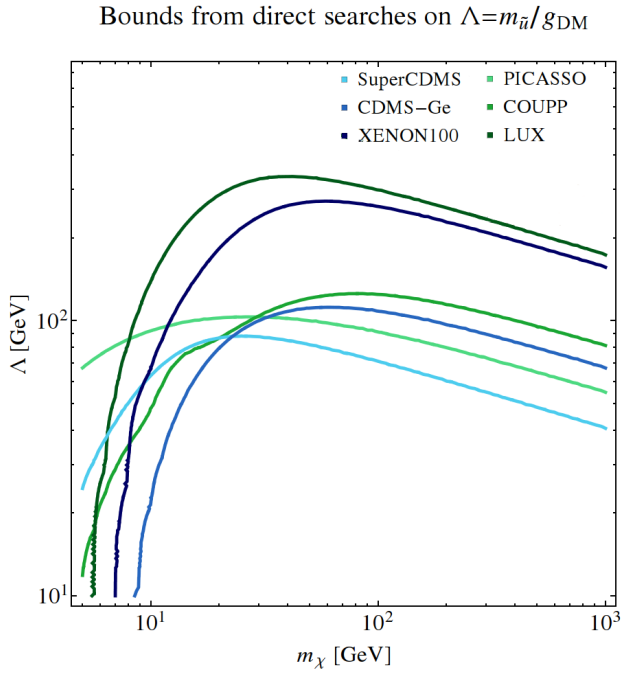

Figure 3.17: Lower limits on the scale $\Lambda = m_{\tilde{u}_R}/g_{\rm DM}$ as a function of m_χ from various direct search experiments.

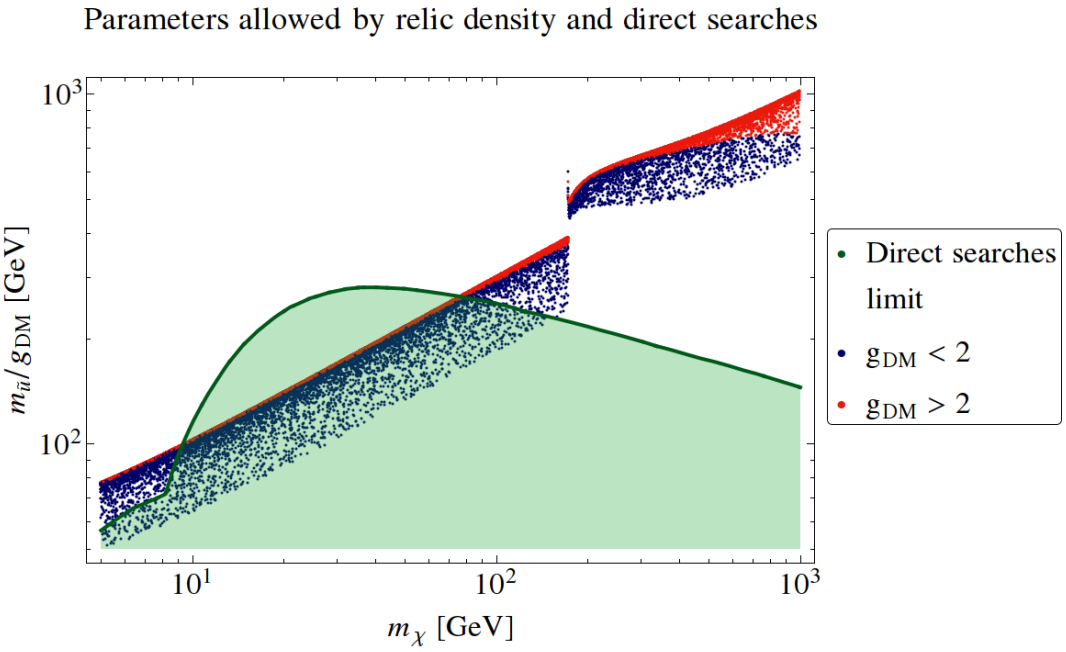

Figure 3.18: Overlay of the lower limit on the cut-off scale $\Lambda = m_{\tilde{u}_R}/g_{\rm DM}$ as a function of m_χ from direct searches with the distribution of the points in the parameter space yielding the correct relic abundance.

In model B, the exclusion limit from direct searches is much more relevant, and excludes the region from 10 to 80 GeV for m_χ. We must keep in mind anyway that the limit from direct searches uses the effective theory, and the result with the complete theory could be different: in particular, the limit will be slightly lower once we take into account a finite β. On the other hand, we have seen in the relic density calculation that this effects should be expected to yield

a difference around $20 - 30\%$, thus the excluded range will shrink but will survive even in the complete theory.

3.5 Constraints from the flux of $\overline{p}$

An important probe for a DM particle interacting with quarks is the observation of the flux of antiprotons in the cosmic rays arriving on the Earth from our galaxy. Indeed, the product of DM annihilations would include protons and antiprotons, and the latter could in principle offer an efficient probe for this type of interaction, given the low amount of antiparticles in the flux of cosmic rays. The background is given by the antiprotons produced during the diffusion of cosmic rays in the galaxy: they can be produced for example through the interactions with the nuclei that populate the interstellar medium, or they could be the result of hadronic interactions of protons accelerated by Supernova remnants; thereafter, they are accelerated by the same sources that accelerate primary cosmic rays [54, 55].

The crucial point, in order to analyse the observations of space-based experiments as PAMELA or FERMI-Lat, is to have a reliable model for the production of cosmic rays and their diffusion in the galaxy, from their origin until they reach the Earth. The starting point for this analysis is a diffusion equation, accounting for the acceleration of astroparticles due to magnetic fields in the galaxy, and energy losses for charged particles. Then, it is necessary to provide a simple geometric model for the galaxy, and reasonable assumptions about the sources of the acceleration of cosmic rays, and the convective motions in the interstellar medium. The variety of models that one can propose are then cross-checked with the experimental observations. Returning back to our goal, it is possible to tune the parameters of the allowed models with the observed flux of protons and the ratio of the observed boron-to-carbon nuclei flux in cosmic rays, in order to predict with these parameters the flux of antiprotons. The agreement with the observed flux is today rather convincing, and the absence of anomalies yields upper exclusion limits on the thermally averaged annihilation cross section of DM to $q\overline{q}$ today. Nevertheless, even if future observations (as the forthcoming results of AMS) were in disagreement with the expected rate of $\overline{p}$ cosmic rays, some caution is in order before claiming that this is an indirect signal of DM annihilation: as discussed in [55], we could have difficulties in testing this possibility against astrophysical explanations for a possible anomaly.

We do not go into further details in this topic. In the following sections, we check the exclusion limits from the observed flux of $\overline{p}$ cosmic rays for models A and B. We take the bounds derived in [54] on the annihilation cross section of DM into $q\overline{q}$ today, as a function of the DM mass, for two sets of astrophysical parameters, called MED and MAX in ref. [54][3].

In order to derive the constraints on our models, we plot the thermally averaged annihilation cross section in the limit of zero temperature (hence $x \to \infty$), that from eq. (B.11) reads

$$\langle \sigma v \rangle = \frac{a}{4g^2 m_{\rm DM}^2} \tag{3.28}$$

for the annihilation into two quarks, and we compare it with the two exclusion limits obtained in [54] with the MED and MAX parameters.

3.5.1 Constraints on model A from the $\overline{p}$ flux

In Model A, the helicity suppression dicussed in section 3.3.2 makes the cross sections for the annihilation into light quarks (up, down, strange, charm) negligible with respect to the annihi-

[3] Ref. [54] uses also another set of parameters called MIN, which is ruled out by [56]. For a recent discussion of the impact of the uncertainties about the propagation model for cosmic rays on the estimate of the $\overline{p}$ flux, see [57]

lation into bottom and top. Thus we plot the distribution of $\langle\sigma v\rangle$ (eq. (3.28)) for the annihilation into bottom (for $m_b < m_X < m_t$) or top (dominant for $m_X > m_t$) quarks, as a function of m_X, for the points in the parameter space that satisfy the relic density constraint. Then we superimpose the upper limit on this quantity from [54], for the MED parameters (which are more conservative in the assumptions on the model for cosmic rays propagation) and the MAX ones. The result is shown in figure 3.19. The lines that we display in the plot correspond to the upper limit on the $X\overline{X} \to b\bar{b}$ thermally averaged cross section: this is indeed nearly identical to the limit $X\overline{X} \to t\bar{t}$, thus the same line can be read as a limit for both annihilation channels.

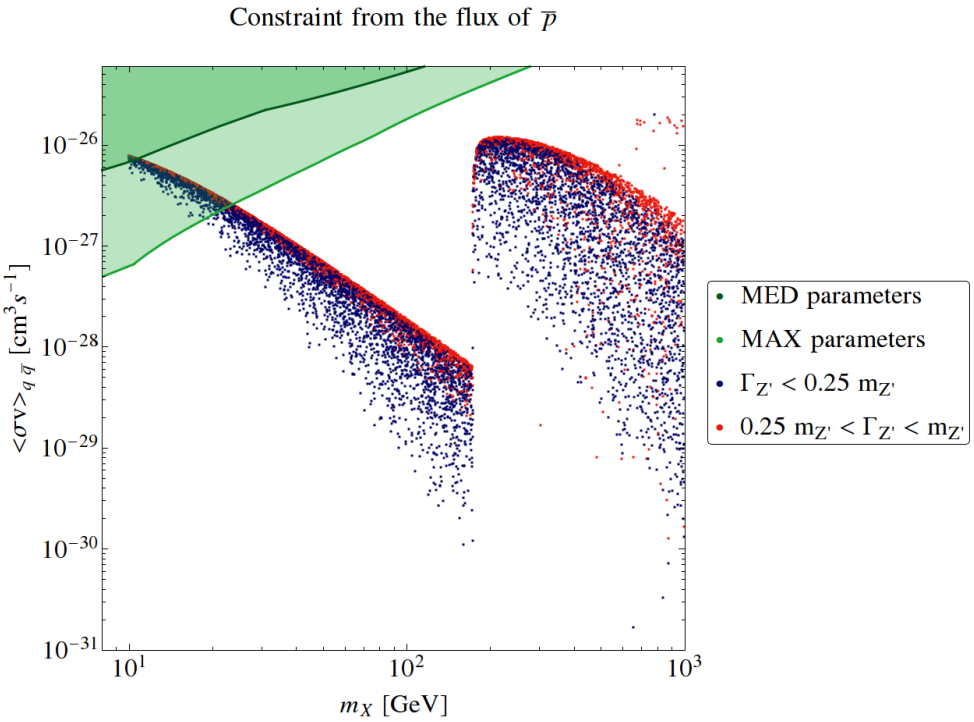

Figure 3.19: Plot of the quantity $\langle\sigma v\rangle$ of eq. (3.28) for the annihilation into bottom (for $m_b < m_X < m_t$) or top (for $m_X > m_t$) quarks, as a function of m_X, for the sample of points in the parameter space that satisfy the relic density constraint. The points in red correspond to a strongly coupled Z' boson. Superimposed in darker and lighter green are the excluded regions from [54] for the MED and MAX parameters, respectively.

We can see that the observation of the flux of $\overline{p}$ in cosmic rays, in model A, poses a bound only for the annihilation into $b\bar{b}$. Indeed, the bound for the annihilation into $t\bar{t}$ is basically identical to the previous one, and the limit is competitive with the relic abundance constraint only for DM masses below $\mathcal{O}(10)$ GeV, thus largely below the top mass threshold. Nevertheless, the bound from $b\bar{b}$ annihilations is not completely negligible: if we trust the MAX astrophysical parameters, they pose a lower limit on m_X around 20 GeV. The more conservative MED bound instead is almoust touching the lower limit of 10 GeV (we recall that this sample was generated for $10 < m_X/\text{ GeV} < 1000$). Nevertheless, this plot shows that the impact of the bound from antiprotons in cosmic rays can be relevant for low DM masses; on the other hand, a possible future anomaly could be at first sight a very interesting hint for DM annihilations, but as discussed for example in [55] it could be difficult to discard alternative astrophysical explanations.

3.5.2 Constraints on model B from the $\overline{p}$ flux

In the case of model B, our initial choice of the quantum numbers of the scalar mediator is crucial for what concerns the constraint from the flux of antiprotons. Indeed, we have chosen $\widetilde{u}_R$ to have the same quantum numbers of the up, right-handed quarks. Thus, given the helicity suppression which makes the coefficient a of eq. (B.9) negligible for $m_\chi < m_t$, the only relevant constraints from the $\overline{p}$ flux in cosmic rays comes from the annihilation to top quarks. The situation would have been very different if at the beginning we had made the DM interact with down-type right-handed quarks (which would have been constrained only by the $\chi\chi \to b\bar{b}$ annihilation) or with the left-handed doublet (bringing to an interaction with all the quark flavours).

We have seen that in model A the relevant limit is the one for the annihilation into $b\bar{b}$. In the case of model B, since there is still the helicity suppression, the annihilation cross section into light quarks (u, c) is completely negligible, then we expect that the bound from $\overline{p}$ does not constrain model B. This is indeed what happens, as we can see from fig. 3.20. Thus, we can conclude that model B is not constrained by this type of indirect search.

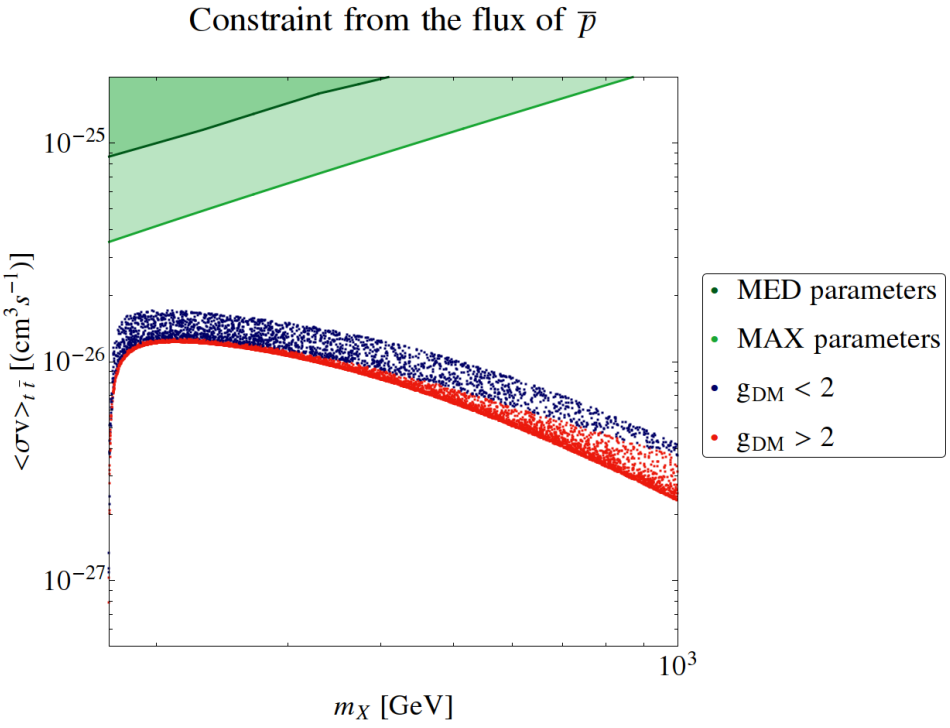

Figure 3.20: Plot of the quantity $\langle\sigma v\rangle$ (eq. (3.28)) for the annihilation into top quarks (in model B, DM interacts only with up-type right-handed quarks) as a function of m_χ, for the sample of points in the parameter space that satisfy the relic density constraint. Superimposed in darker and lighter green respectively are the upper exclusion limits from [54] for the MED and MAX parameters.

3.6 Signals at colliders

In this section, we will review the most relevant limits from hadronic collider searches on the models we consider. The constraints can come from both the search of the mediators and the search of the DM particle in monojet or multijets plus $\not{E}_T$.

As we have also discussed in sec. 2.1.3, collider searches can be in general more constraining than various types of experimental constraints, but are also subject to some limitations in certain domains of the parameter space: on one hand, they are less sensitive to the nature of the interaction of the interaction of DM with quarks, because in the high energy regime effects such as the helicity suppression are no more relevant, and the experimental search does not give sensible differences for vector or axial-vector quark currents. On the other hand, the high energy regime of a collider such as the LHC could also hide the DM particle if it is very weakly interacting and the mass parameters of the model are sufficiently low. Eventually, a problem of the interpretation of collider limits that we have already discussed in sec. 2.1.3 is that the EFT can be mislead to under- or overestimate the limit on specific models, since very often the energy range of the momentum transfer can exceed the cut-off scale.

3.6.1 Constraints on model A from dijet searches

We begin by discussing the relevant search for the mediator of model A. The peculiar signature at an hadronic collider of a vector boson interacting with quarks as the Z' is the so-called *dijet production*, i. e. the production of a high p_{T} quark and antiquark that are dressed in the final state as two jets with nearly opposite direction, through the exchange of the Z' in the s-channel. This type of searches have been performed in all the hadronic colliders of the last decades.

The limits coming from the agreement of these results with the expected rate in the SM bring to exclusion limits on any model introducing additional interactions leading to a dijet final state. A comprehensive analysis of the limits on a massive Z' boson of the same type as in model A has been recently performed in [58]. The most relevant signal of a massive boson exchanged in the s-channel comes near the resonance, thus at a collision energy (at the partonic level) of the order of the mass of the Z'. For a fixed $m_{Z'}$, the energy necessary to excite the resonance is of the order of $m_{Z'}$. It is worth mentioning that in an hadronic collider the exact amount of energy available at the partonic level is not tunable with precision, thus the sensitivity to a resonance is not as strong as in a leptonic collider. Depending on the mass range of the Z' boson, the best limit does not in general come by the collider with the highest energy and luminosity, also because of the different cuts necessary to reduce the strong QCD background at different collision energies. Therefore, in order to get constraints on a large range of $m_{Z'}$ it is necessary to combine the limits from a large range of experiments. Eventually, each exclusion limit for a given value of $m_{Z'}$ can be cast as a limit on the coupling constant g_q of the massive boson to the quark current.

In order to compare the exclusion limits from the dijet searches to the coupling constant g_q of model A, we can exploit the plot obtained in [58], which shows the upper limit on the coupling constant g_q as a function of the $m_{Z'}$ from searches performed in the following experiments: UA1 and UA2 at the SPS, CDF and D0 at the Tevatron, and ATLAS and CMS at the LHC. The result of their analysis is superimposed in figure 3.21 to the distribution in the $(m_{Z'}, g_q)$ plane of the sample of parameter values yielding the correct relic density constraint.

A first remark is that, in order to constrain the Z' mass over a sufficiently large range, it is necessary to include many experiments performed at different energies. The resulting constraints are rather inhomogeneous, in the sense that the upper limit of g_q can range from around 0.7 to values over 2, depending on the mass of the Z', with an irregular behaviour. Thus, there are still open regions with allowed values of g_q of the order of unity. The second important remark concerns the impact of these limits on our model. We can see from the plot in fig. 3.21 that, for g_q higher than $0.7 \div 0.8$, $\Gamma_{Z'} > 0.25\, m_{Z'}$, independently of $m_{Z'}$, m_X and g_X. This is due to the presence of many (up to 6) decay channels of the Z' into quarks, which represent the main contribution to $\Gamma_{Z'}$. Thus this decay width can rapidly increase to non-perturbative

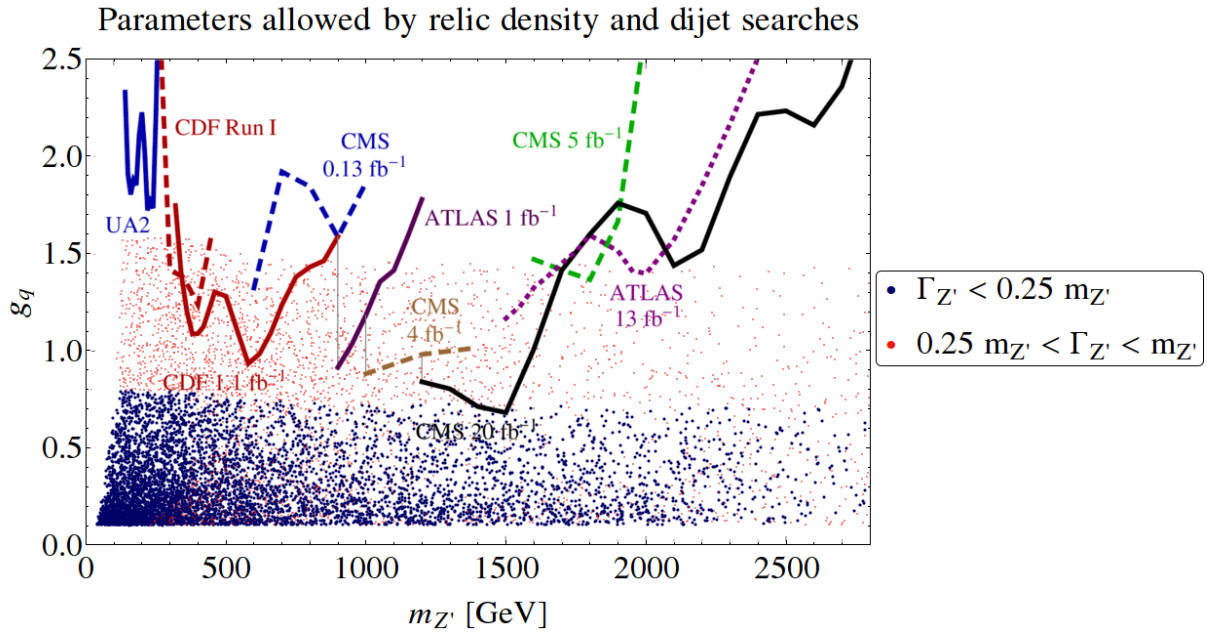

Figure 3.21: Constraints from various dijet searches on the coupling constant g_q as a function of the Z' boson mass [58], superimposed to the points allowed by the relic density constraint. In blue are the points with $\Gamma_{Z'}/m_{Z'} < 0.25$, while the dots with $0.25 < \Gamma_{Z'}/m_{Z'} < 1$ are shown in light red with a smaller size in order to keep the plot readable. See [58, table II] for the details about the experimental searches used to derive these limits.

values for large couplings to the quarks: as we have discussed in section 3.3.3, the increase of $\Gamma_{Z'}$ to non-perturbative values suppresses the annihilation cross section, preventing the relic density from tracking the correct one. This explains why in model A the constraints from dijet searches do not exclude nearly any point with $\Gamma_{Z'}/m_{Z'} < 0.25$.

3.6.2 Constraints on model A from monojet searches

The collider searches which can try to detect the production of DM must select events with a large missing energy and one (or more than one) jet, or a photon (as we have discussed in sec. 2.1.3). At a hadronic collider, the best exclusion limits come from the jet plus $\not{E}_T$ searches. Thus we check the constraint coming from the monojet plus $\not{E}_T$ searches at the LHC. As discussed in sec. 2.1.3, these searches put an upper limit on the production cross section of DM, which can be recast as a lower limit on the cut-off scale of a given effective operator describing the interaction between two quarks and two DM particles. The effective operators used in the CMS and ATLAS searches [29, 30, 31, 32] assume a Dirac fermion as dark matter candidate, and give the limits on the operators (or some of the operators) listed in table 2.3.

In order to derive the constraint on model A from the monojet searches, we take the most stringent limits, coming from [31], on the effective operator with axial-vector couplings, which is exactly the one corresponding to our model (effective Lagrangian (3.2c)). We consider then the limits derived from the analysis of CMS based on 19.5 fb^{-1} at $\sqrt{s} = 8$ TeV, on the cut-off scale Λ for the effective operator, whose coefficient is $1/\Lambda^2$, as a function of m_X^2. We superimpose this limit to the distribution of points allowed by the relic density constraint, together with the limit obtained from direct searches. The result is shown in figure 3.22.

The exclusion limit on the effective operator (eq. (3.2c)) excludes the region of low DM mass: it is important to keep in mind that this limit could be different if obtained with the

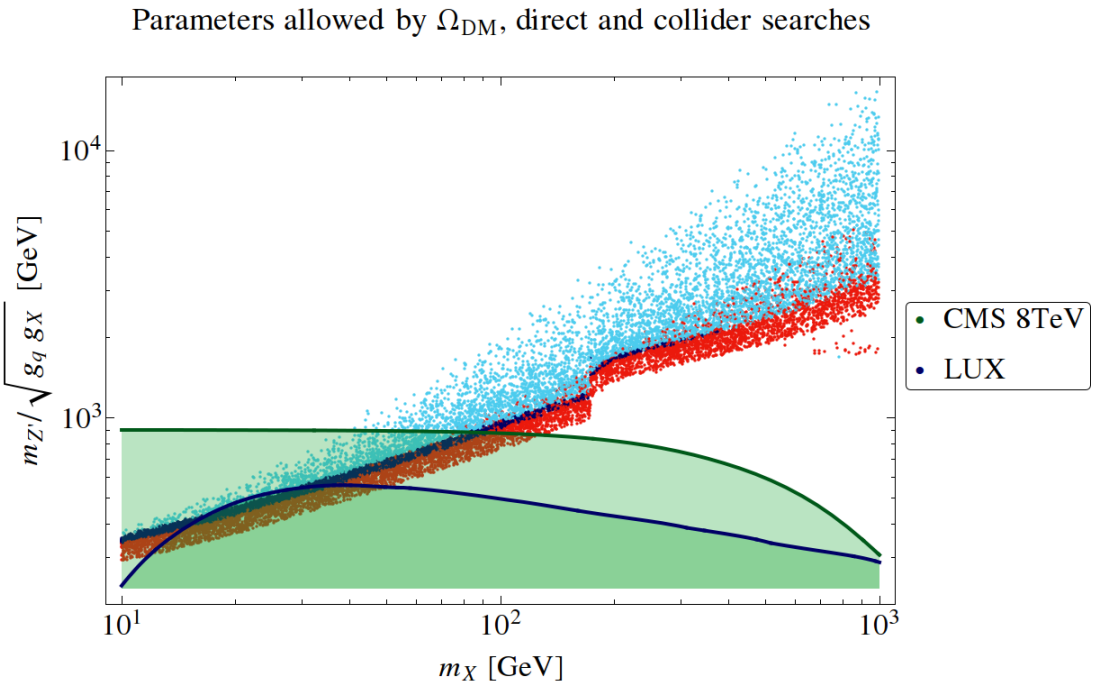

Figure 3.22: Superimposition of the limits from the relic density constraint (coloured dots), the LUX lower limit (blue lower line) and the CMS lower limit (green line) from [31] on the scale $\Lambda = m_{Z'}/\sqrt{g_q g_X}$ as a function of m_X. The red dots are the ones with $0.25 < \Gamma_{Z'}/m_{Z'} < 1$, and the remaining are coloured in dark blue (if $\beta < 0.2$) or lighter blue otherwise.

full theory. For example, in the case of a relatively light resonance, the limit would be much stronger around $m_X \gtrsim m_{Z'}/2$, since in that region the production of the $m_{Z'}$ could be enhanced by the resonance. The most important conclusion that we can draw is that the limit from the relic density that we would have obtained from the EFT (blue line) would have implied a lower limit on m_X around 90 GeV from the CMS limit, while the calculation of the relic density with the complete theory shows that the ligh blue dots remain over the CMS limit even for m_X around 40 GeV. This shows that how much the use of the EFT can distort the exclusion limit that one would obtain from the full theory.

We can also compare the relevance of the CMS limit on the axial-vector operator with the limit from LUX, which is the best limits from direct searches for that same operator. We can see that, in this particular case, the limit from CMS is always stronger than the limit from direct searches. Nevertheless it is important to mention that it is only thanks to the high integrated luminosity reached by the CMS search (19.5 fb^{-1}) that this happens. Indeed, until the first release of the monojet searches [29, 30], the limit from direct searches was higher than the collider one for high DM masses. In order to have a quantitative comparison, we overlay the current limit from LUX on the axial-vector operator with the exclusion limit on that effective operator from [30], which had analysed 4.7 fb^{-1} at $\sqrt{s} = 7$ TeV. The message that we can draw from this comparison is that the limits from monojet and direct searches have been strongly improving in the last few years; however the comparison shown in fig. 3.23 is based on the use of the effective theory, which we have shown to be justified in direct searches for model A, but may not be reliable in collider searches, depending on the mass values of the model.

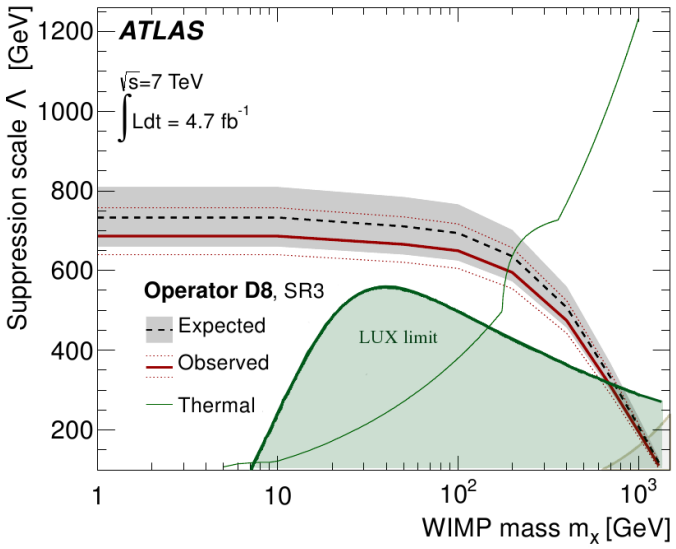

Figure 3.23: Superimposition of the lower limit on the cut-off scale of the vector-axial effective operator obtained by ATLAS in [30] and the current lower limit from the direct search experiment LUX (green line shadowed area). The former is weaker than the second one for $m_X \gtrsim 700$ GeV.

3.6.3 Constraints on model B from mediator searches

We now turn to the discussion of the relevant constraints from collider searches on model B. In this section, we discuss constraints on the search for the mediator $\widetilde{u}_R$, and in the next section we show the limit on the search of the DM particle through the monojet plus $\not{E}_T$ search.

We recall that in model B there are three different mediators $\widetilde{u}_R^{(i)}$, where the index i runs over the three generations. The limits from collider searches thus are relevant only for $\widetilde{u}_R^{(1)}$, the mediator of the first family generation, because of the PDFs. On the other hand, we supposed that the three mediators are degenerate in mass to avoid flavour issues, thus the same limit applies to all the three mediators.

The production of the mediator at colliders brings to a final state composed of jets plus $\not{E}_T$: indeed, $\widetilde{u}_R$ is unstable and decays to $\chi\, u$, and the mediators must be produced in couple if they are charged under the same $\mathbb{Z}_2$ parity as the DM particle (as in the case of supersymmetry). A representative diagram for this process is shown in fig. 3.24.

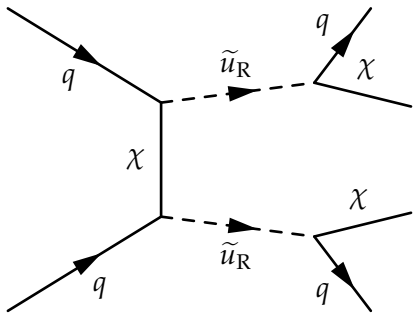

Figure 3.24: A representative Feynman diagram for the production of two $\widetilde{u}_R$, decaying each into DM plus a quark. This is the most relevant production channel if the coupling constant g_{DM} is large enough; for a complete list of the production channels (at tree level) of a couple of $\widetilde{u}_R$ at a hadron collider, and a discussion of their contribution to the total cross section, see [45].

As discussed in [59], also monojet plus $\not{E}_T$ searches are sensitive to the process in fig. 3.24,

because their cuts on additional jets are not so severe to completely discard events with two hard jets. We can derive the limits on the mediator of model B from the searches dedicated to supersymmetric particles. Indeed, this type of searches are sometimes performed within a simplified framework, in order to avoid to specify completely the details of the supersymmetric extension that one is considering, and to show representative results. The latest search of this type performed by ATLAS [60] (analogous results are presented by CMS in [61]) considers also a case which coincides with our model B, where the gluino are decoupled (this is obtained by putting their mass to a value over the TeV threshold). Indeed, gluinos contribute significantly to the process with a final state of multijets plus E_T. Then [60] further distinguishes a case where the 8 squarks (up-type and down-type squarks, each with its two chiralities, for the two lightest families) and a scenario with only one light squark: the latter case coincides with model B, once we take into account the PDFs of the partons which are negligible for c, t quarks.

The corresponding limit of [60, fig. 10c] is a lower limit on the neutralino mass (which corresponds to χ in model B) as a function of the squark mass ($m_{\tilde{u}_R}$ in our model). This limit rapidly decreases for $m_{\tilde{u}_R} \gtrsim 400$ GeV: this comes from the suppression of the PDFs for large parton energy fraction.

We can then superimpose this limit on the distribution of the points of the sample in the parameters space of values that yield the correct relic density, with the result shown in figure 3.25. We can see that the limit from squark searches excludes a large part of the parameter space for $m_{\tilde{u}_R} \lesssim 300 \div 350$ GeV. We recall that the point over the exclusion curve, on the upper right, tend to the limit $m_\chi = 0.9 m_{\tilde{u}_R}$, and that the white region corresponds to $m_\chi > 0.9\, m_{\tilde{u}_R}$ contains the coannihilation region; thus we are not really able to define a general excluded region for $m_{\tilde{u}_R}$, but rather in the limit of low β.

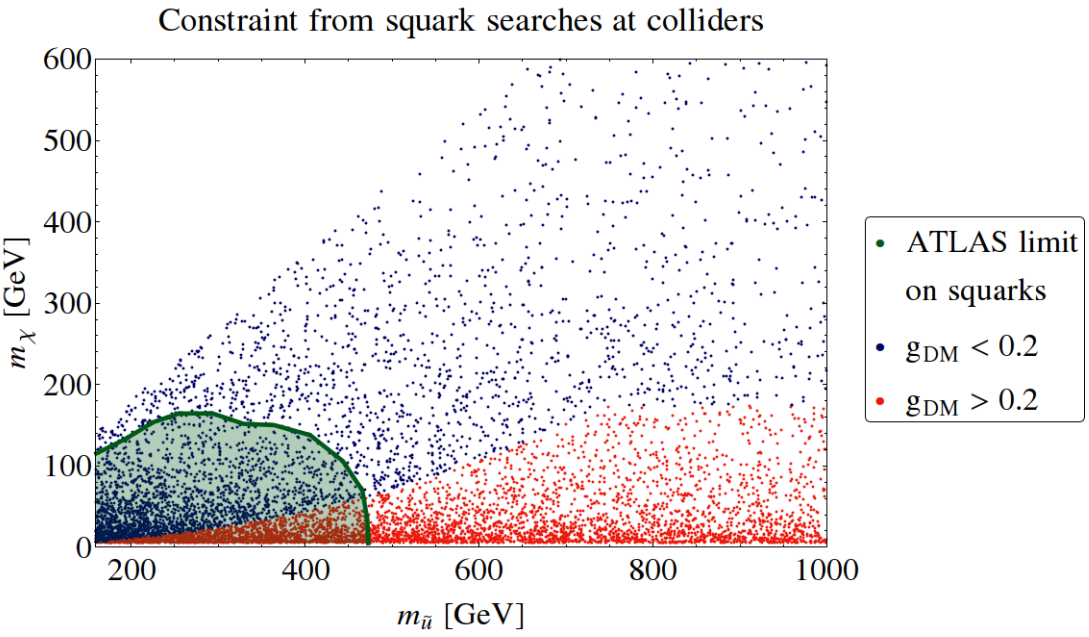

Figure 3.25: Limit on the DM mass m_χ as a function of the mediator mass $m_{\tilde{u}_R}$ (recasting the squark search performed in [60]), superimposed with the distribution of the points of the sample yielding the correct relic density. In red are shown the points with coupling $g_{DM} > 2$.

3.6.4 Constraints on model B from monojet searches

In this section, we will discuss the impact of the limits coming from monojet searches on the effective axial-vector operator, for model B.

In this case, before applying the limit listed by the CMS collaboration [31] as we have done for model A, we must take into account the following differences. The CMS limit on the effective operator $(\overline{\chi}\gamma^\mu\gamma^5\chi\overline{q}\gamma_\mu\gamma^5 q)/\Lambda^2_{\text{CMS}}$ is obtained by assuming that χ is a Dirac fermion, interacting with all the quarks. In model B, the effective theory is described by two operators: one with the contraction of two axial-vector Lorentz bilinears of eq. (3.4b), and one with the contraction of a vector and an axial-vector (eq. (3.4a)). Thus the difference between the limit $\overline{\sigma}_{\text{CMS}}$ from the CMS search on the cross section for the production of $\chi\chi\, j$ and the limit $\overline{\sigma}_{\text{B}}$ that would arise by considering our model must take into account the following numerical factors:

- χ in model B is a Majorana fermion. Then the Feynman rule that we would obtain from an operator $(\overline{\chi}\gamma^\mu\gamma^5\chi\overline{q}\gamma_\mu\gamma^5 q)/\Lambda^2_{\text{B}}$, where χ is a Majorana fermion with its kinetic term normalised accordingly, is twice the amplitude obtained by assuming that χ is a Dirac fermion (as shown in appendix A). This factor 2 gets squared in the modulus squared of the amplitude. Then, an additional factor $1/2$ must be introduced in the case of Majorana DM when computing the phase space integral, because the two particles in the final state are identical. Thus, this first difference gives an factor of 2 in the ratio $\overline{\sigma}_{\text{B}}/\overline{\sigma}_{\text{CMS}}$.

- The EFT of model B also contains the coupling of a vector quark current to a axial-vector DM current (eq. 3.4a). We can show that its contribution to the cross section is identical to the one from the term of eq. (3.4b) in two ways. First, we can think of the chirality of the quarks involved in the two interactions: indeed, the PDFs allow us to restrict to the up and down quarks, which can be considered massless at the energy scale of LHC, thus chiralities of the spinors and helicities of the corresponding particles coincide. Both in the vector and axial-vector quark current, the two spinors involved in the interaction have the same chirality. Thus the two interaction involve equivalently left- or right-handed quarks, without any interference between these contributions. Therefore the contributions of the two operators to the final cross section are equal. Otherwise, we can reach the same conclusion by rewriting the sum of the two interaction terms as

  $$\left(\overline{\chi}\gamma^\mu\gamma^5\chi\overline{q}\gamma_\mu\gamma^5 q\right) + \left(\overline{\chi}\gamma^\mu\gamma^5\chi\overline{q}\gamma_\mu q\right) = 2\left(\overline{\chi}\gamma^\mu\gamma^5\chi\overline{q}\gamma_\mu P_R q\right).$$

  The factor 2 in front of the squared brackets yields a factor 4 in the cross section, while the projection operator P_R selects only one between the two possible chiralities for the two incoming quarks; thus the average over the initial states gets decreased by $1/2$. From both points of view, the factor coming from this issue on the ratio $\overline{\sigma}_{\text{B}}/\overline{\sigma}_{\text{CMS}}$ is 2.

- As a last point, we must recall that in model B the DM interacts only with the up-type quarks. An accurate estimate of the numerical effect of this difference requires the detailed calculation through the PDFs. Since the cut-off scale Λ gets rescaled by this factor raised to the power -4 (as we explain below), also a rough estimate is sufficient for our scope. In the kinematical region of interest, only the up and down quarks have relevant PDFs, and the up quark PDF is twice the down quark one (in first approximation). In model B, only the up quarks interact with DM, while in the CMS model also the interaction with down quarks is included. Then the overall factor in the ratio $\overline{\sigma}_{\text{B}}/\overline{\sigma}_{\text{CMS}}$ is $2/3$.

In conclusion, these three differences imply that the limit $\overline{\sigma}_{\text{B}}$ on the cross section (as predicted in model B) is greater than the value $\overline{\sigma}_{\text{CMS}}$ obtained by CMS by an overall factor $2 \cdot 2 \cdot 2/3 = 8/3$. Thus, since the cross section is proportional to Λ^{-4}, the limit on the cut-off Λ_{B} of the operator

of model B is equal to $(8/3)^{-1/4}\Lambda_{\rm CMS}$. Therefore in figure 3.26 we report the limit on the cut-off scale listed by CMS [31] divided by a factor $\sqrt[4]{8/3}$, superimposed to the distribution of the points yielding the correct relic density.

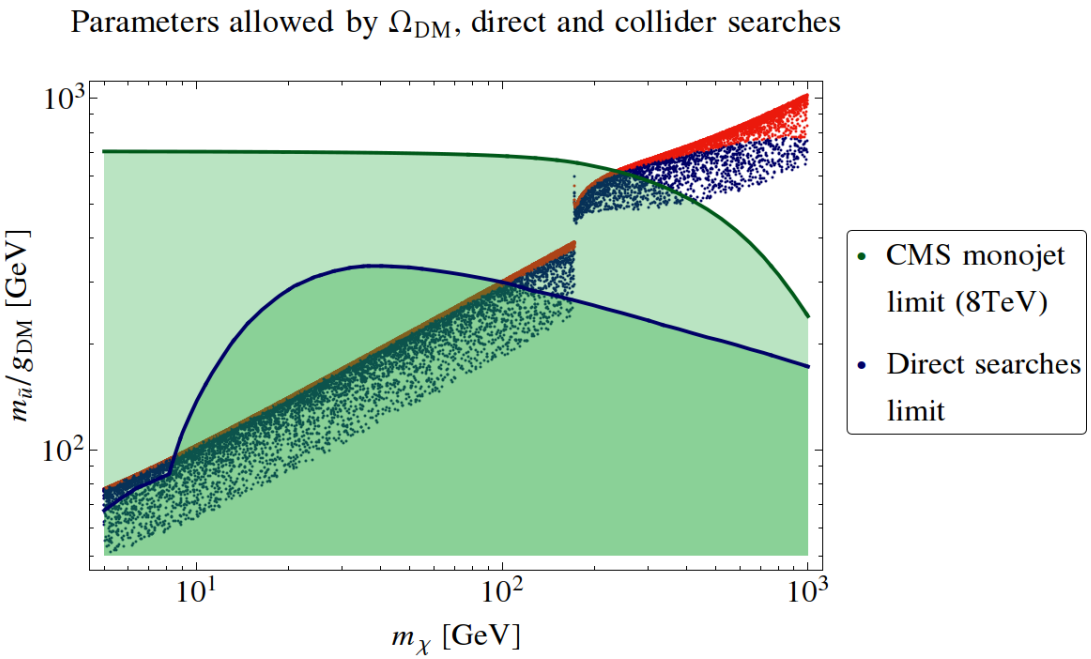

Figure 3.26: Limit from CMS (green line) on the cut-off scale Λ as a function of m_χ from the monojet searches in the framework of the EFT. This limit has been divided by $\sqrt[4]{8/3}$ with respect to the one published in [31]. In the same plane we show with a blue line the limit from direct searches, and the distribution of the points of parameter space yielding the correct relic abundance. The blue dots correspond to points for which $g_{\rm DM} < 2$, while the red ones correspond to $2 < g_{\rm DM} < 4\pi$.

We can see that in model B the constraint from the corresponding effective theory from monojet searches is by far much more constraining with respect to model A. Indeed in this case the lower limit on m_χ is pushed to around 200 GeV. This is basically due to the fact that the cut-off scale needed to reach the correct relic abundance is much smaller than in model A. Indeed, in that case the possibility of a nearly resonant production of the mediator (due to the interaction in the s-channel) increases the cross section, allowing for higher values of Λ in order to keep the correct annihilation cross section: this phenomenon, which happens precisely when departing from the EFT limit, raises the range of allowed values for $\Lambda = m_{Z'}/\sqrt{g_q g_X}$. On the other hand, in model B this phenomenon does not happen because of the mediator exchange in the t and u channel. In this model, the departure from the EFT limit pushes downwards the required value of $\Lambda = m_{\tilde{u}_{\rm R}}/g_{\rm DM}$ that brings to the correct relic density. Thus the exclusion limit on the cut-off scale from monojet searches has a stronger impact on the exclusion limit.

Conclusions

In this thesis we have considered two simplified models for dark matter, to compare critically how experimental data are interpreted in the effective theory and in the complete model. The first model, A, includes a vector mediator with axial vector couplings to the quarks and to a Dirac fermion dark matter. The second model, B, assumes that dark matter is a Majorana fermion interacting with the Standard Model right-handed up-type quarks and some coloured scalars with the same gauge quantum numbers.

First, we have examined the relic density constraint. The result obtained with the complete theory shows the limitations of the effective theory approach: in particular, in model A, the possibility of a resonant production of the mediator and the important effects of its decay width in certain regions of the parameter space are missed by the effective theory. On the other hand, the effective theory is still adequate for a rough estimate of the effective interaction strength, with a difference varying from a factor of two to almost an order of magnitude for increasing dark matter mass.

Then we have moved to direct searches. The kinematic channel in which the mediator is exchanged is relevant for the validity of the effective theory. For model A the effective theory is perfectly adequate in the non-relativistic regime of direct search experiments. In model B its predictions are correct only in the limit of high mass of the mediator with respect to the dark matter particle. However, in model B this effect is not expected to be strongly relevant as long as the masses of the mediator and of the dark matter particle are not very close, as we assumed to avoid some delicate issues in the calculation of the relic density. Therefore, we have used the effective theory to set the limits on our models.

Afterwards, we have compared the relic density constraint with the bound coming from the observed flux of antiprotons in cosmic rays: this is the most relevant indirect search channel because in our models dark matter interacts with quarks. Because of the helicity suppression present in our models, i. e. the vanishing of the cross section for the annihilation of DM particles into quarks in the limit of massless quarks and non-relativistic dark matter, the bound from $\overline{p}$ is relevant only for the annihilation into the heaviest quarks allowed by the interactions. The most relevant constraint turns out to be on the annihilation into b-$\overline{b}$ quarks, and has an impact on model A but not on model B, where the dark matter particle interacts only with up-type quarks.

Finally, we have discussed the collider searches for the mediators and the dark matter particles. It is worth stressing that the full model includes the mediator, which can be directly produced at colliders, while in the effective theory this degree of freedom is absent. In model

A, the limits on the mediator come from the searches for Z' bosons decaying into di-jets, and translate into constraints that are not competitive with the others in the region of perturbative couplings. In model B, the mediator can be identified with a squark, the scalar quark partner in supersymmetry, and some of the limits from squark searches at the LHC can be applied. We find that a large part of the parameter space is excluded for a mass of the mediator below $300 \div 350$ GeV. The search for dark matter at colliders is performed with the analysis of events with a jet and a large amount of missing transverse energy. For simplicity and because of the limited time available, we have taken directly the lower limit on the strength of the effective operator derived by the CMS collaboration, and we have compared that limit with those obtained from direct searches and with the relic density constraint.

The main result of this analysis is that the overall effect of using the effective theory rather than the complete underlying model might still be an acceptable strategy for the interpretation of dark matter searches. However, to reach a firmer and more general conclusion some more work would be needed, which goes beyond the aim and the time constraints of the present thesis. First, it would be interesting to implement a more detailed analysis of the limits from monojet searches, to compare the predictions of the effective theory and those of the underlying model also in this case. We can expect that in model A the most relevant differences will arise when the mass of the mediator is sufficiently low that its resonance can be excited at the LHC. Second, it would be interesting to relax the assumption of pure axial vector coupling in model A: if we allow for a vector component of the couplings, the helicity suppression ceases, and we can expect an increase on the lower bounds on the effective scale, both for the relic density constraint and direct searches, while this should not impact very much collider searches. It would be interesting to check the size and the relative difference of these changes. Then, an assumption of model B whose relevance would be interesting to check is the choice of the quarks with which dark matter is interacting. Depending on the quantum numbers of the mediator (and of dark matter, which we have assumed to be a singlet of the Standard Model), the interaction could be with right-handed down-type quarks or with left-handed quarks. Finally, in model B a region of the parameter space that we have not considered yet is the one in which the dark matter mass approaches (from below) the mass of the mediator: in that regime, also called co-annihilation, the two species decouple simultaneously in the early universe, and the Boltzmann equations for their number densities must be solved together.

APPENDIX A

Spinor conventions

In this appendix we summarise some conventions and useful formulæ on four-components spinors.

We adopt the following sign convention for the four-dimensional flat metric:

$$\eta_{\mu\nu} = \mathrm{diag}(+1, -1, -1, -1)\,, \qquad \eta^{\mu\rho}\,\eta_{\rho\nu} = \delta^{\mu}_{\nu}\,.$$

The Dirac equation is

$$(i\gamma^{\mu}\partial_{\mu} - m)\psi = 0\,,$$

where the field ψ is called *spinor* and the 4×4 Dirac matrices γ^{μ} satisfy

$$\{\gamma^{\mu}, \gamma^{\nu}\} = 2\eta^{\mu\nu}\mathbf{1}_4\,.$$

A convenient basis of dimension 16 for the spinor bilinears with definite Lorentz transformation properties is given by

$$\Gamma^{A} = \{\mathbf{1}_4, \gamma^{\mu}, \sigma^{\mu\nu}, i\gamma_5\gamma^{\mu}, \gamma_5\}\,, \qquad A = 1, \ldots, 16\,, \tag{A.1}$$

where $\sigma^{\mu\nu}$ is defined as $\sigma^{\mu\nu} \equiv i/2[\gamma^{\mu}, \gamma^{\nu}]$ and the matrix γ_5 (where the position of the index 5 is irrelevant) is defined by $\gamma_5 = i\gamma^0\gamma^1\gamma^2\gamma^3$. The basis of eq. (A.1) has been chosen in order to satisfy the normalisation

$$\mathrm{tr}(\Gamma^{A}\Gamma_{B}) = 4\,\delta^{A}_{B}\,, \tag{A.2}$$

where the matrices Γ_A are defined by lowering the space-time indices with the metric $\eta^{\mu\nu}$:

$$\Gamma_{A} = \{\mathbf{1}_4, \gamma_{\mu}, \sigma_{\mu\nu}, i\gamma_5\gamma_{\mu}, \gamma_5\}\,, \qquad A = 1, \ldots, 16\,.$$

The representation of the Lorentz group corresponding to a Dirac spinor is reducible in two representations acting separately on the two 2-dimensional subspaces selected by the projectors

$$P_{\mathrm{L}} = \frac{1 - \gamma_5}{2}\,, \qquad P_{\mathrm{R}} = \frac{1 + \gamma_5}{2}\,. \tag{A.3}$$

We choose the Weyl representation as a specific representation for the γ matrices:

$$\gamma^{\mu} = \begin{pmatrix} \mathbf{0}_2 & \sigma^{\mu} \\ \overline{\sigma}^{\mu} & \mathbf{0}_2 \end{pmatrix}\,, \qquad \gamma_5 = \begin{pmatrix} -\mathbf{1}_2 & \mathbf{0}_2 \\ \mathbf{0}_2 & \mathbf{1}_2 \end{pmatrix}\,,$$

where the σ matrices are defined as follows[1]:

$$\sigma^\mu = \{\sigma^0, \sigma^1, \sigma^2, \sigma^3\}\,, \qquad \overline{\sigma}^\mu = \{\sigma^0, -\sigma^1, -\sigma^2, -\sigma^3\}\,,$$
$$\sigma^0 = \begin{pmatrix} 1 & 0 \\ 0 & 1 \end{pmatrix}, \qquad \sigma^1 = \begin{pmatrix} 0 & 1 \\ 1 & 0 \end{pmatrix}, \qquad \sigma^2 = \begin{pmatrix} 0 & -i \\ i & 0 \end{pmatrix}, \qquad \sigma^3 = \begin{pmatrix} 1 & 0 \\ 0 & -1 \end{pmatrix}.$$

The main advantage of this representation is that the left and right projectors of eq. (A.3) take the simple form

$$P_\mathrm{R} = \begin{pmatrix} \mathbf{0}_2 & \mathbf{0}_2 \\ \mathbf{0}_2 & \mathbf{1}_2 \end{pmatrix}, \qquad P_\mathrm{L} = \begin{pmatrix} \mathbf{1}_2 & \mathbf{0}_2 \\ \mathbf{0}_2 & \mathbf{0}_2 \end{pmatrix},$$

so that a four-component spinor can be neatly decomposed into two two-components spinors, called *Weyl spinors*, which transform under an irreducible representation of the Lorentz group. The usual notation for two-components spinors is the following: right-handed spinors, which are annihilated by P_R, have a dotted greek upper index and an upper bar, while left-handed spinors have a lower undotted greek index,

$$\psi = \begin{pmatrix} \xi_\alpha \\ \bar{\eta}^{\dot{\alpha}} \end{pmatrix}.$$

The transformed under *charge conjugation* of a four-component spinor is obtained through

$$\psi^\mathrm{c} = C(\overline{\psi})^\mathrm{T}\,,$$

where the operator C (which satisfies $C^\dagger C = \mathbf{1}_4$) is given by $C = -i\gamma^2\gamma^0$ and the *Dirac conjugate* $\overline{\psi}$ is $\overline{\psi} = \psi^\dagger\gamma_0$. We quote some relevant properties of the conjugation matrix C that are useful in the calculations of chapter 3:

$$C^{-1} = C^\dagger = -C\,, \quad C^\mathrm{T} = -C\,, \quad C^2 = -\mathbf{1}_4\,, \quad [C, P_\mathrm{L}] = [C, P_\mathrm{R}] = 0\,. \tag{A.4}$$

A *Majorana spinor* (that we will usually denote by χ) is defined as a self-conjugate spinor:

$$\chi = \chi^\mathrm{c} = C(\overline{\chi})^\mathrm{T}\,, \qquad \chi = \begin{pmatrix} \xi_\alpha \\ \bar{\xi}^{\dot{\alpha}} \end{pmatrix}, \tag{A.5}$$

where $\bar{\xi}^{\dot{\alpha}}$ is defined as $\bar{\xi}^{\dot{\alpha}} = \varepsilon^{\dot{\alpha}\dot{\beta}}(\xi_\beta)^*$.

By using the definition (A.5), we can easily show that the Lorentz vector $\overline{\chi}\gamma^\mu\chi$ is 0 if χ is a Majorana spinor by writing explicitely the vector current in terms of two-components spinors.

We now present the so-called *Fierz transformations*, which allow to rewrite the product of two Lorentz bilinears, i. e. of two Lorentz tensors built with two four-component spinors, as the sum of analogous terms with the exchange of some of the spinor fields. In formulæ, we can rewrite a Lorentz bilinear $\overline{\psi}_1\Gamma^A\psi_2\,\overline{\psi}_3\Gamma^B\psi_4$ as

$$\overline{\psi}_1\Gamma^A\psi_2\,\overline{\psi}_3\Gamma^B\psi_4 = \sum_{C,D} C_{CD}^{AB}\,\overline{\psi}_1\Gamma^C\psi_4\,\overline{\psi}_3\Gamma^D\psi_2\,,$$

where the coefficients C_{CD}^{AB} are given, with the normalisation convention chosen in (A.2), by

$$C_{CD}^{AB} = \frac{1}{16}\mathrm{tr}\Big(\Gamma^C\Gamma^A\Gamma^D\Gamma^B\Big)\,. \tag{A.6}$$

In section 3.2.2 we have rewritten the interaction Lagrangian of the effective theory for model B in terms of Lorentz bilinears involving only χ or quark currents: starting from the term

[1] The bar in $\overline{\sigma}^\mu$ has nothing to do with the spinor conjugation.

$\overline{\chi} P_{\mathrm{R}} u\, \overline{u} P_{\mathrm{L}} \chi$, we can use eq. (A.6) to deduce the coefficients of the Fierz transformation. The only non vanishing ones give

$$\left(\overline{\chi} P_{\mathrm{R}} u\right)\left(\overline{u} P_{\mathrm{L}} \chi\right) = \frac{1}{2}\left(\overline{\chi}\gamma^{\mu} P_{\mathrm{L}} \chi\right)\left(\overline{u}\gamma_{\mu} P_{\mathrm{R}} u\right),$$

which can be simplified, by recalling that a vector current for a Majorana spinor is zero, into

$$\left(\overline{\chi} P_{\mathrm{R}} u\right)\left(\overline{u} P_{\mathrm{L}} \chi\right) = -\frac{1}{4}\left(\overline{\chi}\gamma^{\mu}\gamma_5 \chi\right)\left(\overline{u}\gamma_{\mu} P_{\mathrm{R}} u\right). \tag{A.7}$$

We conclude this appendix by recalling some peculiarities of Majorana spinors with respect to Dirac ones when dealing with Feynman diagrams and the corresponding Feynman rules. First, we must remember that the Feynman rule corresponding to a given Lagrangian term containing twice the same Majorana field χ gets an additional factor 2 with respect to the Dirac case. Indeed, eq. (A.5) implies that, in the expansion of the Majorana spinor field χ in terms of the energy eigenstates, the annihilation and creation operators coincide:

$$\chi(x) = \int \frac{\mathrm{d}^3 k}{(2\pi)^3 2E} \sum_{r=1,2} \left[u_r(\vec{k})\, b_r(\vec{k}) e^{-ik\cdot x} + v_r(\vec{k})\, b_r^{\dagger}(\vec{k}) e^{+ik\cdot x} \right] \Bigg|_{k^0 = E = \sqrt{|\vec{k}|^2 + m^2}}, \tag{A.8}$$

where m is the mass of the field χ, r denotes the two possible helicity states, u and v are respectively the positive and negative energy solutions of the Dirac equation in Fourier space, and $k \cdot x$ denotes the four-dimensional scalar product. From eq. (A.8), with the use of the anticommutation rules valid for the creation and annihilation operators b and $b^{\dagger}$, we can check that, for example, the Feynman rule associated to an interaction term containing the Lorentz bilinear $\overline{\chi}\Gamma^A \chi$ would bring to the matrix element

$$\langle 0|\, b(\vec{k}_f) \left(\overline{\chi}\Gamma^A \chi\right) b^{\dagger}(\vec{k}_i)\, |0\rangle = 2\, \overline{u}(\vec{k}_f)\Gamma^A u(\vec{k}_i),$$

where the factor 2 arises from the fact that, for a Majorana spinor, left and right components are simply related by a complex conjugation as in eq. (A.5). This computation shows why we have to insert a $1/2$ factor in front of terms containing twice a given Majorana spinor field.

When computing the Feynman amplitude associated to a diagram containing Majorana fermions, the easiest way to associate the correct spinor to the external legs is to write explicitly the matrix element associated to that diagram. To show an example, we will derive the Feynman amplitude associated to the process $\chi(p_1)\chi(p_2) \to u_{\mathrm{R}}(k_1)\overline{u_{\mathrm{R}}}(k_2)$, with an interaction given by $(\overline{\chi} P_{\mathrm{R}} u)_x (\overline{u} P_{\mathrm{L}} \chi)_y$, where the subscript x or y denotes the point of the spacetime in which the fields must be computed. We must then calculate

$$\begin{aligned}\Big\langle u_{\mathrm{R}}(k_1)\overline{u_{\mathrm{R}}}(k_2)\Big|\left(\overline{\chi} P_{\mathrm{R}} u\right)_x \left(\overline{u} P_{\mathrm{L}} \chi\right)_y \Big|\chi(p_1)\chi(p_2)\Big\rangle \\ = \Big\langle 0\Big|c(k_1)d(k_2)\left(\overline{\chi} P_{\mathrm{R}} u\right)_x \left(\overline{u} P_{\mathrm{L}} \chi\right)_y b^{\dagger}(p_1)b^{\dagger}(p_2)\Big|0\Big\rangle,\end{aligned}$$

where we denote by c and d the destruction operators for up and anti-up quarks, respectively. From this equation it is clear that $c(k_1)$ must be contracted with $\overline{u}(y)$ and $d(k_2)$ with $u(x)$, while both $\overline{\chi}(x)$ and $\chi(y)$ contain an operator b to be contracted with the creation operators $b^{\dagger}$. Depending on whether we contract $b^{\dagger}(p_1)$ with $\chi(y)$ or $\overline{\chi}(x)$, a minus sign arises in the second case because of the anticommutation that must be imposed when switching two fermion fields of the same type. Thus, the Feynman amplitude reads

$$\left(\overline{v}(p_2) P_{\mathrm{R}} v(k_2)\right)\left(\overline{u}(k_1) P_{\mathrm{L}} u(p_1)\right) - \left(\overline{v}(p_1) P_{\mathrm{R}} v(k_2)\right)\left(\overline{u}(k_1) P_{\mathrm{L}} u(p_2)\right). \tag{A.9}$$

We conclude this section by quoting the formulæ for the sums, over the Majorana fermion polarisation, of the associated spinors [48]. Indeed, because of eq. (A.5), the positive and negative energy solutions of the Dirac equation for a Majorana spinor are the conjugate of each other: $u = C\overline{v}^{\mathrm{T}}$, $v = C\overline{u}^{\mathrm{T}}$. These formulæ imply that, together with the usual

$$\sum_{\lambda=1,2} u_{(\lambda)}(p)\overline{u}_{(\lambda)}(p) = \not{p} + M\,, \quad \sum_{\lambda=1,2} v_{(\lambda)}(p)\overline{v}_{(\lambda)}(p) = \not{p} + M\,, \tag{A.10}$$

also the following equations hold:

$$\begin{aligned}
\sum_{\lambda=1,2} u_{(\lambda)}(p)v^{\mathrm{T}}_{(\lambda)}(p) &= (\not{p} + M)C^{\mathrm{T}}\,,\\
\sum_{\lambda=1,2} v_{(\lambda)}(p)u^{\mathrm{T}}_{(\lambda)}(p) &= (\not{p} - M)C^{\mathrm{T}}\,,\\
\sum_{\lambda=1,2} \overline{u}^{\mathrm{T}}_{(\lambda)}(p)\overline{v}_{(\lambda)}(p) &= C^{-1}(\not{p} - M)\,,\\
\sum_{\lambda=1,2} \overline{v}^{\mathrm{T}}_{(\lambda)}(p)\overline{u}_{(\lambda)}(p) &= C^{-1}(\not{p} + M)\,.
\end{aligned} \tag{A.11}$$

APPENDIX B

Thermally averaged cross section and relic density

In this appendix, we discuss a procedure to compute the thermally averaged cross section $\langle \sigma v \rangle$, and to deduce from it the relic abundance of DM today. We will obtain both an exact expression, and an approximate result valid in the assumption of low temperature with respect to the dark matter particle mass.

Throughout this appendix, we will keep the discussion more general, and we will derive the equations for the process in which two identical particles of mass m annihilating into a generic final state.

B.1 Main formulæ and general setup

The equation that controls the time evolution of the number density of a species taking into account its interaction with other species and the expansion of the Universe is the *Boltzmann equation*:

$$\frac{\mathrm{d}n}{\mathrm{d}t} = -3Hn - \langle \sigma v \rangle \left(n^2 - n_{\mathrm{eq}}^2 \right), \tag{B.1}$$

where n is the number density of a given species, g is the number of helicity states of the particle, H is the Hubble parameter, and the equilibrium number density n_{eq} and the thermally averaged cross section $\langle \sigma v \rangle$ are defined[1] as [8, 9]

$$n_{\mathrm{eq}} = g \int \frac{\mathrm{d}^3 p}{(2\pi)^3} \, e^{-\frac{E}{T}}, \tag{B.2}$$

$$\begin{aligned} \langle \sigma v \rangle = & \frac{1}{(n_{\mathrm{eq}})^2} \int \frac{\mathrm{d}^3 p_1}{(2\pi)^3 2E_1} \int \frac{\mathrm{d}^3 p_2}{(2\pi)^3 2E_2} \, e^{-\frac{E_1+E_2}{T}} \cdot \\ & \cdot \left(\prod_i \int \frac{\mathrm{d}^3 k_i}{(2\pi)^3 2E_i'} \right) (2\pi)^4 \delta^4 (p_1 + p_2 - \sum_i k_i) |\mathcal{M}|^2 , \end{aligned} \tag{B.3}$$

[1] In the formula for n_{eq}, we are assuming a vanishing chemical potential and we are neglecting the quantum effects in the distribution function, i. e. we assume a Maxwell-Boltzmann distribution instead of the Fermi-Dirac or Bose-Einstein distribution.

where T is the temperature of the species (which coincides with the one of the thermal bath as long as this is in kinetic equilibrium with the other species), p_i and E_i are the initial state momenta and energies, k_i and E_i' the final ones, and $|\mathcal{M}|^2$ is the modulus squared of the Feynman amplitude for the annihilation process[2], with the sum over the final states and the sum (instead of the average) over the initial ones.

We notice that the second line of eq. (B.3) is simply the (unpolarised) annihilation cross section of the two incoming particles, times the flux factor and the number of initial states. Thus we define

$$(\sigma_{\rm ann}\widetilde{F}) = \left(\prod_i \int \frac{\mathrm{d}^3 k_i}{(2\pi)^3 2E_i'}\right)(2\pi)^4\delta^4(p_1+p_2-\sum_i k_i)|\mathcal{M}|^2\,, \tag{B.4}$$

where $\widetilde{F}$ for a final state of two particles is

$$\widetilde{F} = 4g^2F = 4g^2\sqrt{(p_1\cdot p_2)^2-m^4} = 4g^2\sqrt{s}\sqrt{\frac{s}{4}-m^2} = 2g^2\sqrt{s(s-4m^2)}\,. \tag{B.5}$$

We notice that $(\sigma_{\rm ann}\widetilde{F})$ is a function of the only variable s.

B.2 Derivation of an exact formula for $\langle\sigma v\rangle$

In this section, we will simplify the expression (B.3) into an exact expression containing only one integral over the Mandelstam variable s.

The first step consists in multiplying eq. (B.3) by $1 = \int \mathrm{d}^4K\,\delta^4(K-p_1-p_2)$:

$$\begin{aligned}\langle\sigma v\rangle &= \frac{1}{(2\pi)^6}\frac{1}{(n_{\rm eq})^2}\int\frac{\mathrm{d}^3p_1}{2E_1}\int\frac{\mathrm{d}^3p_2}{2E_2}\,e^{-\frac{E_1+E_2}{T}}(\sigma_{\rm ann}\widetilde{F})\int\mathrm{d}^4K\,\delta^4(K-p_1-p_2) = \\ &= \frac{1}{(2\pi)^6}\frac{1}{(n_{\rm eq})^2}\int\mathrm{d}^4K\,e^{-\frac{K^0}{T}}(\sigma_{\rm ann}\widetilde{F})\left[\int\frac{\mathrm{d}^3p_1}{2E_1}\int\frac{\mathrm{d}^3p_2}{2E_2}\,\delta^4(K-p_1-p_2)\right].\end{aligned}$$

The espression inside squared brackets can be computed explicitly: indeed, it depends only on the four-vector K^μ and is a Lorentz scalar, thus it must be a function of K^2. Moreover, being a Lorentz scalar, it can be computed in any desired frame. We can evaluate it as follows:

$$\begin{aligned}\left[\int\frac{\mathrm{d}^3p_1}{2E_1}\int\frac{\mathrm{d}^3p_2}{2E_2}\delta^4(K-p_1-p_2)\right] &= \int\frac{\mathrm{d}^3p_1}{4E_1E_2}\delta(K^0-E_1-E_2)\int\mathrm{d}^3p_2\,\delta^3(\vec{K}-\vec{p}_1-\vec{p}_2) = \\ &= \int\frac{4\pi|\vec{p}_1|^2\mathrm{d}|\vec{p}_1|}{4E_1E_2}\delta(K^0-E_1-E_2)\,.\end{aligned}$$

The Dirac δ function can be evaluated by observing that in the center-of-mass (c.o.m.) frame $E_1 = E_2$ is a function of the modulus of the momentum $|\vec{p}_1|$; the argument of the δ function vanishes for $|\vec{p}_1| = \sqrt{K^2/4-m^2}$, and the derivative of the argument gives

$$\begin{aligned}\delta(K^0-E_1-E_2) &= \delta\left(|\vec{p}_1|-\sqrt{\frac{K^2}{4}-m^2}\right)\frac{1}{\left|\frac{\mathrm{d}(E_1+E_2)}{\mathrm{d}|\vec{p}_1|}\right|} = \delta\left(|\vec{p}_1|-\sqrt{\frac{K^2}{4}-m^2}\right)\frac{1}{|\vec{p}_1|\left(\frac{1}{E_1}+\frac{1}{E_2}\right)} = \\ &= \delta\left(|\vec{p}_1|-\sqrt{\frac{K^2}{4}-m^2}\right)\frac{E_1E_2}{|\vec{p}_1|(E_1+E_2)}\,.\end{aligned}$$

[2]If there are more than one annihilation channels, a sum over the possible processes is understood in eq. (B.3).

By observing that in the c.o.m. frame we have $\vec{K} = 0$, $E_1 + E_2 = K^0 = \sqrt{K^2}$ where K^2 is the modulus of the 4-vector K^μ, we get

$$\left[\int \frac{\mathrm{d}^3 p_1}{2E_1}\int \frac{\mathrm{d}^3 p_2}{2E_2}\delta^4(K - p_1 - p_2)\right] = \frac{\pi}{\sqrt{K^2}}\int |\vec{p}_1|\mathrm{d}|\vec{p}_1|\delta\left(|\vec{p}_1| - \sqrt{\frac{K^2}{4} - m^2}\right) = \pi\frac{\sqrt{K^2/4 - m^2}}{\sqrt{K^2}}\,.$$

We are now left with an integral in d^4K of a quantity that depends only on K^0, $K^2 = s$. In order to switch to those integration variables, we split $\int \mathrm{d}^4K = 4\pi\int \mathrm{d}K^0\int |\vec{K}|^2\mathrm{d}|\vec{K}|$, and we perform a change of integration variables into $(K^0,\, K^2 = (K^0)^2 - |\vec{K}|^2)$. The Jacobian of this transformation gives

$$\left|\frac{\partial(K^0,\,|\vec{K}|)}{\partial(K^0,\,K^2)}\right| = \begin{vmatrix} 1 & \frac{K^0}{|\vec{K}|} \\ 0 & -\frac{1}{2|\vec{K}|}\end{vmatrix} = -\frac{1}{2|\vec{K}|}\,.$$

The domain of integration is given by $K^0 \in [\sqrt{K^2}, +\infty]$, $K^2 \in [4m^2, +\infty]$. We have then

$$\langle\sigma v\rangle = \frac{1}{(2\pi)^6}\frac{1}{(n_{\mathrm{eq}})^2}2\pi^2\int_{4m_\chi^2}^{\infty}\mathrm{d}K^2\,\frac{\sqrt{K^2/4 - m^2}}{\sqrt{K^2}}(\sigma_{\mathrm{ann}}\widetilde{F})\int_{\sqrt{K^2}}^{\infty}\sqrt{(K^0)^2 - K^2}\,e^{-\frac{K^0}{T}}\mathrm{d}K^0\,.$$

The last integral can be computed analytically: by introducing $y = K^0/\sqrt{K^2}$, it becomes

$$K^2\int_1^\infty \sqrt{y^2-1}\,e^{-y\frac{\sqrt{K^2}}{T}}\mathrm{d}y = K^2\frac{T}{\sqrt{K^2}}\mathscr{K}_1(\sqrt{K^2}/T)\,,$$

where $\mathscr{K}_i(y)$ is the modified Bessel function of order i (for their definition, see ref. [62]).

We now denote K^2 by s. We have obtained

$$\langle\sigma v\rangle = \frac{1}{(2\pi)^6}\frac{1}{(n_{\mathrm{eq}})^2}2\pi^2 T\int_{4m_\chi^2}^{\infty}\mathrm{d}s\,\sqrt{s/4 - m^2}(\sigma_{\mathrm{ann}}\widetilde{F})\mathscr{K}_1(\sqrt{s}/T)\,.$$

For the remainder of this section, we will substitute the flux factor $\widetilde{F}$ by its value (eq. (B.5)) in the case of a two-particles annihilation, to simplify the final expression. We then compute explicitly n_{eq} (eq. B.2):

$$\begin{aligned} n_{\mathrm{eq}} &= g\int\frac{\mathrm{d}^3p}{(2\pi)^3}\,e^{-\frac{E}{T}} = \frac{g}{2\pi^2}\int_m^\infty \mathrm{d}E\,e^{-\frac{E}{T}}E\sqrt{E^2-m^2} = \qquad (y \equiv E/m) \\ &= \frac{g}{2\pi^2}m^3\int_1^\infty \mathrm{d}y\,e^{-y\frac{m}{T}}y\sqrt{y^2-1} = \frac{g}{2\pi^2}m^3\frac{T}{m}\mathscr{K}_2(m/T)\,. \end{aligned} \tag{B.6}$$

By defining $x = m/T$, we get the final expression for $\langle\sigma v\rangle$ (in agreement with [63])

$$\langle\sigma v\rangle = \frac{x}{8m^5}\frac{1}{(\mathscr{K}_2(x))^2}\int_{4m^2}^\infty \sigma_{\mathrm{ann}}\sqrt{s}(s-4m^2)\mathscr{K}_1(x\sqrt{s}/m)\,\mathrm{d}s\,. \tag{B.7}$$

This expression can be easily computed numerically, once m, $\sigma_{\mathrm{ann}}(s)$ and x are fixed.

B.3 Approximate formula for $\langle\sigma v\rangle$

In this section, an approximate formula for $\langle\sigma v\rangle$ in the low temperature limit will be given. This expression will depend on the coefficients of the expansion of $(\sigma_{\mathrm{ann}}\widetilde{F})$ in the low velocity limit. Indeed, $(\sigma_{\mathrm{ann}}\widetilde{F})$ is a function of s, which in turn can be expanded in powers of the module v of the relative 3-velocity between the colliding particles.

The easiest way to derive the expansion of s in terms of the relative speed $v = |\vec{v}_1 - \vec{v}_2|$ between two colliding identical particles is to calculate s (which is a Lorentz invariant) in the c.o.m. frame, where the four-momenta of the two particles are $p_1^\mu = (E, 0, 0, p)$, $p_2^\mu = (E, 0, 0, -p)$: then, $s = (p_1 + p_2)^2 = 4E^2$, where E is the energy of each particle in the c.o.m. frame. In the non-relativistic limit, $E \approx m + m(v^*)^2/2$, where v^* is the speed of each particle in this frame, and is given by $v^* = v_1 - v_{\text{c.o.m.}} = v_1 - (v_1 + v_2)/2 = v/2$. Eventually, $E \approx m(1 + v^2/8)$ and

$$s = m^2(4 + v^2) + \mathcal{O}(v^4) \tag{B.8}$$

Therefore, the low velocity expansion of $(\sigma_{\text{ann}}\widetilde{F})(s)$ will only contain even powers of v:

$$(\sigma_{\text{ann}}\widetilde{F}) \approx a + bv^2\,, \tag{B.9}$$

where a, b are adimensional quantities.

We are going now to expand the integrand in eq. (B.7) in powers of v until the second leading order, in the limit of low temperatures (which corresponds to $x \to \infty$), which is an acceptable approximation since $x_f = m/T_{\text{freeze out}}$ ranges between 20 and 25. We perform then the change of variables $v = \sqrt{s - 4m^2}/m$, whose differential gives

$$\mathrm{d}s = 2m\sqrt{s - 4m^2}\mathrm{d}v\,;$$

by reinserting the flux factor F (eq. (B.5)), the integral in eq. (B.7) reads

$$\int_0^\infty \frac{1}{2g^2}(\sigma_{\text{ann}}\widetilde{F}) \cdot (m^2v^2)\, \mathscr{K}_1(x\sqrt{4 + v^2})2m\,\mathrm{d}v\,.$$

In the simultaneous limit $x \to \infty$, $v \to 0$, the modified Bessel function can be expanded as

$$\begin{aligned}\mathscr{K}_1(x\sqrt{4 + v^2}) &\underset{x\to\infty}{\approx} e^{-x\sqrt{4+v^2}}\left[\sqrt{\frac{\pi}{2}}\frac{1}{\sqrt{x}\sqrt[4]{4 + v^2}} + \mathcal{O}(x^{-3/2})\right] \approx \\ &\underset{v\to 0}{\approx} e^{-2x}e^{-v^2\frac{x}{4}}\frac{\sqrt{\pi}}{2}\frac{1}{\sqrt{x}}\left[1 - \frac{1}{16}v^2\right] + \mathcal{O}(x^{-3/2}, v^4)\,.\end{aligned}$$

We can now use eq. (B.9), and rewrite the integral in eq. (B.7) as (we understand in the following formula factors up to $\mathcal{O}(x^{-3/2}, v^6)$)

$$\frac{m^3}{g^2}\frac{\sqrt{\pi}}{2}\frac{e^{-2x}}{\sqrt{x}}\int_0^\infty (a + bv^2)v^2\left(1 - \frac{1}{16}v^2\right)e^{-v^2\frac{x}{4}}\,\mathrm{d}v \approx \frac{m^3}{g^2}\frac{\sqrt{\pi}}{2}\frac{e^{-2x}}{\sqrt{x}}\int_0^\infty \left[av^2 + \left(b - \frac{a}{16}\right)v^4\right]e^{-v^2\frac{x}{4}}\,\mathrm{d}v\,.$$

After these simplifications, we can explicitly calculate the integrals with the formulæ

$$\int_0^\infty y^{2n}e^{-y^2}\mathrm{d}y = \frac{\sqrt{\pi}}{2}\left|\left(\frac{\mathrm{d}^n}{\mathrm{d}\alpha^n}\frac{1}{\sqrt{a}}\right)_{\alpha=1}\right| \quad\Longrightarrow\quad \int_0^\infty y^2e^{-y^2}\mathrm{d}y = \frac{\sqrt{\pi}}{4}\,,\quad \int_0^\infty y^4e^{-y^2}\mathrm{d}y = \frac{3\sqrt{\pi}}{8}\,.$$

The result of the integration is

$$\frac{\pi}{g^2}m^3\frac{e^{-2x}}{x^2}\left(a + \frac{3(16b - a)}{8x}\right).$$

We are now left with the evaluation of the prefactor in eq. (B.7) in the limit $x \to \infty$: by expanding the Bessel function we get

$$\frac{x}{8m^5}\frac{1}{(\mathscr{K}_2(x))^2} \underset{x\to\infty}{\approx} \frac{x}{8m^5}\frac{1}{\frac{\pi}{2x}e^{-2x}} = \frac{x^2e^{2x}}{4\pi m^5}\,,$$

which gives the final result

$$\langle \sigma v \rangle \approx \frac{1}{4g^2m^2}\left(a + \frac{3(16b-a)}{8x}\right). \tag{B.10}$$

It will be useful in the following to denote

$$\langle \sigma v \rangle \approx \sigma_0 + \frac{\sigma_2}{x}, \qquad \sigma_0 = \frac{a}{4g^2m^2}, \qquad \sigma_2 = \frac{a}{4g^2m^2}\frac{3(16b-a)}{8a} = \sigma_0\left(\frac{6b}{a} - \frac{3}{8}\right). \tag{B.11}$$

B.4 Approximate solution of the Boltzmann equation

In this section, we will derive an approximate solution to the Boltzmann equation.

We can rewrite eq. (B.1) by defining the *yield* $Y = n/s_{\rm ent}$ (and $Y_{\rm eq} = n_{\rm eq}/s_{\rm ent}$), where $s_{\rm ent}$ is the entropy density, in order to get the evolution of the number of particles in a comoving volume. The entropy density is dominated by the contribution of relativistic particles, then with a very good approximation

$$s_{\rm ent} = \frac{2\pi^2}{45} g_{*S} T^3,$$

where g_{*S} is given by

$$g_{*S} = \sum_{\rm bosons} g_i \left(\frac{T_i}{T}\right)^3 + \frac{7}{8}\sum_{\rm fermions} g_i \left(\frac{T_i}{T}\right)^3, \tag{B.12}$$

summed over all the relativistic particles in the Universe.

We can then change the functional dependence on the time t into a dependence on the temperature T by using the relation between time and temperature during the radiation dominated era [9], and then we introduce $x = m/T$. The result is the following form of the Boltzmann equation:

$$\frac{{\rm d}Y}{{\rm d}x} = -\frac{x\langle \sigma v \rangle s_{\rm ent}}{H(m)}\left(Y^2 - Y_{\rm eq}^2\right). \tag{B.13}$$

We want not to derive an approximate value for the final yield Y_∞ after the freeze out. To this aim, we introduce the approximation of low temperature (indeed, x_f ranges between 20 and 25 for our models), in which eq. (B.10) shows that we can write

$$\frac{x\langle \sigma v \rangle s_{\rm ent}}{H(m)} \approx \frac{1}{x^2}\left(\lambda_0 + \lambda_2 \frac{1}{x}\right), \quad \lambda_0 = \sigma_0\left(\frac{x\, s_{\rm ent}}{H(m)}\right)_{x=1}, \quad \lambda_2 = \sigma_2\left(\frac{x\, s_{\rm ent}}{H(m)}\right)_{x=1}. \tag{B.14}$$

The numerical value of $(x\, s_{\rm ent}/H(m))_{x=1}$ is [9]

$$\left(\frac{x\, s_{\rm ent}}{H(m)}\right)_{x=1} = 0.264 \frac{g_{*S}}{\sqrt{g_*}} M_{\rm P} m,$$

where g_* is the number of relativistic degrees of freedom, given by

$$g_{*S} = \sum_{\rm bosons} g_i \left(\frac{T_i}{T}\right)^4 + \frac{7}{8}\sum_{\rm fermions} g_i \left(\frac{T_i}{T}\right)^4, \tag{B.15}$$

summed over all the relativistic particles in the Universe. Notice the difference with respect to eq. (B.12), where the exponent of the temperatures is 3; thus, until when all the relativistic particles share the same temperature, $g_* = g_{*S}$; after the decoupling of neutrinos around $T = 0.5$ MeV, their temperature has been different from the one of photons, thus today $g_* \neq g_{*S}$.

For the temperature regime that will be of interest to us (between 1000 GeV and 10 GeV), g_{*s} is around 100 [9].

Returning back to the Boltzmann equation, it is useful to capture the approximate behaviour during the freeze out to rewrite it in terms of the distance Δ of Y from the equilibrium yield $Y_{\rm eq}$, $\Delta = Y - Y_{\rm eq}$. The differential equation for Δ, after the definitions of eq. (B.14), reads

$$\Delta' = -Y'_{\rm eq} - \frac{1}{x^2}\left(\lambda_0 + \frac{\lambda_2}{x}\right)\Delta(2Y_{\rm eq} + \Delta)\,. \tag{B.16}$$

At early times, Y follows $Y_{\rm eq}$, thus Δ, Δ' can be neglected with respect to Y:

$$\Delta \approx -\frac{Y'_{\rm eq}}{2Y_{\rm eq}}\frac{x^2}{\lambda_0 + \frac{\lambda_2}{x}} \approx \frac{x^2}{2\left(\lambda_0 + \frac{\lambda_2}{x}\right)}\,, \tag{B.17}$$

where we used $Y'_{\rm eq} \approx -Y_{\rm eq}$, that is valid in non-relativistic regime since

$$Y_{\rm eq}(x) = 0.145\frac{g}{g_{*S}}x^{3/2}e^{-x} \equiv \alpha x^{3/2}e^{-x} \quad \Longrightarrow \quad \frac{Y'_{\rm eq}}{Y_{\rm eq}} = \frac{3}{2x} - 1 \approx -1\,.$$

For times after the freeze out, $Y_{\rm eq}$ is negligible and $\Delta \approx Y$, then eq. (B.16) gives

$$\begin{aligned}
\Delta' &\approx -\frac{\left(\lambda_0 + \frac{\lambda_2}{x}\right)}{x^2}\Delta^2\,, \quad \Longrightarrow \quad -\frac{1}{\Delta}\Big|_{x_f}^{\infty} = \left(\frac{\lambda_0}{x} + \frac{\lambda_2}{2x^2}\right)\Big|_{x_f}^{\infty}\,,\\
Y_\infty &= \Delta_\infty = \frac{x_f}{2\left(\lambda_0 + \frac{\lambda_2}{2x_f}\right)}\,.
\end{aligned} \tag{B.18}$$

From this formula, one can finally obtain the approximate value of the asymptotic relic abundance $\Omega_{\rm DM}h^2$, where $h = H/(100\ {\rm km/s/Mpc})$, in terms of σ_0, σ_2 (B.11):

$$\Omega_{\rm DM}h^2 \approx 1.07\cdot 10^{-9}\frac{x_f}{\sqrt{g_*}M_{\rm P}\left(\sigma_0 + \frac{\sigma_2}{2x_f}\right)}\,. \tag{B.19}$$

We need now to estimate x_f: we could define it as the time in which $\Delta(x_f)$ reaches of the same order of $Y_{\rm eq}(x_f)$, say $\Delta(x_f) = cY_{\rm eq}(x_f)$ with c of order unity. Then we can simplify eq. (B.17) into

$$\Delta(x_f) \approx -Y'_{\rm eq}\frac{x_f^2}{\lambda_0 + \frac{\lambda_2}{x_f}}\frac{1}{(2+c)Y_{\rm eq}} \approx \frac{x_f^2}{\left(\lambda_0 + \frac{\lambda_2}{x_f}\right)(2+c)}\,.$$

From this equation, we can rewrite the condition $\Delta(x_f) = cY_{\rm eq}(x_f)$ as

$$\begin{aligned}
\frac{x_f^2}{\left(\lambda_0 + \frac{\lambda_2}{x_f}\right)(2+c)} = c\alpha x_f^{3/2}e^{-x_f} \quad &\Longrightarrow \quad e^{x_f}x_f^{1/2} = \left(\lambda_0 + \frac{\lambda_2}{x_f}\right)\alpha c(2+c)\,,\\
x_f + \frac{1}{2}\ln x_f &= \ln\left[\left(\lambda_0 + \frac{\lambda_2}{x_f}\right)\alpha c(2+c)\right]\,.
\end{aligned}$$

In first approximation, the solution to the previous equation is simply $x_f = \ln[\lambda_0\alpha c(2+c)]$; a better approximation is obtained by replacing this value into the last equation. As a last step, a

definition of c which gives a good fit to the exact numeric solution of the Boltzmann equation is $c(2+c) = 1$ [9]; this gives the final result

$$x_f \approx \ln(\lambda_0 \alpha) - \frac{1}{2}\ln[\ln(\lambda_0 \alpha)] + \ln\left[1 + \frac{\lambda_2}{\lambda_0}\frac{1}{\ln(\lambda_0 \alpha)}\right], \tag{B.20}$$

where we recall that

$$\lambda_0 \alpha = 0.038 \frac{g}{\sqrt{g_*}} M_{\rm P} m \cdot \left(\frac{a}{4g^2 m^2}\right), \qquad \frac{\lambda_2}{\lambda_0} = \frac{3(16b - a)}{8a}.$$

Bibliography

[1] L. E. Strigari, *Galactic searches for dark matter*, Physics Reports **531** (2013) 1-88, arXiv:1211.7090.

[2] G. Bertone, D. Hooper, J. Silk, *Particle dark matter: evidence, candidates and constraints*, Physics Reports **405** (2005) 279-390, arXiv:hep-ph/0404175.

[3] J. L. Feng, *Dark matter candidates from particle physics and methods of detection*, Ann. Rev. Astron. Astrophys. **48** (2010) 495, arXiv:1003.0904.

[4] Planck collaboration, *Planck 2013 results. XVI. Cosmological parameters*, arXiv:1303.5076.

[5] D. Clowe et al., *A direct empirical proof of the existence of dark matter*, Astrophys. J. **648** (2006) L109, arXiv:astro-ph/0608407.

[6] J. D. Bekenstein, *Modified gravity as an alternative to dark matter*, published in G. Bertone (ed.), *Particle dark matter: observations, models and searches*, Cambridge, Cambridge University Press (2010).

[7] S. Dodelson, *The real problem with MOND*, Int. J. Mod. Phys. D **20** (2011) 2749, arXiv:1112.1320.

[8] S. Dodelson, *Modern cosmology*, Burlington, Academic Press (2003).

[9] E. W. Kolb, M. S. Turner, *The early universe*, Redwood City, Addison-Wesley (1990).

[10] L. J. Hall, K. Jedamzik, J. March-Russell, S. M. West, *Freeze-in production of FIMP dark matter*, Journal of High Energy Physics **03** (2010) 80, arXiv:0911.1120.

[11] J. McDonald, *Thermally generated gauge singlet scalars as self-interacting dark matter*, Phys. Rev. Lett. **88** (2002) 091304, arXiv:hep-ph/0106249.

[12] K. M. Zurek, *Asymmetric dark matter: theories, signatures and constraints*, Phys. Rept. **537** (2014) 91-121, arXiv:1308.0338.

[13] A. Falkowski, J. T. Ruderman, T. Volansky, *Asymmetric dark matter from leptogenesis*, Journal of High Energy Physics **05** (2011) 106, arXiv:1101.4936.

[14] M. Shaposhnikov, *Sterile neutrinos*, published in G. Bertone (ed.), *Particle dark matter: observations, models and searches*, Cambridge, Cambridge University Press (2010).

[15] A. Merle, *keV neutrino model building*, Int. J. Mod. Phys. D **22** (2013), arXiv:1302.2625.

[16] R. D. Peccei, *The strong CP problem and Axions*, Lect. Notes Phys. **741** (2008) 3-17, arXiv:hep-ph/0607268.

[17] M. Dine, *TASI lectures on the strong CP problem*, SCIPP-00-30, arXiv:hep-ph/0011376.

[18] L. D. Duffy, K. van Bibber, *Axions as dark matter particles*, New J. Phys. **11** (2009) 105008, arXiv:0904.3346.

[19] P. Sikivie, *Axions*, published in G. Bertone (ed.), *Particle dark matter: observations, models and searches*, Cambridge, Cambridge University Press (2010).

[20] C. Amsler et al., *Review of particle physics, Axions and other similar particles*, Phys. Lett. B **667** (2008).

[21] D. G. Cerdeño, A. M. Green, *Direct detection of WIMPs*, published in G. Bertone (ed.), *Particle dark matter: observations, models and searches*, Cambridge, Cambridge University Press (2010).

[22] M. Cirelli, E. Del Nobile, P. Panci, *Tools for model-independent bounds in direct dark matter searches*, JCAP 10 (2013) 019, arXiv:1307.5955.

[23] C. Armendariz-Picon, J. Neelakanta, *How cold is cold dark matter?*, JCAP 1403 (2014) 049, arXiv:1309.6971.

[24] N. Mirabolfathi, *Dark Matter Direct Detection With Low Temperature Detectors*, arXiv:1308.0044.

[25] CDMS Collaboration (R. Agnese et al.), *Silicon Detector Dark Matter Results from the Final Exposure of CDMS II*, Phys. Rev. Lett. **111** (2013) 251301, arXiv:1304.4279.

[26] AMS Collaboration (M. Aguilar et al.), *First result from the Alpha Magnetic Spectrometer on the International Space Station: precision measurement of the positron fraction in primary cosmic rays of 0.5-350 GeV*, Phys. Rev. Lett. **110** (2013) 141102.

[27] E. Bulbul, M. Markevitch, A. Foster, R. K. Smith, M. Loewenstein, S. W. Randall, *Detection of an unidentified emission line in the stacked X-ray spectrum of galaxy clusters*, arXiv:1402.2301.

[28] A. Boyarsky, O. Ruchayskiy, D. Iakubovskyi, J. Franse, *An unidentified line in X-ray spectra of the Andromeda galaxy and Perseus galaxy cluster*, arXiv:1402.4119.

[29] CMS collaboration (S. Chatrchyan et al.), *Search for dark matter and large extra dimensions in monojet events in pp collisions at* $\sqrt{s} = 7$ *TeV*, JHEP 1209 (2012) 094, arXiv:1206.5663.

[30] ATLAS collaboration (G. Aad et al.), *Search for dark matter candidates and large extra dimensions in events with a jet and missing transverse momentum with the ATLAS detector*, JHEP 1304 (2013) 075, arXiv:1210.4491.

[31] CMS collaboration, *Search for new physics in monojet events in pp collisions at* $\sqrt{s} = 8$ *TeV*, CMS PAS EXO 12-048.

[32] ATLAS collaboration, *Search for new phenomena in monojet plus missing transverse momentum final states using 10* fb^{-1} *of pp collisions at* $\sqrt{s} = 8$ *TeV with the ATLAS detector at the LHC*, ATLAS-CONF-2012-147.

[33] CMS collaboration (S. Chatrchyan et al.), *Search for dark matter and large extra dimensions in pp collisions yielding a photon and missing transverse energy*, Phys. Rev. Lett. **108** (2012) 261803, arXiv:1204.0821.

[34] ATLAS collaboration (G. Aad et al.), *Search for Dark Matter Candidates and Large Extra Dimensions in events with a photon and missing transverse momentum in pp collision data at $\sqrt{s} = 7$ TeV with the ATLAS detector*, Phys. Rev. Lett. **110** (2013) 011802, arXiv:1209.4625.

[35] G. Busoni, A. De Simone, E. Morgante, A. Riotto, *On the validity of the effective field theory for dark matter searches at the LHC*, Physics Letters B **728** (2014) 412-421, arXiv:1307.2253.

[36] G. Busoni, A. De Simone, J. Gramling, E. Morgante, A. Riotto, *On the validity of the effective field theory for dark matter searches at the LHC Part II: Complete Analysis for the s-channel*, JCAP 1406 (2014) 060, arXiv:1402.1275.

[37] G. Busoni, A. De Simone, T. Jacques, E. Morgante, A. Riotto, *On the validity of the effective field theory for dark matter searches at the LHC part III: Complete Analysis for the t-channel*, arXiv:1405.3101.

[38] S. P. Martin, *A supersymmetry primer*, arXiv:hep-ph/9709356.

[39] G. Mack, J. Beacom, G. Bertone, *Towards closing the window on strongly interacting dark matter: far-reaching constraints from Earth's heat flow*, Phys.Rev. D76 (2007) 043523, arXiv:0705.4298.

[40] J. Goodman, M. Ibe, A. Rajaraman, W. Shepherd, T. Tait, H. Yu, *Constraints on dark matter from colliders*, Phys.Rev. D82 (2010) 116010, arXiv:1008.1783.

[41] G. Servant, *Dark matter at the electroweak scale: non-supersymmetric candidates*, published in G. Bertone (ed.), *Particle dark matter: observations, models and searches*, Cambridge, Cambridge University Press (2010).

[42] M. Cirelli, A. Strumia, *Minimal Dark Matter: Model and results*, New J.Phys. 11 (2009) 105005, arXiv:0903.3381 .

[43] Y. Bai, P. Fox, R. Harnik, *The Tevatron at the frontier of dark matter direct detection*, JHEP 1012 (2010) 048, arXiv:1005.3797.

[44] A. De Simone, G. F. Giudice, A. Strumia, *Benchmarks for dark matter searches at the LHC*, 1402.6287, arXiv:1402.6287.

[45] M. Garny, A. Ibarra, S. Rydbeck, S. Vogl, *Majorana dark matter with a coloured mediator: collider vs direct and indirect searches*, JHEP06 (2014) 169, arXiv:1403.4634.

[46] M. Srednicki, R. Watkins, K. Olive, *Calculations of relic densities in the early universe*, Nuclear Physics B310 (1988) 693-713.

[47] O. Lebedev, Y. Mambrini, *Axial dark matter: the case for an invisible Z'*, arXiv:1403.4837.

[48] H. E. Haber, G. L. Kane, *The search for supersymmetry: probing physics beyond the Standard Model*, Physics Reports **117** (1985), 75-263, and Erratum SCIPP 85/47.

[49] H. K. Dreiner, H. E. Haber, S. P. Martin, *Two-component spinor techniques and Feynman rules for quantum field theory and supersymmetry*, Physics Reports 494 (2010) 1-196, arXiv:0812.1594.

[50] S. Chang, R. Edezhath, J. Hutchinson, M. Luty, *Effective WIMPs*, Phys. Rev. D89 (2014) 015011, arXiv:1307.8120.

[51] A. DiFranzo, K. Nagao, A. Rajaraman, T. Tait, *Simplified models for dark matter interacting with quarks*, JHEP 1311 (2013) 014, arXiv:1308.2679.

[52] H. An, L. Wang, H. Zhang, *Dark matter with t-channel mediator: a simple step beyond contact interaction*, Phys. Rev. D89 (2014) 115014, arXiv:1308.0592.

[53] A. Fitzpatrick, W. Haxton, E. Katz, N. Lubbers, Y. Xu, *The effective field theory of dark matter direct detection*, JCAP 1302 (2013) 004, arXiv:1203.3542.

[54] N. Fornengo, L. Maccione, A. Vittino, *Constraints on particle dark matter from cosmic-ray antiprotons*, JCAP 04 (2014) 003, arXiv:1312.3579.

[55] V. Pettorino, G. Busoni, A. De Simone, E. Morgante, A. Riotto, W. Xue, *Can AMS-02 discriminate the origin of an anti-proton signal?*, arXiv:1406.5377.

[56] G. Di Bernardo, C. Evoli, D. Gaggero, D. Grasso, L. Maccione, *Cosmic ray electrons, positrons and the synchrotron emission of the Galaxy: consistent analysis and implications*, JCAP 1303 (2013) 036, arXiv:1210.4546.

[57] M. Cirelli, D. Gaggero, G. Giesen, M. Taoso, A. Urbano, *Antiproton constraints on the GeV gamma-ray excess: a comprehensive analysis*, arXiv:1407.2173.

[58] B. A. Dobrescu, F. Yu, *Coupling–mass mapping of di-jet peak searches*, Phys. Rev. D **88** (2013) 035021, arXiv:1306.2629.

[59] M. Papucci, A. Vichi, K. M. Zurek, *Monojet versus rest of the world I: t-channel models*, arXiv:1402.2285.

[60] ATLAS collaboration (G. Aad et al.), *Search for squarks and gluinos with the ATLAS detector in final states with jets and missing transverse momentum using* $\sqrt{s} = 8$ *TeV proton–proton collision data*, arXiv:1405.7875.

[61] CMS collaboration (S. Chatrchyan et al.), *Search for new physics in the multijets and missing momentum final state in proton-proton collisions at 8 TeV*, CMS-PAS-SUS-13-012.

[62] G. Arfken, H. Weber, *Mathematical methods for physicists*, Amsterdam, Elsevier (2005).

[63] P. Gondolo, G. Gelmini, *Cosmic abundances of stable particles: improved analysis*, Nucl. Phys. B360 (1991) 145-179.